Design of a Remote, Integrated, Automatic and Continuous Bedload Sediment Transport Monitoring Station and Application in a Rural Stream in Southern Ontario

by

Matthew Iannetta

A thesis

presented to the University of Waterloo

in fulfillment of the

thesis requirement for the degree of

Master of Applied Science

in

Civil Engineering (Water)

Waterloo, Ontario, Canada, 2021

Author's Declaration

I hereby declare that I am the sole author of this thesis. This is a true copy of the thesis, including any required final revisions, as accepted by my examiners.

I understand that my thesis may be made electronically available to the public.

Abstract

The form and function of a stream network is directly influenced by natural processes and human activities that occur within the watershed. Human modifications in the form of urban and agricultural development alter natural water and nutrient cycles, which adversely affects stream health and stability. As new stormwater management techniques that aim to mitigate these impacts become more commonly implemented, it is prudent to investigate if we can continue modifying the landscape and alternatively realize a net benefit to stream health and stability. To evaluate the effectiveness of stream restoration efforts, baseline flow and bedload sediment transport characteristics should be characterized. However, many commonly used bedload monitoring methods often yield limited inter-flood or discontinuous data, which restricts our understanding of bedload transport dynamics. Field efforts involved in collecting these data can be difficult, expensive, and dangerous in some circumstances of significant flow.

This thesis presents a new remote, integrated, automatic and continuous bedload monitoring station. The station configuration is relatively inexpensive, easy to deploy in the field, and designed for remote applications. The station was deployed at a semi-alluvial headwater creek located in an agricultural watershed in Southern Ontario where baseline flow and bedload sediment transport characteristics were studied. The station integrates two indirect monitoring devices including an in-situ radio frequency identification (RFID) antenna tracker and “Benson-Type” seismic impact plates. 400 synthetic RFID tracer stones divided into four size classes were seeded upstream of the station to be tracked automatically as they gradually pass over the in-situ RFID antenna. The “Benson-Type” seismic impact plates rest along the creek bed surface and function by converting mechanical energy exerted by mobile bedload particles that strike the plates into electrical energy recorded as total counts. A sediment trap was installed to help calibrate the continuous impact

plate data record. Supplemental inter-flood tracer tracking surveys were completed to monitor tracer movement along the study reach. Field observations were used to build a predictive model of bedload sediment transport. The predictive model was used in combination with hydrologic model outputs to make relative comparisons of tracer displacement under alternative land-use scenarios.

The field study was limited by technical shortcomings that ultimately prevented consistent operation of the station during the study period and uncertainty in impact plate device performance limited the usefulness of the recorded dataset. Technical improvements were gradually added to the bedload monitoring station throughout the study period and additional planned upgrades should allow for more consistent operation in the future. It is recommended that the impact plates undergo flume experimentation in a future study to clarify uncertainties related to device performance.

Acknowledgements

For the better part of the past nine years I have been studying at the University of Waterloo. I would like to acknowledge that during this time I have lived and worked on the traditional territory of the Neutral, Anishinaabeg and Haudenosaunee peoples. The University of Waterloo is situated on the Haldimand Tract, the land promised to the Six Nations that includes ten kilometres on each side of the Grand River. The lands studied for this thesis are situated within the traditional and treaty territory of the Mississaugas and Chippewas of the Anishinaabeg, known today as the Williams Treaties First Nations.

I would like to thank my academic supervisor Dr. Bruce MacVicar for providing continued support and mentorship throughout my time as a grad student. Whether it was a research related discussion or career advice, I could always count on Bruce for guidance. Thank you Bruce.

Thank you John Koke, Amanda Santo and the team at Dorsay Development Corporation for making this research possible by providing industry funding through a Mitacs Accelerate Fellowship and NSERC Engage grant. It was truly encouraging to have an industry partner take such an active interest in supporting this project.

I would like to express my sincerest gratitude to the team at GeoProcess Research Associates for providing guidance throughout my grad school journey. Thank you to Jeff Hirvonen, Ben Plumb, Pete Thompson, Ian Roul, Tom Arsenault, Cal Jefferies, Chris McKie, Cailey McCutcheon, and Lorenzo Brignoli. Jeff and Ben inspired the foundation of this research project and coordinated the opportunity to collaborate with Dorsay. Jeff, Ben and Pete generously offered their time to discuss research ideas and provide suggestions on a continual basis.

I would like to thank external researchers and collaborators Dr. Peter Downs, Dr. Philip Soar and Ian Benson for providing knowledge and expertise regarding the modified Benson Type-A impact plates used for this research project.

There are many members of the University of Waterloo Department of Civil and Environmental Engineering who have helped me along the way. I would like to thank the following staff and faculty: Mark Sobon, Mark Hummel, Mark Merlau, Anne Allen, Peter Volcic, Doug Hirst, Richard Morrison, Colin Van Niejenhuis, Dan Jessel and Victor Lewis. I would like to express special thanks to Mark Sobon, the jack of all trades who was always happy to help without a second thought, and Mark Hummel who was a key contributor in the execution of field instrumentation.

Thank you to friends and fellow colleagues who helped with my research: Dirk Friesen, Jackie Wintermeyer, Elli Papangelakis, Aryn Cain, Asal Montakhab, Chris Muirhead, Sara Gopaul, Jaclyn Iannetta, Jasmine Romero, Kevin Morwood and Paul Chiocchio. A special mention goes to Jackie Wintermeyer who worked tirelessly during the Spring 2019 co-op term to manufacture 400+ tracer stones and helped instrument the field site. Another special mention goes to Dirk Friesen who was essential to the project and an absolute pleasure to work with; Dirk was the technological expert who seamlessly integrated research monitoring devices into an automated system.

Commenting on the quality of the year 2020 (or lack thereof) has quickly become a cliché, but I would be remiss not to mention how critical the support of my family has been during these unprecedented times. To my Grandma, I will always appreciate your keen interest in river hydraulics and enthusiastic greeting of “did your rocks move?”. To my parents and sister, thank you for accommodating a sometimes fatigued, anxious and impatient, perpetually caffeine deficient grad student during the pandemic lockdown. It is very rare that we are all home together with Jaclyn for more than one or two weeks a year; I will always cherish that time. Jaclyn, thank

you for keeping me grounded. Finally, to Jasmine, you are such a bright, kind-hearted, and strong individual. You are a determined leader and passionate advocate for social justice. You are my inspiration.

Table of Contents

Author's Declaration ii
Abstract iii
Acknowledgements v
List of Figures x
List of Tables xiii
1 Introduction 1
2 Literature Review 6
2.1 Channel Morphology and Evolution 6
2.2 Influence of Agricultural Development on Stream Morphology in Southern Ontario 10
2.2.1 Quaternary Period History 10
2.2.2 Deforestation and Riparian Vegetation Removal 14
2.2.3 Anthropogenic Modifications 17
2.2.4 Urbanization of Rural Areas 20
2.3 Bedload Monitoring Methods 21
2.3.1 Integrated Automatic Continuous Bedload Monitoring 24
2.3.2 Passive Acoustic Bedload Monitoring 25
2.3.3 Passive Integrated Transponder Tags 30
2.4 Summary of Research Gaps 34
3 Remote, Integrated, Automatic and Continuous Bedload Monitoring Station 37
3.1 Bedload Monitoring Method Selection 37
3.2 Station Overview 39
3.2.1 Power Supply and Storage 40
3.2.2 System Controller 41
3.2.3 Network Communication 42
3.2.4 Protective Housing 43
3.2.5 Water Level Measurement 44
3.2.6 Bedload Sediment Transport Measurement 45
3.3 Modified Benson Type-A Impact Plate Performance Testing 49
3.3.1 Manufacturer Sensitivity Rating 49
3.3.2 Threshold Test and Spatial Sensitivity Analysis 51
3.3.3 Cold Temperature Performance Analysis 54
3.3.4 Recommendations 56

4 Baseline Flow and Sediment Characterization of a Semi-Alluvial Creek 57
4.1 Study Site 57
4.1.1 Stream Power Analysis 58
4.1.2 Site Reconnaissance 60
4.2 Methods 61
4.2.1 Hydrology 62
4.2.2 Substrate Characterization 62
4.2.3 Geomorphic Survey 63
4.2.4 Photographic Inventory 64
4.2.5 Bedload Transport Monitoring 64
4.2.6 Field Installation 71
4.3 Results 73
4.3.1 Geomorphic Characterization 73
4.3.2 Critical Threshold Assessment 78
4.3.3 Tracer Particle Tracking 81
4.3.4 Bedload Impact Detections 90
4.3.5 Direct Physical Sampling 98
4.4 Alternative Land Use Modelling 99
4.4.1 Hydrologic Model Scenarios 100
4.4.2 Cumulative Excess Discharge Analysis 101
4.5 Conclusions 103
5 Conclusions and Recommendations 104
References 108
Appendix A: CIVE 781 Principles of Hydrologic Modelling Final Project Report 119

List of Figures

Figure 1. Dynamic relationship between channel form and process in gravel bed rivers. From (Ashworth & Ferguson, 1986). 6
Figure 2. Classic Lane balance scale diagram. From (Rosgen, 1996). 7
Figure 3. Incised channel evolution model developed by (Schumm, 1984) and (Simon, 1989). From (Shields Jr., 1998)..... 9
Figure 4. Canadian quaternary period timeline. From (Fulton, 1986). 11
Figure 5. Quaternary Period Glacial Extents. From (Killey, 2007). 12
Figure 6. Cross-section schematic demonstrating transitions between aquatic, riparian and upland ecosystems. From (Stevens et al., 1995). 15
Figure 7. Visualization of Subsurface Tile Drainage. From (Blann et al., 2009). 18
Figure 8. Conceptual model of agricultural drainage impacts on aquatic ecosystems. From (Blann et al., 2009). 19
Figure 9. Sediment Transport Classifications and Mechanisms. From (Dey, 2014). 22
Figure 10. Habersack integrated bedload monitoring station, a) bedload slot sampler, b) station during maintenance, c) bedload sample retrieval, d) slot sampler operational schematic. From (Habersack et al., 2017). 24
Figure 11. Continuous passive acoustic bedload monitoring station at the Erlenbach stream, Switzerland. From (Rickenmann et al., 2012). 26
Figure 12. Continuous passive acoustic bedload monitoring at the River Avon, UK. From (Downs et al., 2016). 28
Figure 13. Schematic of Wobblestone conceptual design. From (Papangelakis, Muirhead, et al., 2019). 31
Figure 14. Muirhead Station water level gauge and in-stream antenna (left), and electrical components housed within a storage bin (right) at Schneider Creek. From (Muirhead, 2018).... 32
Figure 15. Bedload monitoring station conceptual diagram. 40
Figure 16. Electronics enclosure mounted to tabletop frame. Figure shows early version of station setup with only one solar panel. 43
Figure 17. Seametrics PT2X pressure sensor. (A) Sensor and cable connection. Retrieved from: https://www.nexsens.com/products/sensors/water-level/seametrics-pt2x-water-level-loggers. (B) Well housing. 44
Figure 18. Solidworks schematic of PVC housing for in-stream antenna. (A) Zoomed in view of single modular segment showing inner channels and bumps. (B) View of housing assembly. ... 46
Figure 19. Impact plate mounted to concrete block. View of electrical wire conduit routed through inner channel. 48
Figure 20. Bunte sediment trap (Bunte et al., 2007). 48
Figure 21. Benson Type-A impact plate manufacturer sensitivity test. A) Experimental setup. B) Test results (Photo credits: Ian Benson, 2019). 50
Figure 22. Impact plate detection threshold analysis. Impacts were exerted upon the plate centre using a Dynapulse™ impulse hammer to measure peak impact force. 51

Figure 23. Impact plate spatial sensitivity analysis. Impacts were exerted upon a transect along the plate centre running parallel to the length of the plate using a Dynapulse™ impulse hammer to measure peak impact force. Statistical outliers are presented as individual points. 52
Figure 24. Impact plate detection threshold test experimental setup. Burette stand and clamp positioned above the plate centre to release a fine gravel particle at a measurable height. 53
Figure 25. Impact plate detection threshold analysis. Impacts were exerted upon the plate centre by dropping a gravel particle (Particle-A) from measured heights..... 54
Figure 26. Impact plate detection threshold analysis under cold operating temperatures. Impacts were exerted upon the plate centre by dropping a gravel particle (Particle-B) from measured heights. 55
Figure 27. Carruthers Creek watershed basin and study sub-basin area..... 58
Figure 28. Carruthers Creek specific stream power analysis. 59
Figure 29. Pebble count particle shape categorized by half-phi class. 65
Figure 30. Wobblestone insert parts and assembly stages. (A) Raw part cast from HDPE injection mold. (B) Weighted inner ball bottom halves containing RFID tags. (C) Assembled Wobblestone inserts. 67
Figure 31. Particle tracking synthetic tracer stones, stone molds, and original stones. 68
Figure 32. Linear interpolation method applied to obtain total bedload sediment yield from BLIP model outputs. From (Soar & Downs, 2017). 71
Figure 33. Carruthers Creek bedload monitoring station. (A) Tabletop frame, solar panels, and electronic equipment enclosure located within river-left overbank zone. (B) View facing upstream showing water level sensor (top-right), in-stream antenna (centre) and impact plates (bottom). (C) View facing downstream showing sediment trap. (D) Seeded tracer stone (photo credit: Bruce MacVicar). 72
Figure 34. Electronics enclosure contents including MotoMaster deep cycle battery, Steca solar charge controller, OregonRFID SAR, and Raspberry Pi. Wire and cables enter enclosure via water-tight feedthrough seals. 73
Figure 35. Study reach longitudinal profile displaying locations of the volumetric bedload samples (SED), pebble counts (PC), monitoring station and upstream tracer stone seeding limit. 74
Figure 36. Carruthers Creek monitoring station riffle crest cross-section and bankfull stage. 74
Figure 37. Grain size distributions of pebble count and volumetric bedload samples. 74
Figure 38. Profile view of headcut advancement over study period..... 76
Figure 39. Visual comparison of headcut over study duration. (A) Headcut location on May 23, 2019. (B) Significant advancement first observed on March 17, 2020. (C) View of gravel particles embedded within till on June 1, 2020 (Photo credit: Bruce MacVicar). 77
Figure 40. Conceptual diagram of cumulative flow metrics. From (Papangelakis, 2019). 78
Figure 41. In-flood RFID tracer stone movement during January 2020 flow event. Red shading signifies the duration for which tracer stone 8513 remained within the antenna detection zone. 82
Figure 42. Tracer stone fractional mobility. 84
Figure 43. Tracer stone scaled travel lengths compared to literature relationships. 85

Figure 44. Comparison of surveyed weighted median travel lengths against estimates derived from cumulative excess discharge analysis. Estimates correspond to varying dimensionless critical shear stress values assumed for the median grain size. 86
Figure 45. Tracer stone mean annual velocity. Comparing Carruthers Creek results (left) to Papangelakis (2019) (right) including results from Ganatsekaigon Creek, Wilket Creek, and Morningside Creek. From (Papangelakis, 2019). 88
Figure 46. Study reach tracer stone layout. Plan-view of seeded locations on August 15, 2019 (left) and locations documented during the final tracking survey on June 12, 2020 (right). 89
Figure 47. Aggregate bedload impacts summed over 5-minute time intervals. GRA gauge record superimposed onto station water level timeseries. 91
Figure 48. Study reach under-ice water profile over an uncovered impact plate on January 24, 2020 (viewing upstream). Ice previously covering the impact plate was removed to visualize flow conditions. 92
Figure 49. December 2019 flow event. Aggregate bedload impacts summed over 5-minute time intervals. 93
Figure 50. December 2019 flow event data quality analysis. (A) Frequency of time between successive raw data point observations. (B) Magnitude frequency of aggregated bedload impacts. (C) Normal probability plot of aggregated bedload impacts. 94
Figure 51. December 2019 flow event instantaneous stage versus predicted unit bedload rates (plate 1 and 2 average) derived from Soar & Downs (2017) BLIP model. Stage is specified for points of interest including bankfull discharge, critical threshold estimates, and the automatically tracked movement of tracer stone 8513. 96
Figure 52. Bunte sediment trap sealed by ice and vegetation on January 24, 2020. (A) Ice and vegetation removed from trap opening. (B) Sand and gravel substrate found resting on top of sediment trap netting. 99
Figure 53. Raven model outflow hydrograph for 5-year return period 3-hour Chicago distribution design storm. 101

List of Tables

Table 1. Summary of Bedload Monitoring Method Characteristics 39
Table 2. Bedload Monitoring Station Power Summary 41
Table 3. Summary of Bedload Monitoring Method Characteristics 64
Table 4. Carruthers Creek In-stream Antenna Characteristics 69
Table 5. Carruthers Creek Study Reach General Characteristics 75
Table 6. Summary of Tracer Stone Critical Thresholds ($\boldsymbol{\tau cD50}* = 0.047$ [-]) 80
Table 7. Summary of Tracer Stone Critical Thresholds ($\boldsymbol{\tau cD50}* = 0.07$ [-]) 81
Table 8. Summary of Tracer Stone Critical Thresholds ($\boldsymbol{\tau cD50}* = 0.082$ [-]) 81
Table 9. Weighted Median Travel Length Estimates for Study Tracking Period 81
Table 10. Summary of K-Means Analysis Total Within-Cluster SSE Results 90
Table 11. Cumulative Excess Discharge Results for Modelled Outflow Hydrographs 102

1 Introduction

The health of a stream network is the product of natural processes and human activities within the watershed. The establishment of modern agriculture is known to have adversely affected stream health as a result of deforestation, clearing of riparian vegetation, straightening of surface channels, and implementation of subsurface tile drainage. Such modifications disrupt the natural water and nutrient cycles and can change the quantity, quality, and timing of water routed to stream networks (Blann et al., 2009). These stressors typically manifest into responses observed within stream networks of agricultural lands including degraded channel morphology, degraded habitat and reduced biodiversity (Blann et al., 2009; Weijters et al., 2009). While restoration efforts have been shown to mitigate adverse responses in localized areas, the immense scale of watershed disturbances can make local restoration efforts futile with respect to improving the overall stream network (Wohl et al., 2015). Agriculture is unquestionably a fundamental component in sustaining our population; however, agricultural practices lead to a consistent pattern of degraded stream network health.

Water regulators and governing authorities generally operate under the assumption that we need to maintain the current state of watershed health in areas that have not been subjected to urban development; however, the current state of stream networks in agriculturally impacted watersheds is not necessarily healthy from an ecological or morphological perspective. It is a misconception to equate agricultural lands as natural areas due to the disturbances that agricultural development imposes upon natural hydrology and ecosystem integrity. This study aims to investigate the question: can an urban development undertaking be leveraged as a remedial opportunity that improves upon the adverse responses observed in agriculturally impacted stream networks? The

answer to this question is beyond the scope of this thesis, but here systems are put in place to begin exploring this proposition.

Urbanization is commonly associated with well-known adverse impacts that are consistently observed in stream systems that drain urban lands. This relationship is referred to as the 'urban stream syndrome' and is characterized by a variety of symptoms including reduced water quality, reduced biotic richness, and altered channel stability and morphology (Meyer et al., 2005; Walsh et al., 2005; Wenger et al., 2009). Urban areas typically integrate stormwater management practices that treat stormwater as waste rather than a resource. These practices are generally one-dimensional as they reserve very little consideration for objectives related to ecological enhancement (Ontario Ministry of the Environment & Climate Change, 2017). Stormwater management infrastructure attenuates flooding and erosive flows but significantly alters the flow and sediment regimes of the receiving stream network posing as a discontinuity in the system (Bledsoe & Watson, 2001; A. Chin, 2006; Walsh et al., 2012). Low impact development (LID) is an alternative stormwater management practice that reduces overall surface runoff volumes routed to adjacent streams and has potential in remedying urban stream symptoms (Askarizadeh et al., 2015). LID encompasses a wide variety of different features such as permeable pavement, green roofs, infiltration galleries, etc. that manage precipitation where it falls. There is significant potential in utilizing LID as an alternative stormwater management practice as it is a naturalized approach that targets a wider variety of technical design objectives including ecological enhancement (Walsh et al., 2012). However, LID is relatively untested on a large scale within the context of Canada and has been historically limited in application to minor localized features that supplement a traditional end-of-pipe treatment design (Ontario Ministry of the Environment & Climate Change, 2017).

Using LID as a primary stormwater management technique that mimics natural hydrology subsequently prompting improvements to stream network health may sound promising; however, a significant data gap exists when it comes to understanding the effectiveness and relevance of any sort of stream restoration effort. We often have an inability to define specific restoration goals and targets largely due to two issues. One, to inform meaningful restoration we require an adequately undisturbed reference reach that demonstrates natural conditions with which restoration targets can be modelled after; however, such undisturbed reaches are seldom found in watersheds influenced by human activity (Downs et al., 2011). Two, in the absence of a reference reach we can approximate reference conditions through various analytical methods; however, an analytical approach requires the collection of baseline field data which is difficult to obtain and rarely collected in general (Downs et al., 2011). Collecting baseline bedload transport data is particularly challenging as existing methods are typically laborious, expensive, and sometimes dangerous (Gray, Laronne, Osterkamp, et al., 2010). These limitations ultimately translate into restoration targets that are poorly understood, ambiguously defined, and difficult to quantify performance with little way of knowing if they are even significant in restoring the stream network.

The goal of this study is to develop a robust field method capable of collecting comprehensive baseline data that can be used to inform stream restoration targets and land use decision making. This goal will be accomplished by completing a field- and model-based numerical approach as defined through the following objectives: (1) develop a bedload transport monitoring system capable of automatically measuring bedload transport during competent flow events; (2) characterize the baseline flow and sediment regime of a study reach situated within an agricultural watershed, and; (3) make predictions regarding how the study reach flow and sediment

characteristics may change in response to altered watershed land use, specifically urban development with LID stormwater management.

The realization of these objectives is feasible for this thesis due to recent well-established research completed by fellow members of the University of Waterloo River Hydraulics Research Group. Additional resources include technical expertise provided by Dirk Friesen of the University of Waterloo Structural Dynamics Identification and Controls (SDIC) lab, collaboration with Dr. Peter Downs (University of Plymouth) and Dr. Philip Soar (University of Portsmouth), and extensive industry support provided by Dorsay Development Corporation and GeoProcess Research Associates Inc. Objective (1) builds upon the design of an in-stream automated station developed by Muirhead (2018). The new station incorporates seismic impact plates (Downs et al., 2016) and Radio Frequency Identification (RFID) tracer stone technology with an in-stream antenna to automatically collect bedload transport data in real time during a competent flow event. In support of Objective (2), the station was deployed at Carruthers Creek, situated within a rural watershed in Pickering, Ontario. In addition to the station data record, inter-flood particle tracking surveys and geomorphic survey data were collected along the study reach to characterize baseline conditions. Study results are contrasted against field data records observed at three neighbouring watershed research sites in Southern Ontario characterized by a variety of land use and stormwater management practices (Cain, 2019; Papangelakis, 2019; Raso, 2017). In support of Objective (3), a semi-distributed hydrologic Raven model (Craig et al., 2020) of the Carruthers Creek sub-watershed was used to simulate streamflow under alternative land use scenarios. The Raven model was previously built and calibrated for the University of Waterloo Principles of Hydrologic Modelling short course (CIVE 781) during the Spring 2019 term. Hydrologic model outputs were used in combination with a cumulative excess discharge equation developed by Papangelakis et

al. (2020) to demonstrate a workflow process that predicts and compares bedload transport dynamics under alternative land use conditions.

The content of this thesis begins with a literature review of fundamental concepts and recent advancements related to bedload transport monitoring in Chapter 2. Chapter 3 presents the design of the newly developed bedload monitoring station. Chapter 4 introduces the study site at Carruthers Creek and outlines the methods and results of the baseline field study. Chapter 4.4 presents the results of the alternative land use hydrologic modelling exercise. Final conclusions and recommendations are outlined in Chapter 5.

2 Literature Review

The following chapter is organized into three sections. The first section describes fundamental concepts pertaining to how watercourses respond to evolving driving variables. The second section places this general framework of channel evolution into the historical context of Southern Ontario, specifically regarding agricultural areas and stream health. The third section describes sediment transport monitoring techniques and recent advancements.

2.1 Channel Morphology and Evolution

Scientists and researchers commonly study stream morphology and geomorphic processes to characterize riverine systems. Stream morphology refers to the shape and size of a channel, and the unique configuration of bedforms that are present while geomorphic processes refer to the conveyance of water and sediment which influence stream morphology (E. W. Lane, 1955; Rosgen, 1996). Stream morphology, synonymous with channel form, shares a coupled relationship with geomorphic processes characterized by significant feedback as demonstrated in Figure 1 (Ashworth & Ferguson, 1986; S. N. Lane & Richards, 1997).

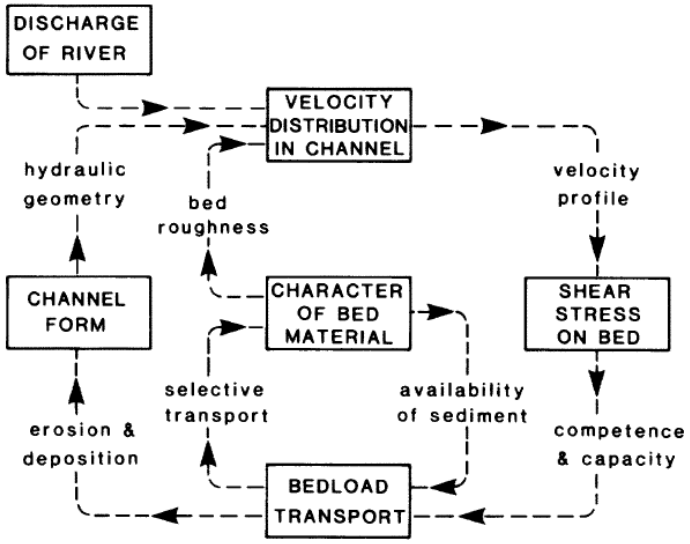

Figure 1. Dynamic relationship between channel form and process in gravel bed rivers. From (Ashworth & Ferguson, 1986).

Figure 1 illustrates how channel processes influence cycles of erosion and sedimentation and consequentially channel form. Conversely, channel form contributes towards the distribution of in-channel velocity and bed shear, thus impacting channel process. Channel form is also indicative of watershed hydrology and geology which govern the quantity of water delivered and the properties of sediment supplied to the channel network respectively (Emmett & Wolman, 2001; Mackin, 1948; M Gordon Wolman, 1967). In summary, a watercourse can be described as a dynamic system with a natural tendency to self-maintain and adjust towards a state of quasi-equilibrium whereby erosive forces emanating from the flow of water and resistive frictional forces of channel materials are balanced (E. W. Lane, 1955; Mackin, 1948). E. W. Lane (1955) presented the coupled nature of channel form and process as a conceptual model, depicted in Figure 2, which relates the proportionality of sediment discharge and grain size with stream flow and slope.

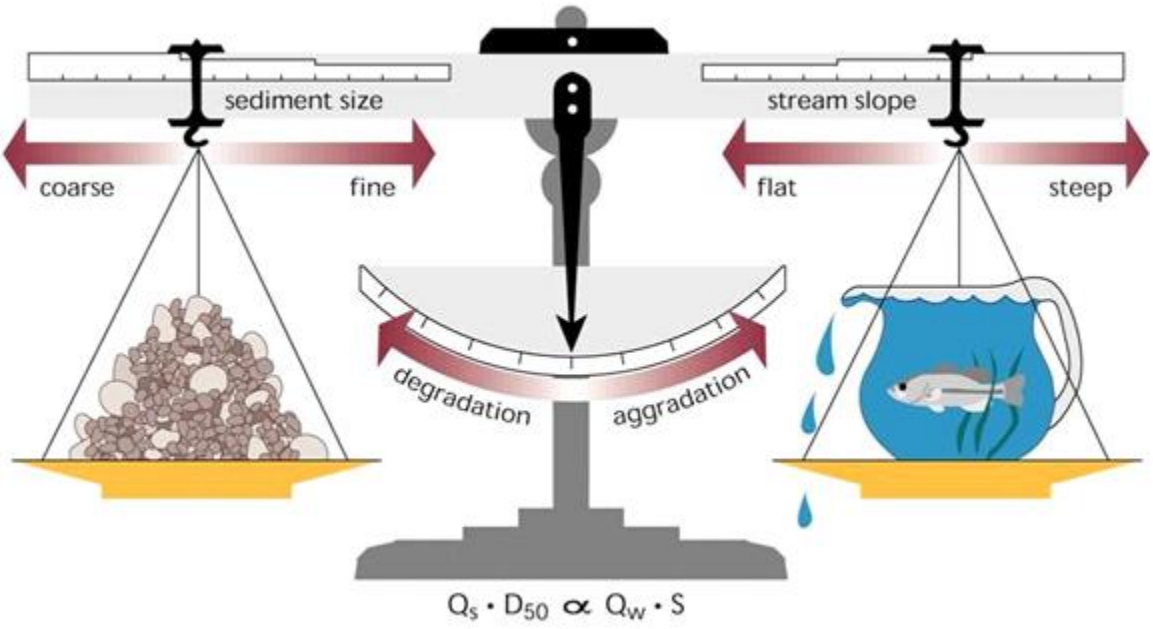

Figure 2. Classic Lane balance scale diagram**.** From (Rosgen, 1996).

The evolution of a channel is a complex process of cause and effect, which can be described in many ways depending on the spatial extents of a system and the temporal scale that is considered

(S. N. Lane & Richards, 1997; Schumm & Lichty, 1965). S. N. Lane & Richards (1997) described channel evolution as a trajectory such that the future state of a channel is a temporal function of past and present conditions, and a spatial function of upstream and downstream environments. The Lane scale helps anticipate how a channel will evolve in response to changes in watershed-scale parameters. For example, an increase in stream flow will cause the system response (represented by the bottom scale) to shift to a state of degradation, thus prompting the watercourse to restore system balance by adjusting other parameters. The reason behind this activity can be explained by the concepts of base-level change, and supply- and transport- limited systems. Base-level refers to the level of a body of water such as a lake or ocean which controls the level of watercourses that discharge into the waterbody (E. W. Lane, 1955). A rise or decline in base-level will decrease or increase the energy grade of a watercourse causing aggradation or degradation respectively (E. W. Lane, 1955; Mackin, 1948; Schumm, 1984). When the energy and sediment transport capacity of a channel exceeds the quantity of sediment physically supplied and available for transport, it is said to be supply-limited. This excessive energy results in downcutting of the stream bed which increases the slope of tributary streams and subsequently increases sediment supplied to the main channel. In contrast, a transport-limited system does not have enough energy to transport the sediment supplied which prompts an opposite system response of aggradation. When transport capacity and sediment supply are balanced, the system is also in a quasi-equilibrium state of balance.

Schumm (1984) outlined the concept of geomorphic thresholds which helps to explain how imbalances in parameters of the Lane scale can be instigated. Geomorphic thresholds can be either extrinsic or intrinsic; extrinsic threshold exceedance occurs when progressive changes in some sort of external variable, such as land use or climate, eventually cause a sudden change within the

stream system (Schumm, 1984). Conversely, intrinsic threshold exceedance occurs when progressive change of an internal variable, such as slope weathering, is the cause for abrupt system change (Schumm, 1984). Erosional development of concentrated drainage pathways, referred to as channel incision, occurs when geomorphic thresholds are exceeded (Graf, 1979; Schumm, 1984). Figure 3 illustrates the progressive evolution of a pre-modified, sinuous channel that is straightened, which results in channel incision.

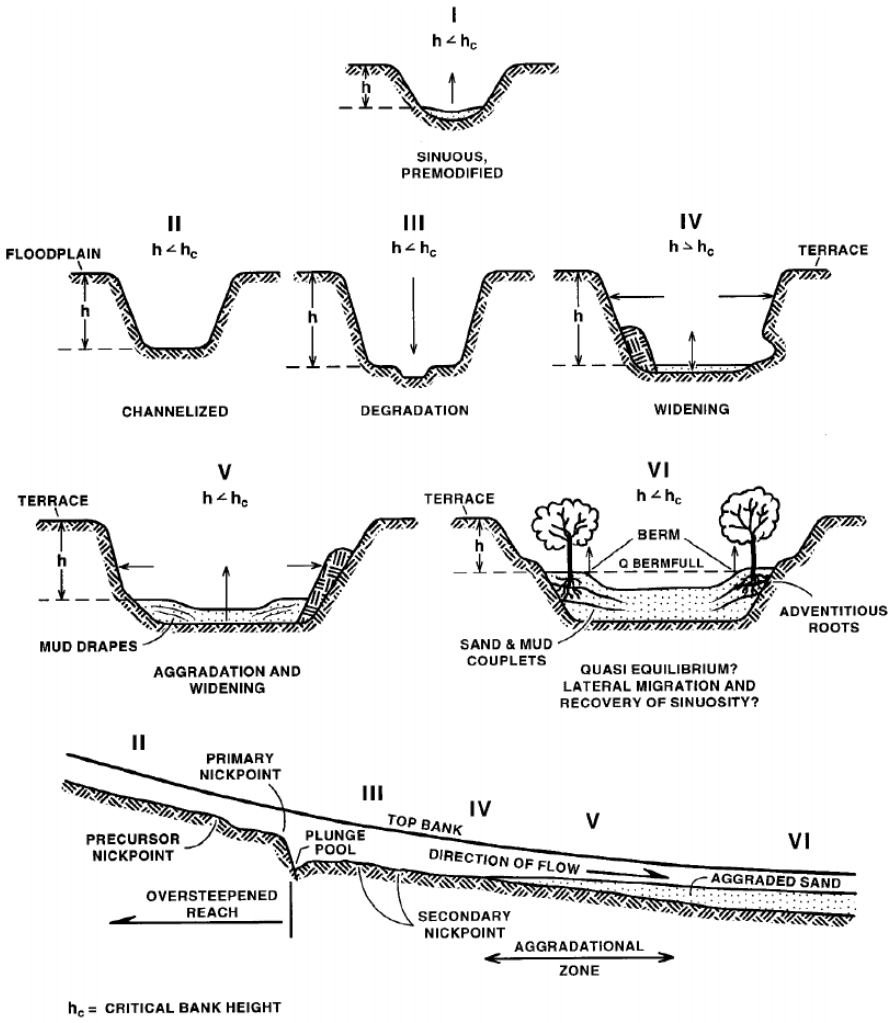

Figure 3. Incised channel evolution model developed by (Schumm, 1984) and (Simon, 1989). From (Shields Jr., 1998).

Significant changes to valley floor vegetation and peak discharge can result in substantial incision (Schumm, 1984). Anthropogenic activities such as agriculture and urban development substantially alter the drainage properties and vegetation cover of a watershed and significantly contribute to this process. A detailed review of adverse impacts to stream morphology originating from agricultural development is presented in Chapter 2.2.

2.2 Influence of Agricultural Development on Stream Morphology in Southern Ontario

The following chapter describes how anthropogenic activities leading up to and including agricultural development have significantly modified the natural morphology of stream systems in Southern Ontario. A brief history of the Quaternary period is described to provide context regarding the true natural conditions bestowed upon the Southern Ontario area following glacial activity. The causes and effects of agricultural development on stream morphology are explored in detail.

2.2.1 Quaternary Period History

Prior to the development of modern agriculture in Southern Ontario nearly 240 years ago, much of the landscape remained relatively undisturbed for over 10,000 years (Elliott, 1998; Lacroix, 2019). To fully appreciate how humans have changed the Southern Ontario landscape, one must consider what the area originally looked like in its *most recent* historical natural state and how it came to be during the events of the Quaternary Period (Figure 4).

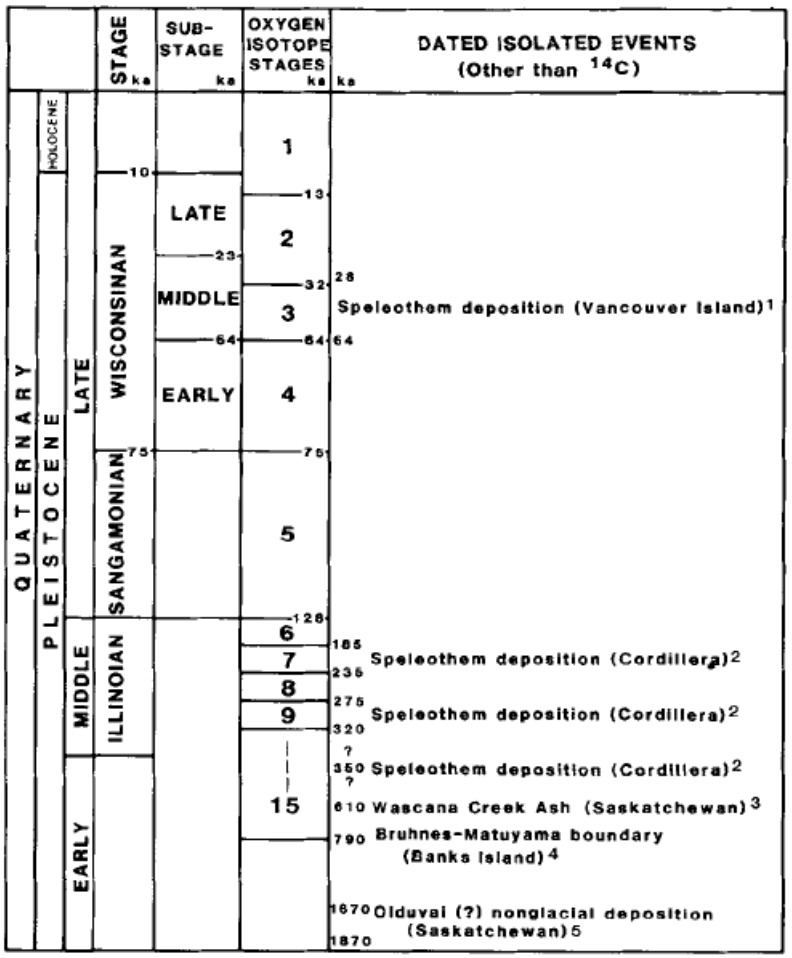

[1]Gascoyne *et al.*, 1980; [2]Harmon *et al.*, 1977; [3]Westgate *et al.*, 1977; [4]Vincent *et al.*, 1983; [5]Foster and Stalker, 1976.

Figure 4. Canadian quaternary period timeline. From (Fulton, 1986).

During the Quaternary period beginning approximately 1.87 million years ago, all of Southern Ontario and most of Canada was repeatedly glaciated (Fulton, 1986; Trenhaile, 2007). The cycles of glacier advancement and retreat exerted massive forces upon the earth scraping up and carving out the ground, depositing sediments, burying and evacuating previous glacial deposits, and repeating these processes over again (Fulton, 1986). Glacial activity during the quaternary period has left behind a diverse geological landscape around Southern Ontario characterized by features such as the Great Lakes, extensive river drainage networks, moraines, and underlain glacial till units. Most daylighted glacial materials found today were originally deposited during the last

glaciation of the late Wisconsin stage (Fulton, 1986). During this stage, most of Canada and some of the Northern United States were covered by large glacial formations including the Cordilleran and Laurentide ice sheets as illustrated in Figure 5.

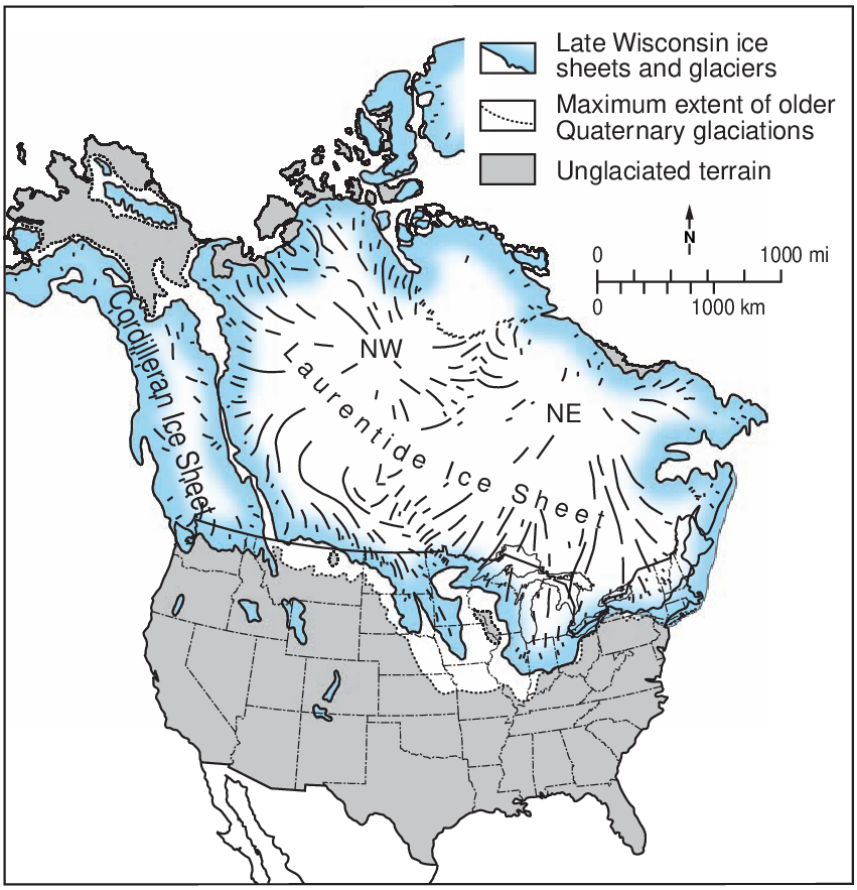

Figure 5. Quaternary Period Glacial Extents. From (Killey, 2007)**.**

The conclusion of the last glaciation marked the beginning of the current Holocene epoch and set our current surficial landscape conditions in place. The geologic and climatic conditions of the Great Lakes region in Southern Ontario support mixed coniferous and deciduous forest growth which dominated the area prior to European colonization. Indigenous communities made minor alterations to the landscape by clearing areas for farming and creating favourable hunting conditions (Elliott, 1998; Lambert & Pross, 1967; Riley & Mohr, 1994). However, the scale of land cultivation by Indigenous communities is somewhat unclear as historians have widely ignored

or dismissed Indigenous agrarian activities (Classens, 2017; Dawson, 2003). Beginning in the late 1400's, Indigenous populations were devastated by diseases carried to North America by European explorers (Royal Commission on Aboriginal Peoples, 1996). A lack of immunity to these diseases in addition to armed hostile encounters and starvation resulted in a substantial decline to Indigenous populations (Royal Commission on Aboriginal Peoples, 1996). During this period, previously cultivated areas were left to re-wild for hundreds of years prior to European colonization.

European settlers introduced a new period of anthropogenic change and systematic deforestation that severely altered drainage characteristics of the landscape during the 19th century (Elliott, 1998; Lambert & Pross, 1967). Large scale logging activities began in 1776 to provide timber resources to the British and French navies (Elliott, 1998; Ontario Royal Commission on Forestry, 1947). At the end of the American War of Independence in 1783, American colonists who supported the Crown (referred to as the United Empire Loyalists) were offered land grants in Ontario and other parts of Canada with the condition that 5 acres of land and a road right-of-way were to be cleared within 3 years in order for the Crown to honour the land title (Elliott, 1998; Lacroix, 2019; Lambert & Pross, 1967). Establishing settlements and agriculture was prioritized over reserving timber resource plots in Southern Ontario thus land was primarily designated as land grants (Elliott, 1998). Settlers quickly transformed forested lands into divided agricultural plots, sometimes by means of setting fire to clear large areas (Elliott, 1998). As agriculture developed in Southern Ontario, so too did anthropogenic modifications to the landscape with the intention of creating ideal drainage conditions to improve crop yields and extend the overall growing season to begin earlier in the spring with dry workable field conditions (Blann et al., 2009). The conversion of forests to agricultural lands introduces many adverse changes to hydrology and stream morphology

primarily through disruptions to the natural water and nutrient cycle (Blann et al., 2009). This process can be simplified into two main stages of historical transformation: first, the initial clearing of forested lands and riparian vegetation; and second, physical modifications made to the natural landscape and stream network to maintain drainage conditions that are favourable for productive agriculture. These disruptive characteristics and artificial features are explored in detail in Chapters 2.2.2 and 2.2.3.

2.2.2 Deforestation and Riparian Vegetation Removal

Upland forests and riparian vegetation play an integral environmental role offering many hydrologic and ecologic benefits that affect stream health and stability. Aquatic species have varying tolerances to changes in the natural flow, sediment, thermal, and water chemistry regimes, which are all related to riparian vegetation and upland forest cover (Eaton & Scheller, 1996; Statzner & Highler, 1986; Todd & Kaltenecker, 2012; Ward & Stanford, 1982). The riparian zone represents a significant transitional area which bridges aquatic and upland terrestrial environments supporting a diverse ecosystem as illustrated in Figure 6 (Gregory et al., 1991; Naiman & Décamps, 1997).

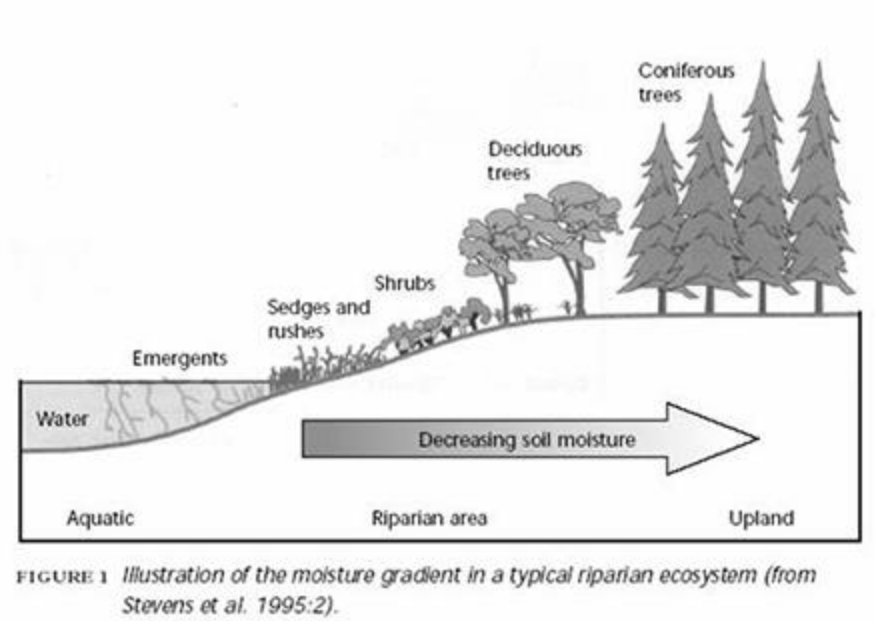

FIGURE 1 *Illustration of the moisture gradient in a typical riparian ecosystem (from Stevens et al. 1995:2).*

Figure 6. Cross-section schematic demonstrating transitions between aquatic, riparian and upland ecosystems. From (Stevens et al., 1995).

Riparian vegetation directly serves as habitat for insects and other terrestrial species, but also indirectly supports aquatic habitat. Riparian zones supply stream networks with organic inputs that support water and aquatic habitat quality such as large woody debris and leaf litter (Sweeney et al., 2004). Many studies have demonstrated that riparian vegetation helps filter nonpoint source nutrients and pollutants, reducing concentrations that enter the aquatic zone (Jordan et al., 1993; Osborne & Kovacic, 1993; Peterjohn & Correll, 1984; Sweeney et al., 2004). Vegetation canopy cover within the riparian zone helps regulate the aquatic thermal regime and inhibits in-stream vegetation growth by providing shade and limiting the amount of photosynthetically active solar radiation (Sweeney et al., 2004).

Upland and riparian vegetation help manage rainfall events through a number of mechanisms which increase abstraction and subsequently reduce runoff volumes, and fluvial erosive energy. Studies have shown that forest canopy cover can abstract up to 48% of annual rainfall (D. A. Chin, 2013; Leyton et al., 1967). A large portion of rainfall returns to the atmosphere through the process

of evapotranspiration. The roots of vegetation increase void spaces in the soil profile allowing for added moisture storage capacity (Nir, 1983). Rainfall that is not captured by canopy interception, soil storage, or evapotranspiration is subsequently routed as surface runoff. Vegetation and decaying organic matter create treacherous pathways meaning increased surface roughness, which reduces runoff velocities and erosive forces. These treacherous pathways inhibit flow paths from becoming concentrated forming rills and gullies (Nir, 1983; Schumm, 1984). Root mass also helps stabilize land preventing loss to erosion.

Deforestation and the clearing of riparian vegetation during the historic development of agricultural lands greatly diminished these hydrologic and ecologic benefits. Sweeney et al. (2004) completed a robust field study to scientifically quantify the effects of riparian deforestation on stream ecosystem quality, quantity, and pollutant processing ability. Sweeney et al. (2004) studied 16 streams in Eastern North America containing paired forested and deforested reaches absent of adjacent anthropogenic disturbances such as agriculture or urbanization. The study reaches were evaluated based on information obtained through geomorphic surveys, macroinvertebrate and fish surveys, and a variety of sampled water quality parameters. Sweeney et al. (2004) found that riparian deforestation generally results in stream narrowing, or entrenchment, which minimizes streambed area per unit channel length and consequentially reduces aquatic habitat and pollutant attenuation. The data collected by Sweeney et al. (2004) demonstrates that forested reaches are characterized by equal or greater ecosystem services, health, and stability than comparable deforested reaches. While Sweeney et al. (2004) investigated stream impacts by isolating a single study variable (the presence or absence of riparian forest), Peterjohn & Correll (1984) contrastingly described an entire agricultural system through developing a nutrient budget of a small watershed in Maryland, U.S.A. Peterjohn & Correll (1984) quantified nutrient dynamics for

the agricultural watershed and observed that riparian forests perform an extremely significant ecological function with respect to nutrient sequestration.

2.2.3 Anthropogenic Modifications

The next significant transformation that occurred during the development of agriculture in Southern Ontario and most of North America was the construction of artificial surface and subsurface drainage features. Croplands were often outfitted with artificial drainage features to improve agricultural efficiency, offering many advantages to farm operators which have been shown to result in annual yield gains of 5–25% (Blann et al., 2009; Eidman, 1997). The implementation of artificial surface drainage began with efforts to straighten and enlarge existing stream networks to rapidly convey water away from agricultural lands (Blann et al., 2009). Floodplain areas were drained and leveed to contain flood waters while maximizing cultivatable table lands (Blann et al., 2009). Ditches were constructed to connect poorly drained agricultural plots to existing stream networks, thus improving drainage efficiency (Blann et al., 2009). Smaller ditch networks were dug across fields to help facilitate drainage but were often inadequate and made operating large equipment difficult, thus artificial subsurface drainage became more appealing (Madramootoo et al., 2007). Artificial subsurface drainage, commonly referred to as tile drainage, was initially developed to help drain particularly wet areas that would frequently accumulate ponded water (Blann et al., 2009). These systems initially consisted of shallow, haphazardly placed clay, concrete, or wood tiles (Blann et al., 2009; Madramootoo et al., 2007). Tile drains evolved over time into strategic pipe systems buried across entire fields in parallel rows typically 10 – 30 m apart at depths of 0.6 – 1.2 m, and directly discharged into ditches or streams (Blann et al., 2009). In the 1970's, perforated corrugated polyethylene tubes began replacing clay and concrete materials for added longevity (Blann et al., 2009; Madramootoo et al., 2007). These

strategic systems provide relatively consistent and uniform soil moisture conditions by lowering the groundwater table as illustrated in Figure 7 (Blann et al., 2009).

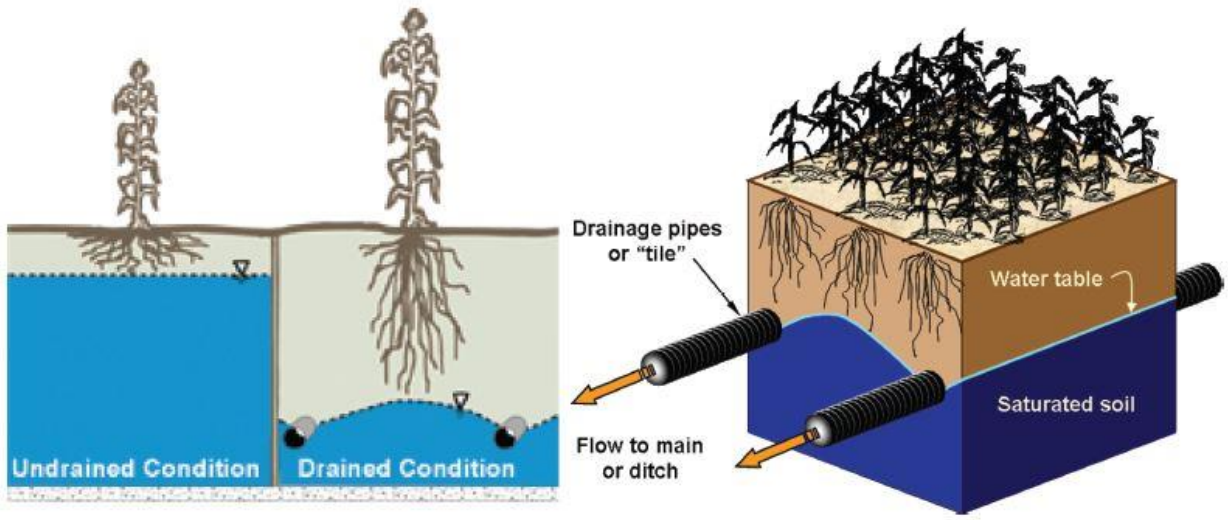

Figure 7. Visualization of Subsurface Tile Drainage. From (Blann et al., 2009).

Despite the many benefits to farm operators, these anthropogenic modifications were historically implemented unknowingly at the cost of watershed health. Artificial drainage features exacerbate the impacts of deforestation and riparian vegetation removal, and contribute to changes in the quantity, quality, and timing of water routed to stream networks as shown in Figure 8 (Blann et al., 2009).

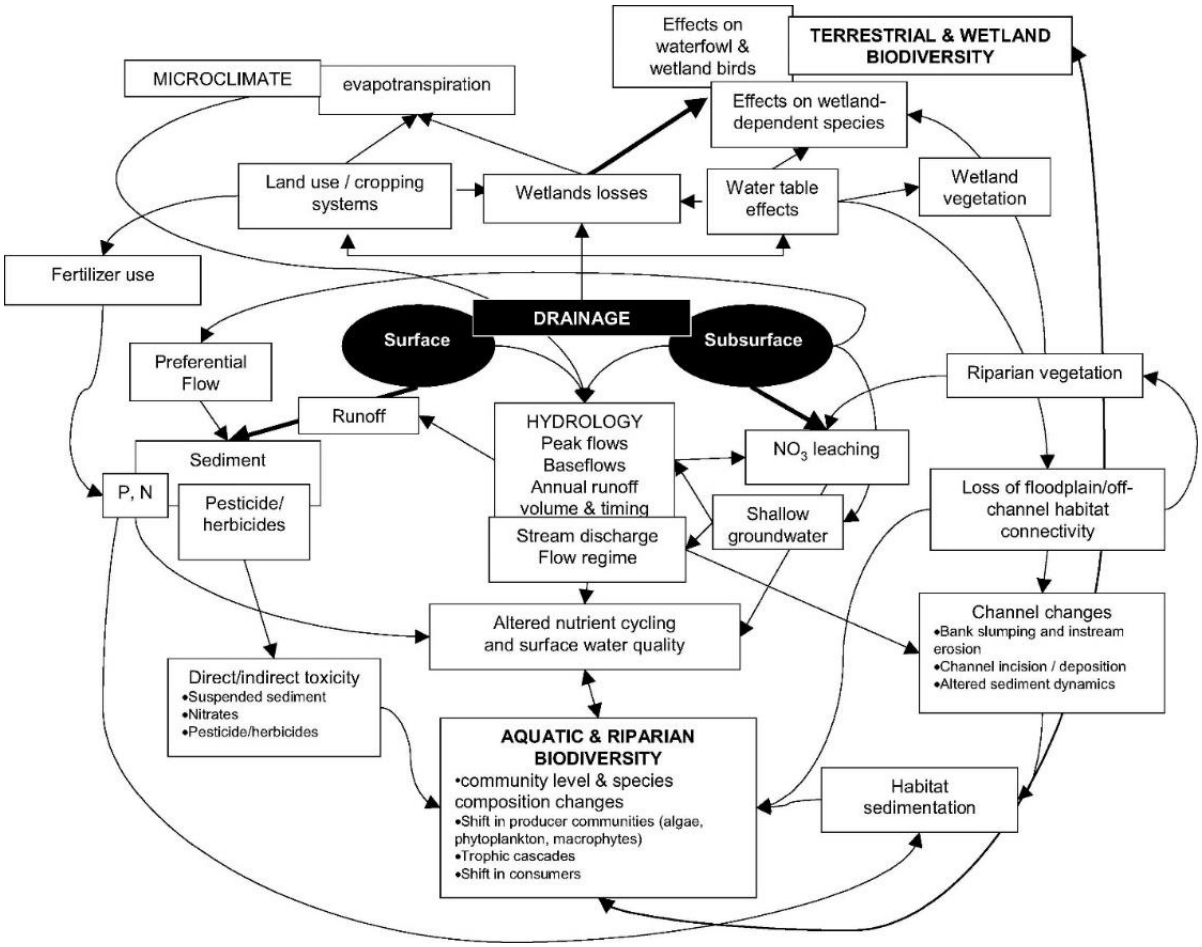

Figure 8. Conceptual model of agricultural drainage impacts on aquatic ecosystems. From (Blann et al., 2009)**.**

Figure 8 illustrates an interrelated cascade of adverse effects stemming from agricultural drainage, which can all be summarized as follows: the implementation of artificial drainage physically subtracts from available terrestrial, wetland and riparian environments and habitats, and the impacts of these drainage features lead to degraded aquatic biodiversity. Shifts in the natural water and nutrient cycles are the dominant processes which manifest into degraded aquatic health.

Surface and subsurface drainage features increase the quantity of water routed to the stream network and expand physical connectivity between streams and agricultural lands (Blann et al., 2009; Robinson & Rycroft, 1999). Increased connectivity reduces the time it takes for rainfall to access the stream network. These changes alter the natural flow regime which generally translate

into greater forces exerted upon the stream boundary with greater frequency. Shifts in the natural flow regime place the system in a transitional or unstable state that will correspondingly attempt to reestablish equilibrium by shifting the sediment regime by means of localized channel incision and downstream sedimentation (Schumm, 1984). Historic straightening of natural stream networks and leveeing of floodplains compounds this process with elevated erosional forces due to increased channel slope and restricted floodplain energy dissipation respectively (Schumm, 1984). Transitional erosion and sedimentation activity greatly disturb aquatic biota due to the destruction of habitat features and increased turbidity. Numerous scientific studies have demonstrated that sedimentation and turbidity results in adverse impacts to fish species including elevated physiological stress, reduced ability to feed, altered spawning patterns, and decreased survival rates among larvae, which all contribute to degraded diversity (Blann et al., 2009; Burkhead & Jelks, 2001; Johnston & Shute, 1997; Mion et al., 1998; Newcombe & Jensen, 1996; Owens et al., 2005; Pimentel et al., 1995; Sweka & Hartman, 2001; Wichert & Rapport, 1998).

2.2.4 Urbanization of Rural Areas

Rural areas situated near heavily populated regions in Southern Ontario, such as the Greater Toronto Area, are likely to endure another phase of transformation: urbanization. Urbanization is commonly associated with well-known adverse impacts that are consistently observed in stream systems that drain these urban lands. This relationship is referred to as the ‘urban stream syndrome’ and is characterized by symptoms that include reduced water quality, reduced biotic richness, and altered channel stability and morphology (Meyer et al., 2005; Walsh et al., 2005; Wenger et al., 2009). The urban stream syndrome is driven by a variety of complex mechanisms but is primarily attributed to the improved ability of urban stormwater to access the stream network (Meyer et al., 2005; Walsh et al., 2005; Wenger et al., 2009). Traditional stormwater management typically

involves end-of-pipe treatment such that stormwater runoff is collected and routed through a closed pipe network to a stormwater management pond where stormwater accumulates and is released to the stream network at a controlled rate.

The urbanization of agricultural lands presents a new challenge: anticipating channel response to a new stress and the likely influence of previous agricultural stressors. Plumb et. al (2017) studied the event-based bedload transport dynamics of the highly urbanized Mimico Creek located in Toronto, Ontario. Plumb et al. (2017) found that the frequency, time, and volume of flow events capable of performing geomorphic work increase with urbanization. Furthermore, urbanization shifts the geomorphic significance of events towards more frequent, lower magnitude discharge. Papangelakis (2019) studied the characteristics of streams situated within rural and urban watersheds in Southern Ontario including Ganatsekiagon Creek (rural), Wilket Creek (urban), and Morningside Creek (urban with SWM). Papangelakis (2019) found that SWM shifted the sediment regime of Morningside Creek from a supply-limited to transport-limited system. This shift was instigated by SWM flood attenuation causing excess shear stress reduction and subsequent channel narrowing and bed coarsening. Morningside Creek is one example of the many ways which anthropogenic modification can change the trajectory of a watercourse.

2.3 Bedload Monitoring Methods

Bedload sediment transport refers to the discharge of coarse sediments in a watercourse that primarily remain in contact with the bed during transportation. The physical transportation of individual bedload particles occurs through the mechanisms of rolling, sliding, and saltating as illustrated in Figure 9. Fluvial scientists are able to study channel stability by monitoring bedload sediment transport. Bedload transport data provides an indication of channel trajectory (degradation or aggradation) and the effects of hydrology over a full range of floods.

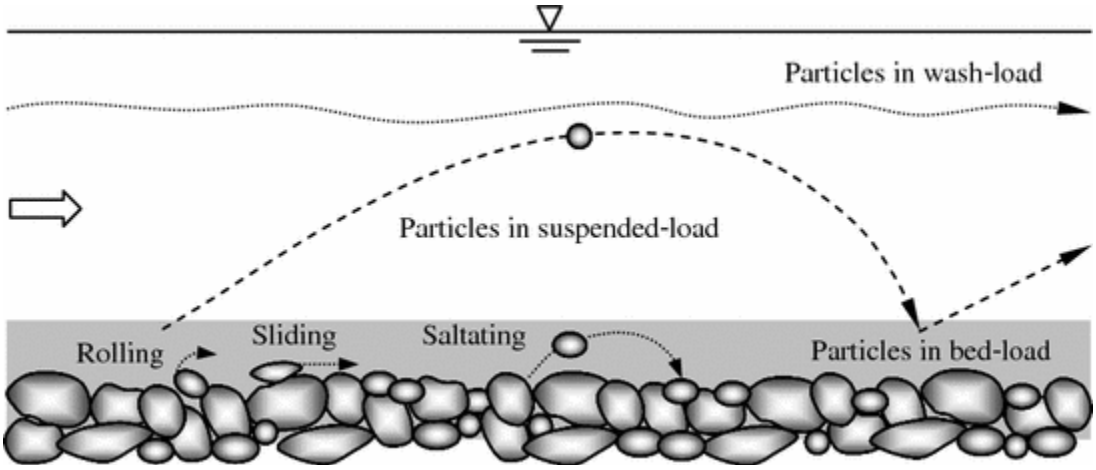

Figure 9. Sediment Transport Classifications and Mechanisms. From (Dey, 2014)**.**

There are a wide variety of well-studied field methods that have been developed by researchers to help quantify bedload transport dynamics. These field methods can all be classified as either direct or indirect monitoring techniques (Habersack et al., 2010, 2017). Direct monitoring methods specifically refer to physical in-situ sampling or collection of bedload particles using some sort of sampling device such as a bag, box, basket, pan, tray, trough, pit, etc., to ascertain specific bedload discharge and grain size distribution (Gray, Laronne, & Marr, 2010; Habersack et al., 2010, 2017). Indirect (surrogate) methods refer to non-invasive techniques that do not physically sample bedload particles, but rather actively or passively monitor and infer bedload dynamics using sensing technology (Habersack et al., 2017).

Bedload has traditionally been monitored through direct monitoring methods that use physical sampling devices (Gray, Laronne, Osterkamp, et al., 2010). In the mid-2000's, attention within the river science community grew regarding the uncertainties and temporal limitations of data gathered from these direct monitoring methods. This notion became a theme at the 2007 International Bedload Surrogate Monitoring Workshop, where Gray (2010) said that our general understanding of bedload transport processes was limited by the lack of "reliable, accurate, and temporally dense datasets" (Gray, Laronne, Osterkamp, et al., 2010). Many direct monitoring

methods are highly laborious, relatively expensive, dangerous, and accompanied by an abundance of difficulties (Gray, Laronne, Osterkamp, et al., 2010). Physical sample collection requires a device to be placed in direct contact with the streambed, which can obstruct flow and interfere with bedload transport processes. The physical dimensions of a device limit the maximum particle size that can be sampled and thus samples may not be representative of the entire range of mobilized bedload. Physical sampling devices often require an operator to be continually or periodically present during periods of bedload activity, which typically results in temporally sparse data. The reliability and accuracy of physical sampling results can be negatively affected by poor device deployment and operator bias. These affects are further amplified by the very nature of bedload transport, which is highly variable both spatially and temporally.

The difficulties associated with direct monitoring methods can result in considerable uncertainty in estimated bedload transport rates, as was demonstrated by Vericat (2006), which ultimately creates a research data gap and necessitates a more reliable alternative method (Gray, Laronne, Osterkamp, et al., 2010; Vericat et al., 2006). Gray (2010) explained how indirect bedload monitoring techniques can fill this data gap with the only caveat being that rigorous field calibration is necessary to provide proper context to monitoring results (Gray, Laronne, Osterkamp, et al., 2010). Thus, direct physical sampling devices still play an integral niche role in monitoring bedload dynamics as they are a useful complimentary method that can be used to calibrate indirect surrogate monitoring technology that operates using active- or passive- sensors (Gray, Laronne, & Marr, 2010). Recent advancements in the use of continuous indirect passive bedload monitoring methods have helped to address these dataset limitations stressed by Gray (2010).

2.3.1 Integrated Automatic Continuous Bedload Monitoring

Habersack (2017) theorized that no single monitoring technique can fully describe bedload transport dynamics. Individual techniques quantify specific parameters and provide some insight into the driving processes/mechanisms but are associated with unique limitations (Habersack et al., 2017). In order to gain a wider understanding of bedload dynamics, multiple complimentary monitoring methods can be employed into a single integrated monitoring station allowing for a more comprehensive interpretation. Habersack (2017) developed an integrated automatic continuous bedload monitoring system at the Drau River, Dellach, Austria which combines the use of a mobile bag sampler, bedload slot samplers, and plate geophones as shown in Figure 10 (Habersack et al., 2017).

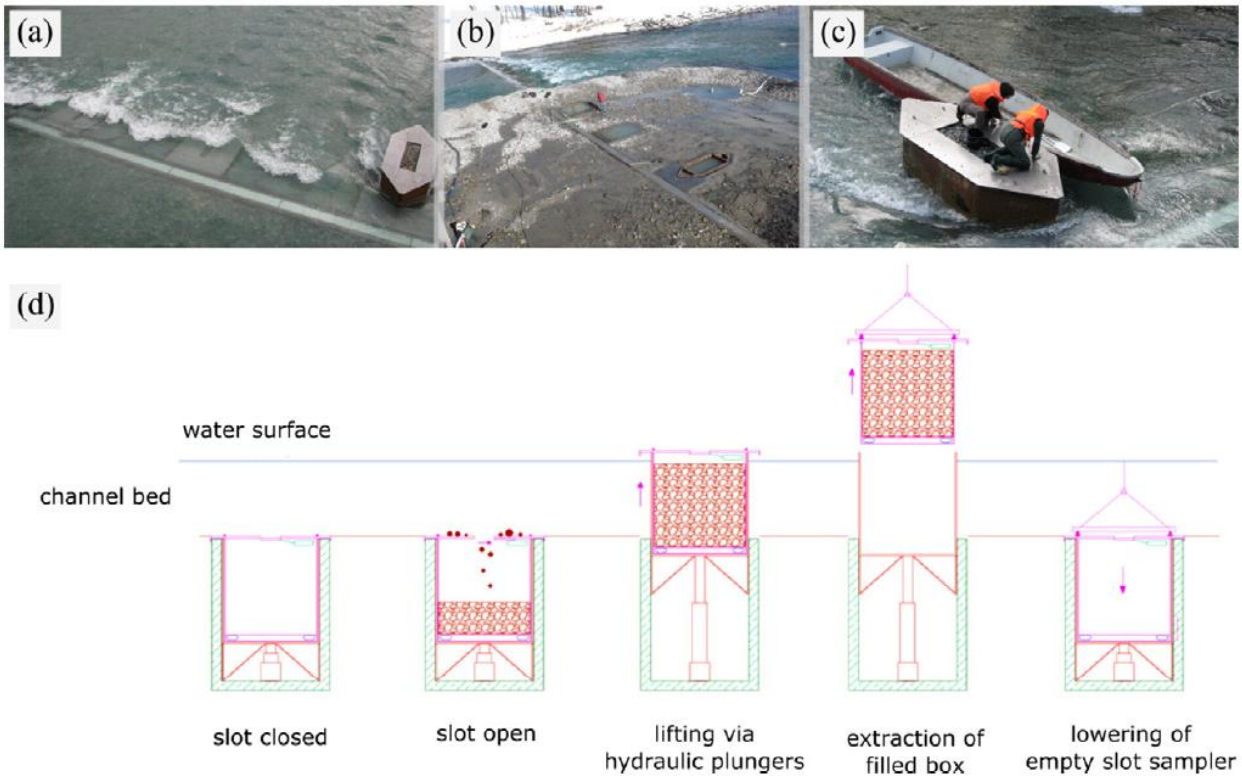

Figure 10. Habersack integrated bedload monitoring station, a) bedload slot sampler, b) station during maintenance, c) bedload sample retrieval, d) slot sampler operational schematic. From (Habersack et al., 2017).

The station integrates two (2) direct sampling methods with plate geophones that indirectly and automatically collect continuous high-resolution bedload transport data (Habersack et al., 2017). The direct sampling methods are used as reference techniques that help calibrate the indirect plate geophone monitoring method (Habersack et al., 2017). Habersack et al. (2017) found that the direct and indirect monitoring results were very well correlated and was able to confidently adopt an integrated bedload discharge calculation approach which contributed towards a more reliable estimation.

The integrated station is very comprehensive and sophisticated, however the level of complexity introduces several practical limitations as explored by Habersack et al. (2017). Notably, the excessive cost to install, maintain, and operate the hydraulic bedload slot sampling system is a substantial drawback. Furthermore, a reliable power source is required to operate the slot sampler, and the plate geophone to a lesser extent.

2.3.2 Passive Acoustic Bedload Monitoring

Extensive research into continuous indirect passive acoustic bedload monitoring methods has been completed at the Erlenbach stream in Switzerland by Rickenmann estimation (Rickenmann, 1997, 2017; Rickenmann et al., 2012, 2014, 2018; Rickenmann & Fritschi, 2010; Rickenmann & McArdell, 2007; Turowski & Rickenmann, 2009). In 1986 the Erlenbach streambed was first instrumented with an array of nine (9) piezoelectric bedload impact sensors (PBIS) at a monitoring cross-section as shown in Figure 11.

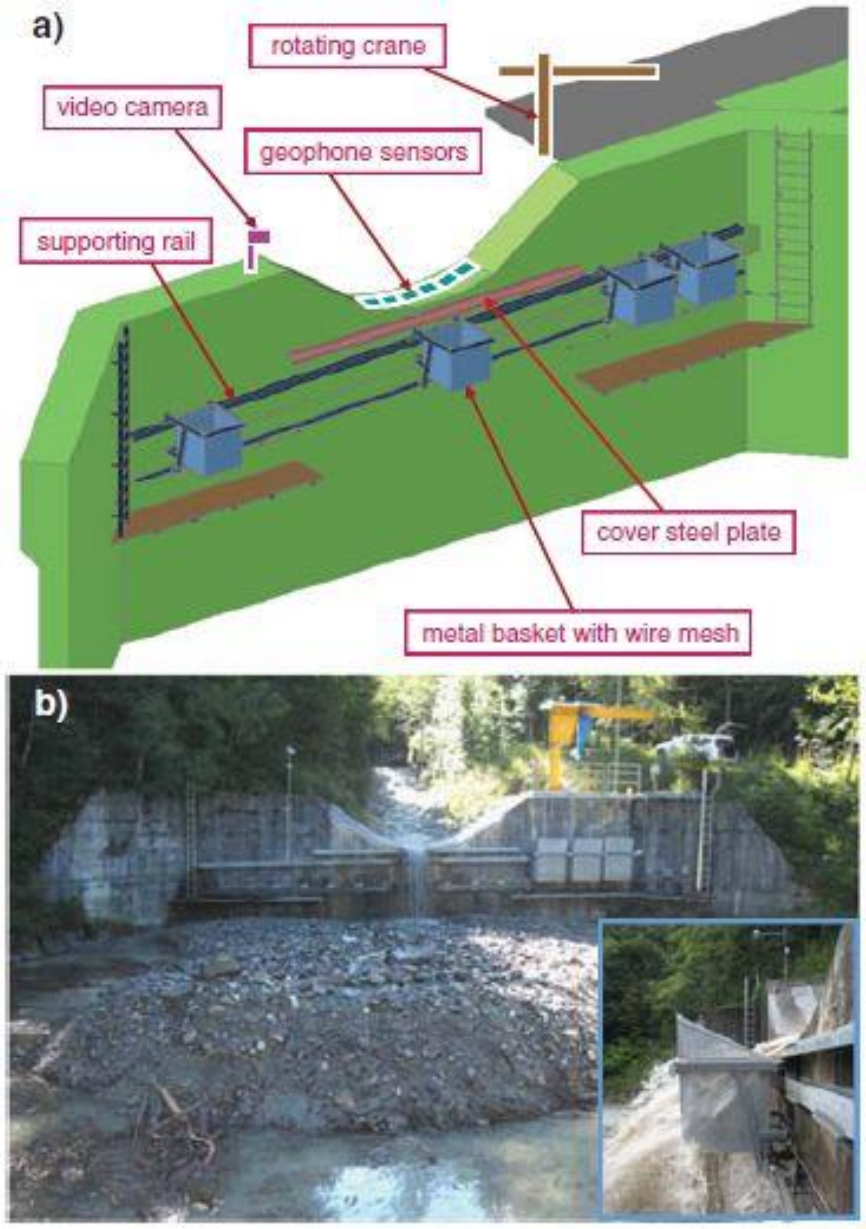

Figure 11. Continuous passive acoustic bedload monitoring station at the Erlenbach stream, Switzerland. From (Rickenmann et al., 2012).

Each PBIS consist of a piezoelectric crystal that is acoustically isolated and housed within a steel frame and surface plate (Rickenmann & McArdell, 2007). Whenever a bedload particle strikes the surface plate, the impact is transmitted to the piezometric crystal which deforms and subsequently generates an electric potential recorded as an impulse when exceeding a threshold voltage (Rickenmann & McArdell, 2007). In 1999 some of the piezoelectric crystals had reached the end

of their life cycle, so all crystals were removed and replaced by six (6) geophone sensors for the sake of consistency (Rickenmann et al., 2014). The retrofitted monitoring section, referred to as the Swiss impact plate geophone system, fundamentally operates similar to its predecessor. Each geophone sensor contains an inductive coil and a magnet which produces an electric current when a bedload particle strikes the surface plate causing the magnet to vibrate within the coil (Rickenmann et al., 2014). The electric current is proportional to the magnet's velocity and is recorded as an impulse when exceeding a specified threshold voltage (Rickenmann et al., 2014). A moving basket mechanism was installed at the station in 2009 to automatically collect and weigh bedload samples which are used to calibrate the geophone impulse dataset.

Rickenmann compared calibration results from the Erlenbach stream with four (4) similar Swiss impact plate geophone systems located at the Fischbach, Reutz, and Rofenache streams in Austria, and the Nahal Eshtemoa in Israel (Rickenmann et al., 2014). For each dataset, Rickenmann performed linear regression analyses upon a variety of geophone summary metrics and found a consistently strong linear relationship between impulse counts and bedload mass (Rickenmann et al., 2014). It was also noted that impulse amplitude contains some information regarding bedload particle size, however further flume and field experimentation are required before reliable conclusions can be made (Rickenmann et al., 2014).

Downs et al. (2016) completed a field study at the River Avon, Devon, UK which demonstrated that passive continuous bedload monitoring can provide valuable insight into bedload transport dynamics through the collection of high-resolution data over extended time periods using portable relatively inexpensive instrumentation. For this particular study, four (4) 'Benson-type' seismic impact plates were deployed along the river bed as shown in Figure 12.

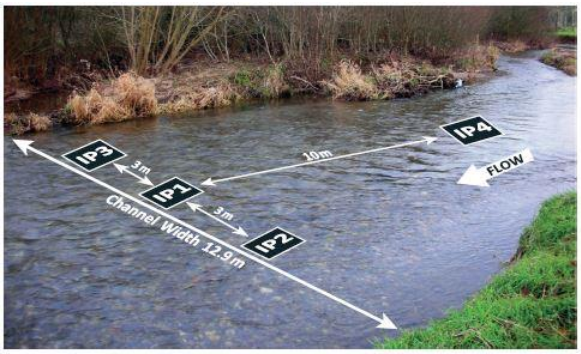

Figure 12. Continuous passive acoustic bedload monitoring at the River Avon, UK. From (Downs et al., 2016).

The 'Benson-type' impact plate is a rectangular stainless steel plate (150 x 130 x 6 mm) with a stainless steel barrel welded to the underside that houses an accelerometer. The accelerometer converts mechanical energy exerted by bedload particles striking the plate surface into an electric voltage which is subsequently recorded as an impact when the signal amplitude exceeds 20 mV (typically exerted by a particle weighing 0.5 g) (Downs et al., 2016). The 'Benson-type' impact plate has a relatively small surface area and a sampling frequency limit of 5 Hz (measurements recorded at least 0.2 s apart) which helps prevent over counting of bedload particles transported via rolling motions (Downs et al., 2016; Reid et al., 2007).

As concluded by Rickenmann (2014, 2017), there is a great deal of uncertainty associated with using impulse amplitude to infer bedload particle size and transport rates. In contrast, numerous research studies demonstrate that impulse counts collected by passive acoustic monitoring devices share a strong linear correlation with total bedload mass motions (Beylich & Laute, 2014; Downs et al., 2016; Rickenmann et al., 2012, 2014). For these reasons, Downs et al. (2016) elected to only analyze impulse counts but carried out innovative approaches to study bedload transport dynamics. During a particularly wet 12-month observation period, Downs et al. (2016) revealed the role of transport- and supply- limited behaviors during bedload mobilizing events by comparing instantaneous discharge and 5-minute aggregated impulse counts to explain count variability

(Downs et al., 2016). An incremental flow magnitude, impact frequency analysis also provided insight into the observed effective discharge based on impulse activity (Downs et al., 2016).

In addition to the techniques employed by Downs et al. (2016) to analyze impact plate counts, Soar & Downs (2017) developed a probabilistic model that works in conjunction with impact counts to produce a high-resolution time-series of supply-limited bedload transport rates. The model relies specifically on impulse counts (consistently shown to strongly correlate with total bedload mass) rather than impulse amplitude to derive these estimates (Soar & Downs, 2017). Consequentially, this model bridges the gap of linking data collected from indirect passive acoustic bedload monitoring devices and the prospect of inferring bedload transport rates while incorporating the inherently stochastic nature of bedload transport (Soar & Downs, 2017).

Although passive acoustic monitoring is a promising method capable of providing high resolution bedload transport data with relative ease, there are notable uncertainties associated with this technology. The transport mechanism of a bedload particle is highly dependent on particle shape and can present unique complications when making impact detections. For example, rounded particles will tend to roll during transportation which introduces the possibility of a single particle registering multiple impacts (Turowski & Rickenmann, 2009). A smaller impact plate surface, such as the design adopted by Downs et al. (2016), and a lower detection frequency can help mitigate against multiple detections registered by rolling particles (Downs et al., 2016; Reid et al., 2007). However, flat or irregularly shaped particles with a tendency to saltate may be underrepresented by a smaller plate, particularly during significant flow events as saltation lengths increase (Chatanantavet et al., 2013). The nuances between particle shape and detection response are typically assumed by researchers to even out, with justification drawn only from the

consistently strong correlation observed between impulse counts and total bedload (Downs et al., 2016).

2.3.3 Passive Integrated Transponder Tags

Passive integrated transponder (PIT) tags are a bedload particle tracking method which incorporates radiofrequency identification (RFID) to track the movement of uniquely identifiable tracer stones (Lamarre et al., 2005). Tracer stones can be constructed from particles collected from the streambed by drilling out a small cavity to embed a PIT tag, or they can be synthetically cast for greater control over the consistency of physical dimensions. PIT tags are typically seeded along the streambed and tracked over time following bedload mobilizing flow events using a mobile antenna reader and survey equipment. As the mobile antenna scans over a tracer stone, the PIT tag becomes inductively charged and subsequently transmits its unique identification number to the antenna reader (Lamarre et al., 2005).

Pit tags have become increasingly popular due to the many advantages they possess compared to other particle tracking techniques (Papangelakis, Muirhead, et al., 2019). PIT tag tracer stones are relatively inexpensive to produce, have superior recoverability in small stream systems, are durable, and their life span is not restricted by a battery techniques (Allan et al., 2006; Cassel et al., 2017; Lamarre et al., 2005; MacVicar et al., 2015; Nichols, 2004; Papangelakis, Muirhead, et al., 2019; Tsakiris et al., 2015). Although popular, PIT tag tracking is associated with a number of technological limitations primarily related to variability in RFID detection range. Tracers can get buried in sediment bars beyond their detection range and become temporarily lost, particularly true for smaller tracer stones (Chapuis et al., 2014; Lamarre et al., 2005; Rollet et al., 2008). The shape of a PIT tag detection field relative to an antenna depends on the orientation of the tag (Arnaud et al., 2015; Chapuis et al., 2014; Papangelakis, Muirhead, et al., 2019). Tsakiris et al. (2015)

demonstrated that changing the orientation of a PIT tag relative to an antenna from parallel (vertical) to perpendicular (horizontal) reduced the maximum detection range by 26 % - 76 % depending on bed material composition. Tracers that are positioned too close to one another can become masked due to interference created by overlapping detection fields (Cassel et al., 2017; Chapuis et al., 2014; Papangelakis, Muirhead, et al., 2019). Furthermore, irregularly shaped detection fields generated by inconsistently oriented tags can exacerbate masking effects (Cassel et al., 2017; Chapuis et al., 2014; Papangelakis, Muirhead, et al., 2019).

Papangelakis et al. (2019) developed a new synthetic RFID tracer stone design to help overcome the limitations related to variable stone orientation. The new synthetic tracer stone design, referred to as a *Wobblestone*, ensures that the embedded PIT tag remains vertical regardless of the tracer stone orientation as illustrated in Figure 13.

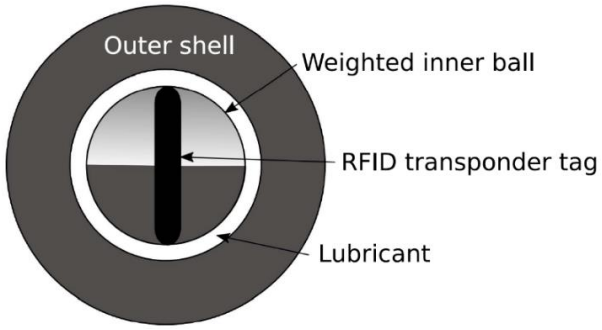

Figure 13. Schematic of Wobblestone conceptual design. From (Papangelakis, Muirhead, et al., 2019).

The Wobblestone incorporates a nested plastic ball design where the inner weighted ball is free to rotate keeping the RFID tag oriented vertically regardless of the exterior stone orientation. The Wobblestone can reduce the uncertainty associated with PIT tag tracking as it increases precision when locating tracer stones, reduces signal interference from clustered tracers, and permits estimation of burial depth due to the consistent detection field shape (Cain & MacVicar, 2020; Papangelakis, Muirhead, et al., 2019).

From a methodology perspective, PIT tag tracking presents two persisting challenges. First, PIT tag tracking only provides limited insight into bedload transport dynamics because observations are made in between flood events after transport activity subsides. Second, collection of this inter-flood data can be fairly time intensive depending on the quantity of seeded traces, the distance of tracer dispersion, and the surrounding vegetation and topographic conditions that influence survey efficiency (Papangelakis, Muirhead, et al., 2019). Muirhead (2018) developed an in-stream automated antenna tracking station that was designed to address these methodological challenges. The Muirhead station was deployed along a naturalized reach of Schneider Creek, Kitchener, Ontario in November 2016 and was decommissioned during the Fall of 2018. The station consisted of a loop antenna buried slightly below the streambed surface that was connected to a commercial RFID multi antenna reader (MAR), and a Raspberry Pi system brain as illustrated in Figure 14 (Muirhead, 2018). The station was intended to automatically track RFID tracer stones when the creek water level rose during a competent flow event to a set high-water threshold (Muirhead, 2018).

Figure 14. Muirhead Station water level gauge and in-stream antenna (left), and electrical components housed within a storage bin (right) at Schneider Creek. From (Muirhead, 2018).

The Muirhead station was powered by a single marine battery, which meant that power conservation was essential to allow the system to function for extended periods of time. For this reason, all station components including the Raspberry Pi system controller, in stream antenna, and RFID MAR were connected to a float switch hardware piece. The float switch was mounted within a perforated standpipe along the stream bed and rested in an 'off' position during periods of low flow when the water level rested below the float. While the float switch was in the 'off' position, the power delivery circuit connecting the marine battery to the station components remained disconnected. At times when the water level rose to the float switch, the free-moving float would be lifted into an 'on' position, thus completing the power delivery circuit to turn on the station. During these times of high flow, the Muirhead station RFID MAR would track previously seeded tracer stones as they were transported over the in-stream antenna detection field. The Muirhead station Raspberry Pi system controller would simultaneously execute a python code that would relay any detections made by the RFID MAR to a .csv file located on a USB flash drive or Dropbox cloud.

The Muirhead station was limited by several constraints, the most significant of all being an inability to output any data. A lab duplicate of the Muirhead station was used to both troubleshoot these issues and make improvements to the system. Upon inspection of the system programming code, it was discovered that the code was unable to establish a proper serial device communication connection between the Raspberry Pi and the RFID MAR. As a result, the Raspberry Pi was incapable of accessing the detections made by the RFID MAR and therefore had no data to write to the .csv output file. After rectifying this bug in the code, several new errors arose as the system was able to proceed further through the programming script. These additional errors remain unresolved. Another constraint of the Muirhead station was the reliance on a custom circuit board

and wiring to supply power to the Raspberry Pi and RFID MAR. The custom circuitry setup had a poor electrical ground that would activate bare metal surfaces of the system controller into live weak electrical contacts. The wiring that connected the float switch to the system was inadequately insulated and unlikely to provide durability for long term use in the field. Furthermore, most of the field deployed station components were housed within a sealed plastic storage bin buried at the top of the valley wall adjacent to the in-stream antenna. Although the storage tote was located beyond the floodplain extents, it would frequently accumulate water placing the electrical components at risk of damage.

The Muirhead station deployed at Schneider Creek was unable to function as intended and was subsequently decommissioned before long-term field testing could be observed. As a result, it is unclear whether the system was designed with sufficient weather resistance, durability, and power capacity to operate for reasonably extended periods of time in the field. However, the concept of an in-stream automated tracking station is a promising idea that can improve upon the limitations of PIT tag tracking and other bedload tracking stations.

2.4 Summary of Research Gaps

Numerous research studies have demonstrated that agricultural development places an enormous level of stress upon the natural water and nutrient cycles, which consequentially degrade the health and stability of fluvial systems diversity (Blann et al., 2009; Burkhead & Jelks, 2001; Johnston & Shute, 1997; Mion et al., 1998; Newcombe & Jensen, 1996; Owens et al., 2005; Pimentel et al., 1995; Sweka & Hartman, 2001; Wichert & Rapport, 1998). Rural areas situated near heavily populated regions in Southern Ontario, such as the Greater Toronto Area, are likely to endure further development in the form of urbanization. This begs the question: can an urban development undertaking be leveraged as a remedial opportunity that improves upon the adverse responses

observed in agriculturally impacted stream networks. In order to explore this idea in practice, there must be robust monitoring methods put in place to gain a solid understanding of baseline stream health and stability, and use this baseline information to make predictions about stream stability in response to the modified landscape.

When it comes to monitoring bedload sediment transport, a significant research gap exists within the scientific community as there are a lack of low-cost, reliable, robust, and comprehensive methods for quantifying bedload sediment transport. Many existing monitoring methods are unable to yield high-resolution and temporally dense data, which contributes to our limited understanding of bedload transport dynamics (Gray, Laronne, Osterkamp, et al., 2010). Among existing methods, direct physical sampling is a commonly employed technique but provides limited insight and is laborious, costly, sometimes dangerous to operate, and accompanied by an abundance of difficulties (Gray, Laronne, Osterkamp, et al., 2010). However, direct sampling methods function well as a complimentary technique when used in tandem with indirect monitoring methods for calibration purposes (Gray, Laronne, Osterkamp, et al., 2010). Popular indirect monitoring methods such as PIT tag particle tracking only provide limited inter-flood data and are labour intensive. Muirhead (2018) attempted to reconcile the limitations of PIT tag tracking through the conception of an automated tracking station but was ultimately limited by technical shortcomings. Recent studies have demonstrated the potential behind passive acoustic bedload monitoring as a technique that can provide valuable insight into bedload transport dynamics through the collection of high-resolution data over extended time periods using portable relatively inexpensive instrumentation.

Habersack et al. (2017) shared the philosophy that no single monitoring technique can completely characterize bedload transport dynamics. Rather, a variety of integrated monitoring methods can

provide a broader understanding of bedload dynamics by offering distinct yet temporally comparable perspectives of bedload activity. The aforementioned research gap and Habersack's philosophy motivated the direction of this thesis to incorporate several unique monitoring techniques into a newly developed remote, integrated, automatic, and continuous bedload monitoring station as described in Chapter 3. The station is based on the advancements made by Muirhead (2018) and combines automated PIT tag particle tracking, a direct physical sampler, and passive acoustic monitoring to collect high-resolution, temporally dense, and continuous bedload transport data. The station setup is designed to be relatively inexpensive compared to similar stations devised by other researchers and can be easily deployed in remote settings for both industry and research applications.

3 Remote, Integrated, Automatic and Continuous Bedload Monitoring Station

The following chapter presents the design of a newly developed remote, integrated, automatic and continuous bedload monitoring station. The justification and advantages behind the selected bedload monitoring methods incorporated into the station are reviewed in Chapter 3.1. A high-level conceptual overview of the bedload monitoring station design is presented in Chapter 3.2, followed by details regarding the specific components incorporated into a functional version of the station. Preliminary lab test results of a key bedload monitoring device are presented in Chapter 3.3.

3.1 Bedload Monitoring Method Selection

Three complimentary bedload monitoring methods were incorporated into the station design. These methods include particle tracking with synthetic RFID tracer stones, passive acoustic monitoring using modified Benson Type-A impact plates, and direct physical sampling using a Bunte sediment trap. RFID particle tracking was selected because of its unique advantages as a monitoring technique (Table 1). RFID tracer stones can be tracked either manually between flood events by a survey team, or automatically during competent flow events by the station, which uses an RFID antenna reader and in-stream antenna. RFID particle tracking is an indirect method that provides specific information regarding travel paths of a tracer population, which can link flood events to tracer movement between measured coordinates. Recent methodological advancements made by Papangelakis (2019) and Muirhead (2018) at the University of Waterloo made this method a very practical choice in that the bedload monitoring station design builds off the knowledge and developments of their research. Researchers at the University of Waterloo have amassed an extensive RFID particle tracking dataset across several field sites in Southern Ontario, which provides an additional benefit of data comparison. Some of these field sites are located

within the Greater Toronto Area and share similar properties, but are characterized by different land-use and stormwater management infrastructure. The contextual similarities of these study sites permit comparison of particle tracking results as they pertain to various land development conditions.

Modified Benson Type-A impact plates were also selected for bedload transport monitoring. These plates are complementary to RFID particle tracking because they use a passive acoustic approach to monitoring. These plates are an indirect method that provides high-resolution continuous data on a full census of bedload particles. Further advantages are that they are low cost, portable, and measure transport in an unobstructive manner. The method requires calibration, however, largely due to single rolling particles triggering multiple detections and spatial variations in bedload transport.

Direct physical sampling using a Bunte sediment trap was incorporated into the station design to verify the results of the indirect monitoring methods and calibrate the impact plates. In theory the sediment trap would eventually be removed from the monitoring station once the impact plates are satisfactorily calibrated, which would subsequently enable the entire system to operate automatically. The Bunte sediment trap is a portable, inexpensive, and non-intrusive instrument that offers several advantages over other physical sampling devices such as ease of installation and sample collection, and the ability to relocate the instrument. Overall, the three selected methods offer a diverse range of potential bedload monitoring insight as summarized in Table 1.

Table 1. Summary of Bedload Monitoring Method Characteristics

Method	Device	Method Type	Sample Type	Measurable Bedload Parameters*
Particle tracking	Synthetic RFID tracer stones; in-stream antenna & reader	Indirect	Tracer	Virtual velocity [m/year] Travel length [m] Burial depth [m] Temporal variability [-] Incipient motion [-]
Passive acoustic monitoring	Modified Benson Type-A impact plate	Indirect	Census	Bedload discharge [kg/s] Total bedload transport [kg] Temporal variability [-] Spatial variability [-] Incipient motion [-]
Physical sampling	Bunte sediment trap	Direct	Census	Specific bedload discharge [kg/m/s] Total bedload transport [kg] Grain size distribution [-] Incipient motion [-]

*Transcribed from (Habersack et al., 2010).

3.2 Station Overview

The bedload monitoring station is intended to function as a remote system that integrates several bedload monitoring methods to automatically collect high-resolution continuous data. It is a low cost and robust system that is well suited for monitoring small rivers and creeks. The monitoring station consists of the following main design components, which are depicted in Figure 15:

1. Power supply and storage
2. System controller
3. Network communication
4. Protective housing for electronic components
5. Water level measurement
6. Bedload sediment transport measurement

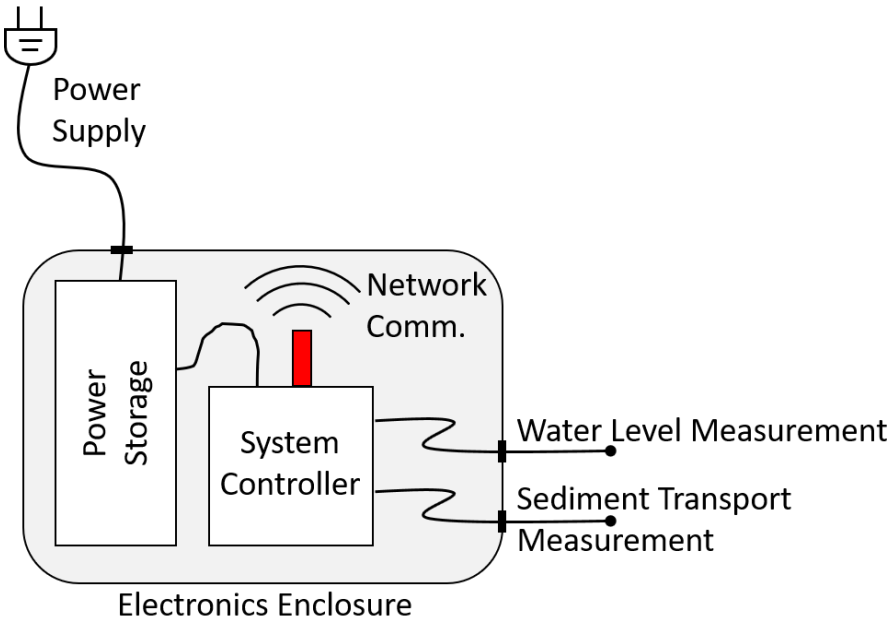

Figure 15. Bedload monitoring station conceptual diagram.

A functional version of the bedload monitoring station conceptual design was assembled and deployed at a field site along Carruthers Creek, Pickering, Ontario as explored in Chapter 4. The specific features of the assembled station are described in Chapters 3.2.1 to 3.2.6.

3.2.1 Power Supply and Storage

The station requires some form of power supply and power storage to operate in remote conditions during intermittent periods of bedload activity. In its current configuration, power is supplied to the station from two solar panels (Renogy 100 Watt 12 Volt Monocrystalline) and stored in two batteries wired in parallel (MotoMaster Nautilus Group 31 Deep Cycle). A solar charge controller (Steca Solsum 8.8F) regulates power delivery from the solar panels to the batteries. Power conservation is a critical element in ensuring that the station remains operational during significant storm events when the batteries are placed under sustained load and solar radiation may not be available for immediate recharge. The RFID single antenna reader (SAR) consumes the most power out of all station components, and as a result, it remains on standby during periods of low

flow to conserve power when bedload activity is not anticipated. Table 2 provides a summary of power drawn or supplied by each device.

Table 2. Bedload Monitoring Station Power Summary

Station Component	Device	Type	Voltage [V]	Amperage [A]	Power [W]
System controller	Raspberry Pi	Load	5	0.35	1.75
Water level meas.	Seametrics PT2X Sensor	Load	12	0.015	0.18
Bedload meas.	OregonRFID SAR & Antenna	Load	12	0.18	11.6
Bedload meas.	Benson Type-A Impact Plate	Load	13	0.004	0.052
Power storage	MotoMaster Battery	Supply	12	105	1260
Power supply	Renogy Solar Panel	Supply	17.9	5.72	100

The fully charged batteries will last for approximately 160 hours (or just under 7 days) if the station is placed under sustained full load with no solar radiation available to supply additional power through the solar panels. The solar panels require approximately 13.3 hours of solar radiation to fully charge the depleted batteries under zero load. Average daily hours of solar radiation vary seasonally between 2.13 and 3.98 hours in the Toronto area meaning it may realistically take up to 6 - 7 days to fully charge the depleted batteries under this scenario (Integrated Power Systems, n.d.).

3.2.2 System Controller

The monitoring station is controlled by a Raspberry Pi 3B+ single-board computer that runs a Node-RED software program to execute system operations. Node-RED is a programming tool that is well suited for communicating with hardware devices and network services. Node-RED is a visual software that is accompanied by a browser-based graphical user interface (GUI) providing users with a palette of pre-programmed and customizable nodes that can be arranged into a ‘flow’ to execute a desired task.

Through the Node-RED program, the Raspberry Pi is able to communicate with the PT2X pressure sensor, RFID SAR and impact plates via buried wire connections. The Raspberry Pi polls the stream water level from the PT2X pressure sensor and if it exceeds a user specified threshold (signifying a competent flow event) then the RFID SAR is initiated from standby to begin tracking tracer stones. At the time of threshold exceedance, a short messaging service (SMS) notification is sent to the user and repeats on an hourly basis while the system remains above threshold. After the passing of a competent flow event when the water level remains below threshold for a duration of 30 minutes, the Raspberry Pi switches the RFID SAR back into standby mode. The Raspberry Pi saves all data records to its local hard drive as comma separated value (.csv) files that can be retrieved remotely by the user as described in Chapter 3.2.3.

3.2.3 Network Communication

Network communication between the station and user is an essential design component that allows for application in remote settings. Network communication is used to send notifications and permit the user to remotely off-load data and update software. Network communication is facilitated by a Hologram Nova USB dongle attached to the Raspberry Pi, which establishes a 3G network connection. To optimize data usage and battery consumption, the Raspberry Pi is programmed to connect to the 3G network only twice per week for a duration of 1 hour per session (Tuesdays and Thursdays at 10:00 am EST). At this time, a user can establish a remote connection to the system through a secured shell (SSH) network communication protocol and off-load data according to the following steps. First, a user must execute Hologram's *SpaceBridge* service on their own device to establish an encrypted authenticated tunnel to the Raspberry Pi device. Next, the user must run an SSH client (such as *OpenSSH* or *PuTTY*) to transmit an SSH request to the Raspberry Pi device through the *SpaceBridge* tunnel. Once the request is accepted, a terminal command line interface

window will open and allow the user to access data records stored on the Raspberry Pi device. The user can then off-load data (for example by using the secure copy (scp) command) and clear previous records on the Raspberry Pi.

3.2.4 Protective Housing

The electronic components of the station are housed within a robust Pelican Vault V600 weather resistant enclosure. In the field, the enclosure rests off the ground on a tabletop frame to promote long-term station durability by protecting the electronic components from rain and flood water as displayed in Figure 16. All electronic cabling enters the enclosure through cable feedthrough seals that prevent moisture ingress. The enclosure is bolted to the frame and can be secured shut with a padlock to discourage vandalism and theft.

Figure 16. Electronics enclosure mounted to tabletop frame. Figure shows early version of station setup with only one solar panel.

3.2.5 Water Level Measurement

The station measures water depth and temperature with a Seametrics PT2X pressure sensor. The sensor is housed within a stainless-steel perforated well where it freely hangs from the well cap at a fixed depth above the creek bed as displayed in Figure 17. The well cap contains a cable feedthrough seal that grasps the sensor cable keeping it at a consistent depth and routes the cable wiring to the Raspberry Pi system controller. The PT2X contains an atmospheric intake hose located outside of the station electronics enclosure that automatically compensates water depth measurements for barometric pressure. The intake hose is filled with a colour indicating granular desiccant that prevents moisture accumulation and changes colour when absorbing capacity has exhausted.

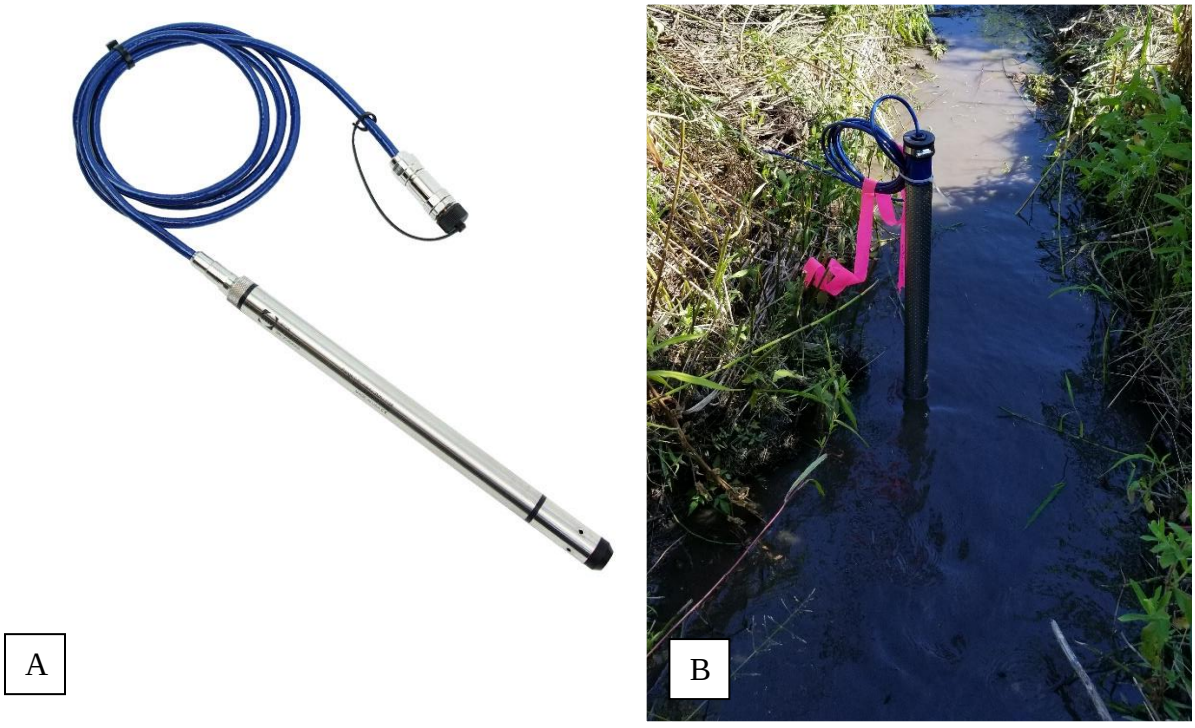

Figure 17. Seametrics PT2X pressure sensor. (A) Sensor and cable connection. Retrieved from: https://www.nexsens.com/products/sensors/water-level/seametrics-pt2x-water-level-loggers. (B) Well housing.

3.2.6 Bedload Sediment Transport Measurement

3.2.6.1 Automated RFID Tracer Stone Particle Tracking

The station is designed to automatically track synthetic RFID tracer stone particles using an in-stream loop antenna, an OregonRFID automatic tuning capacitor (ATC), and an OregonRFID half-duplex (HDX) long range PIT tag SAR. The loop antenna is buried slightly below the mean streambed surface and is connected to the ATC, which is then routed to the SAR housed within the electronics enclosure using buried twinax cable. The in-stream antenna configuration must adhere to OregonRFID design guidelines to ensure that the antenna setup is compatible with the ATC and SAR. The guidelines specify that an antenna needs to be configured as a loop of wire capable of generating a magnetic field that agrees with the tuning range of the capacitor. In the case of the ATC, an antenna must have a magnetic capacity (a measurable property referred to as inductance) of 25 – 102 µH (Oregon RFID, 2019). Antenna inductance is influenced by antenna size, antenna geometry, and the number of loop turns made by the wire (Oregon RFID, 2019).The ATC is required to tune the antenna frequency to an international standard value of 134.2 kHz, which alleviates electromagnetic disturbances to organisms (Oregon RFID, 2019).

The antenna wiring is inserted into a custom PVC housing manufactured by the University of Waterloo Creation Lab computer numerical control (CNC) machine. The housing is intended to protect the antenna from field damage by forming a durable but semi-flexible conduit. A Solidworks design of the PVC housing originally rendered by Muirhead (2018) was slightly modified for the station as displayed in Figure 18. The PVC housing consists of several segments that contain rounded modular ends allowing for flexibility when installed along a streambed. A series of parallel channels are cut along the centre of the PVC segments to contain the turns of the antenna loop. The antenna loop wire is secured within the channels by a series of alternating inset

bumps. The segments can be fastened together by feeding zip ties through the sets of holes located at either end of each segment.

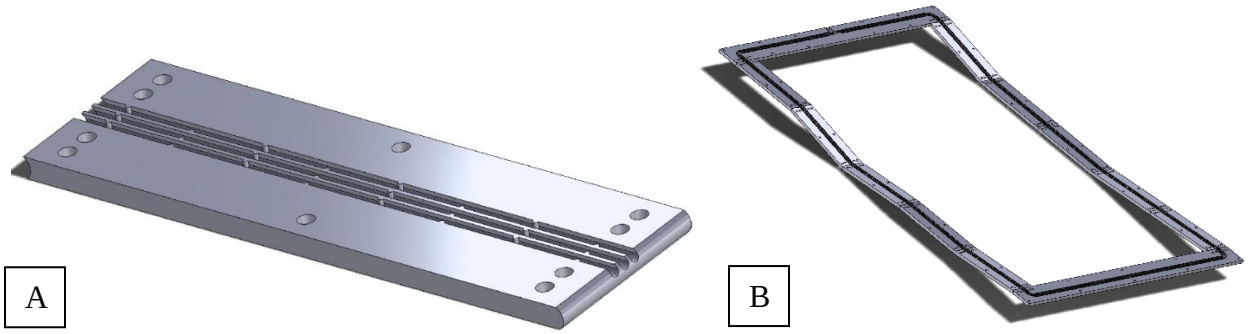

Figure 18. Solidworks schematic of PVC housing for in-stream antenna. (A) Zoomed in view of single modular segment showing inner channels and bumps. (B) View of housing assembly.

When the water level at the station increases to the user specified high-water threshold, the Raspberry Pi system controller initiates the SAR and begins tracking tracer stones that are mobilized over the antenna detection field. The SAR tracks tracer stones by emitting a short magnetic pulse from the antenna to inductively charge nearby RFID tags, and then listening for return radio signaling from nearby tags that are deciphered as unique identification numbers (Oregon RFID, 2019). Each magnetic charge and listening sequence make up one scan cycle that is referred to as HDX cycling. For each detection, the SAR records the unique tag ID, a timestamp, and the duration with which the tracer remains in the antenna detection field. The primary challenge associated with this automated method of tracking RFID tracer stones is determining an optimal high-water threshold that minimizes battery load by avoiding excessive triggering, but is set low enough to initiate tracking before the smallest sized tracer stone is entrained. The high-water threshold can be initially estimated through an analysis of critical shear stress using the creek cross-sectional geometry and adjusted over time based on trial and error.

3.2.6.2 Modified Benson Type-A Impact Plates

The station incorporates two modified Benson Type-A impact plates, herein referred to as "plates". The plates are made of stainless steel and consist of a rectangular slab with a barrel welded to its underside to house electrical components. Each plate contains a seismic sensor capable of detecting the mechanical energy of bedload impacts exerted upon the plate that exceed the device's lower sensitivity limit. The manufacturer indicates that the modified Type-A plates are capable of detecting impacts from particles with a b-axis diameter of 10 – 12 mm as described in Chapter 3.3.1. The mechanical energy of an impact is converted into an electrical pulse that is recorded as a singular count accompanied by a timestamp.

Each plate is mounted to a custom-made concrete block buried in the streambed such that the surface of the plates rest flush with the local mean streambed surface. A water-tight seal is maintained with a rubber stopper and silicone applicant that plug the barrel of the plate. The plates are lightly modified as the internal data loggers typically installed by the manufacturer have been removed and replaced with hard-wired connections to directly link each plate to the Raspberry Pi system controller via underground water-tight conduits. A brass barb fitting is connected to the centre of each plate rubber stopper leading the electrical wires through 3/8" air brake hose conduits to the monitoring station electronics enclosure. The custom concrete mounting blocks contain open channels that accommodate the conduits and allow for easy plate removal while leaving the mounts in-situ as displayed in Figure 19.

Figure 19. Impact plate mounted to concrete block. View of electrical wire conduit routed through inner channel.

3.2.6.3 Bunte Sediment Trap

A Bunte sediment trap was included in the station setup to compliment the indirect monitoring techniques with a direct physical sampling method. The Bunte sediment trap was constructed following the specifications listed in Bunte et al. (2007) and is displayed in Figure 20.

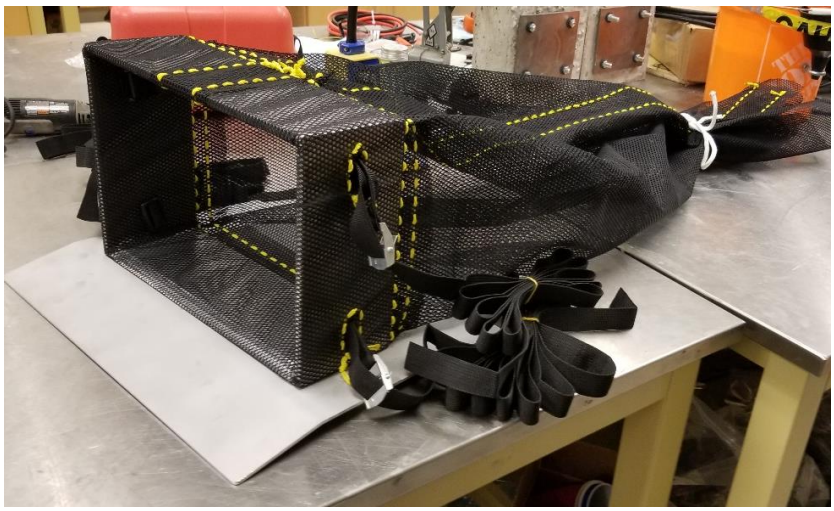

Figure 20. Bunte sediment trap (Bunte et al., 2007).

The trap consists of an aluminum ground plate and an aluminum frame that is sewn into an open-ended net. The aluminum parts were digitally rendered using Solidworks software and then manufactured by the University of Waterloo Engineering Machine Shop. In the field, the ground

plate is centred with the creek thalweg lying flush to the mean bed elevation and is secured in place with rebar posts. The frame rests on top of the ground plate and is fastened to the rebar posts with metal friction buckles. The end of the net is tied off for sediment sample collection and can be untied to easily retrieve samples. The net is a semi-rigid mesh that allows passage of particles with a b-axis diameter less than 3 mm.

3.3 Modified Benson Type-A Impact Plate Performance Testing

The Benson Type-A impact plates are a relatively new bedload monitoring device with limited but growing use in research applications (Downs et al., 2016; Reid et al., 2007; Soar & Downs, 2017). There is a degree of uncertainty surrounding the performance and limitations of the plates due to their limited use to date. The plates are manufactured in the UK where they have been largely geographically limited in application, thus it is unclear how the plates perform under cold operating conditions such as that regularly observed in Southern Ontario. A series of brief laboratory tests were completed using a modified Benson Type-A impact plate mounted to a custom-made concrete block to evaluate plate functionality under controlled lab conditions and cold operating temperatures. The results of these tests and sensitivity information provided by the manufacturer are described in the following chapters and concluded with general recommendations.

3.3.1 Manufacturer Sensitivity Rating

The manufacturer of the impact plates provided an approximate sensitivity rating for the Type-A plate as derived from an experimental test. The experimental setup consisted of the plate being placed at the bottom of a tote bin that contained a 10 cm deep water profile. A variety of stones were dropped from 30 mm above the water profile onto the impact plate. The results of the test were presented as the b-axis diameter of stones that were *normally detected* by the impact plate compared to the b-axis diameter of stones that were *normally missed* as displayed in Figure 21.

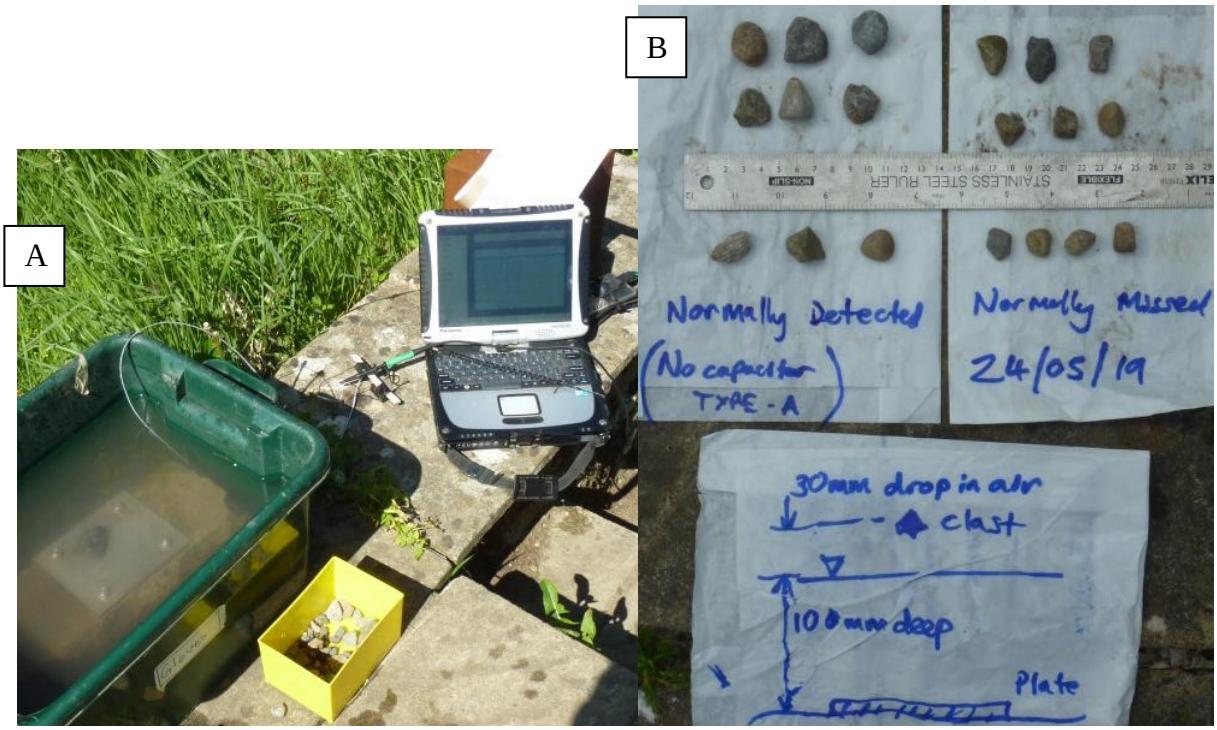

Figure 21. Benson Type-A impact plate manufacturer sensitivity test. A) Experimental setup. B) Test results (Photo credits: Ian Benson, 2019).

Based on this test, the manufacturer reports that the Type-A plate normally detects particles with a b-axis diameter of approximately 18 mm. However, the test results highlight the uncertainty associated with this bedload monitoring device as the plates are seemingly unable to consistently replicate detections for a given particle.

A modified version of the Type-A impact plate with increased sensitivity was ordered from the manufacturer and used in the bedload monitoring station setup. The manufacturer reports that the modified Type-A plate normally detects particles with a b-axis diameter of approximately 10 – 12 mm based on past flume experimentation (personal correspondence, Ian Benson). Additional sensitivity tests were completed at the University of Waterloo to assess this reported threshold for detection.

3.3.2 Threshold Test and Spatial Sensitivity Analysis

A plate detection threshold test and spatial sensitivity analysis were performed using a Dytran Dynapulse™ impulse hammer. An impulse hammer measures the electromotive force exerted upon striking the hammer against a surface and can be equipped with a nylon or aluminum tip. To determine an approximate plate detection threshold, consecutive hammer strikes were delivered to the center of the plate using the nylon tip. The peak force of each strike was recorded and compared to the corresponding impact plate signal displayed through an oscilloscope. A total of 39 successive strikes were exerted to converge upon an approximate plate detection threshold as demonstrated in Figure 22.

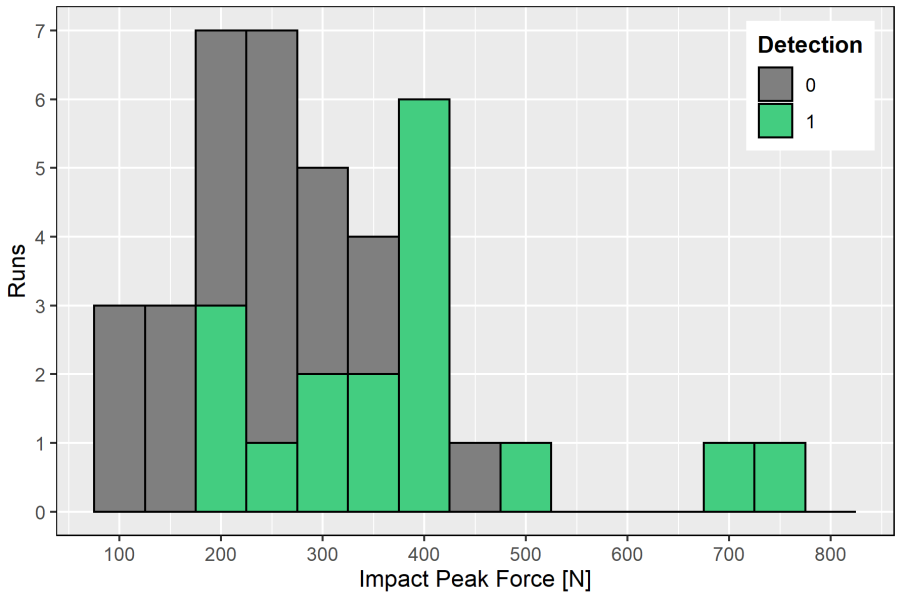

Figure 22. Impact plate detection threshold analysis. Impacts were exerted upon the plate centre using a Dynapulse™ impulse hammer to measure peak impact force.

The results of the detection threshold analysis reveal that the impact plate centre was typically triggered by a peak force of approximately 400 N. To evaluate the spatial sensitivity of the plate, consecutive strikes were delivered with the impulse hammer along a transect running through the plate center, parallel to the longest plate dimension (150 mm). The plate was divided into 9 equal

segments along the transect with which approximately 20 successive strikes were exerted per segment as demonstrated in Figure 23.

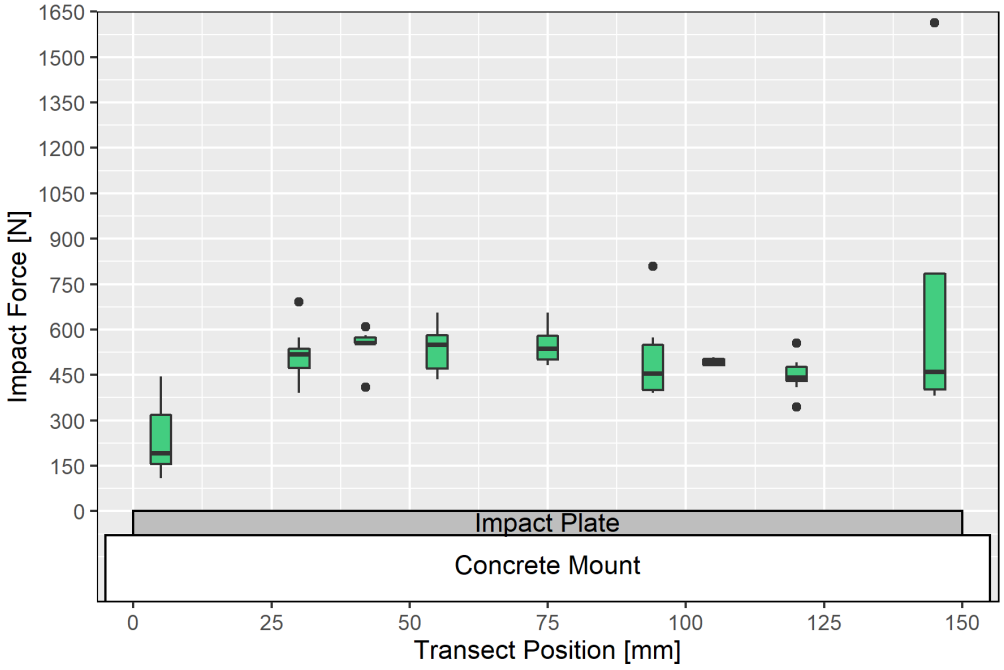

Figure 23. Impact plate spatial sensitivity analysis. Impacts were exerted upon a transect along the plate centre running parallel to the length of the plate using a Dynapulse™ impulse hammer to measure peak impact force. Statistical outliers are presented as individual points.

The results of the spatial sensitivity and detection threshold analyses generally agree with one another as similar peak forces typically triggered a plate detection. The spatial sensitivity analysis reveals that the impact plate was typically triggered by a peak force of approximately 500 N along the transect, in exception to segment 1 positioned at 5 mm. Segment 1 was typically triggered by a peak force of 200 N, which is considerably less than the other 8 transect locations. Following the impulse hammer tests, it was noted that although the plate was securely fastened to the concrete mount, not all edges of the impact plate rested flush against the concrete surface due to the curvature of the plate and uneven torqueing of the nut fasteners. This provides a possible explanation as to why transect segment 1 was more sensitive during the spatial sensitivity analysis, as this edge was in direct contact with the mount while majority of the opposing edge was lifted

off the mount. This observation leads to the belief that mounting an impact plate is not trivial, rather it is important to ensure that the plate is evenly secured to the mount.

Following this observation, metal washers were added to the underside of the plate keeping all edges of the plate evenly lifted off the surface of the concrete mount to repeat the threshold test; however, plate response to subsequent impulse hammer strikes became highly inconsistent. The impulse hammer nylon tip was exchanged with the aluminum tip, but the plate response did not change noticeably. While the plate was generally unresponsive to the impulse hammer, other metal objects (such as the aluminum handle of a small screwdriver) would cause a plate detection with little force. This observed inconsistency indicates that factors other than peak impact force (such as strike duration, impact rebound, object material, etc.) might have a considerable influence on plate detection.

It was decided that the impulse hammer was not a suitable measuring device for the purpose of determining a plate detection threshold with respect to the intended application of bedload transport monitoring. An alternative experimental approach was adopted that also improved replicability between runs. A vertical burette stand and clamp were assembled next to the impact plate with the clamp resting above the centre of the plate as displayed in Figure 24.

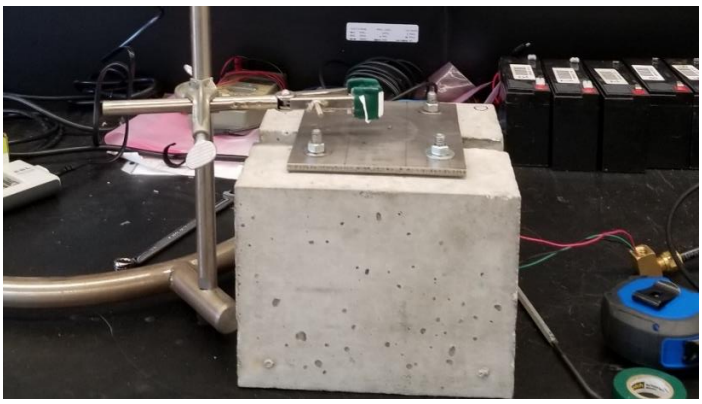

Figure 24. Impact plate detection threshold test experimental setup. Burette stand and clamp positioned above the plate centre to release a fine gravel particle at a measurable height.

A 3/8” diameter stainless steel ball bearing was placed in the clamp and released at measured heights above the plate to converge upon the plate detection threshold. The plate was able to detect the ball bearing when dropped from very small heights, so the ball bearing was replaced with a fine gravel particle. The particle, herein referred to as Particle-A weighed 0.1 g and possessed a b-axis diameter of 3.48 mm. Particle-A was consistently oriented in the clamp between successive runs such that the a- and b-axis were parallel and perpendicular to the plate surface, respectively. A total of 30 runs were completed as demonstrated in Figure 25.

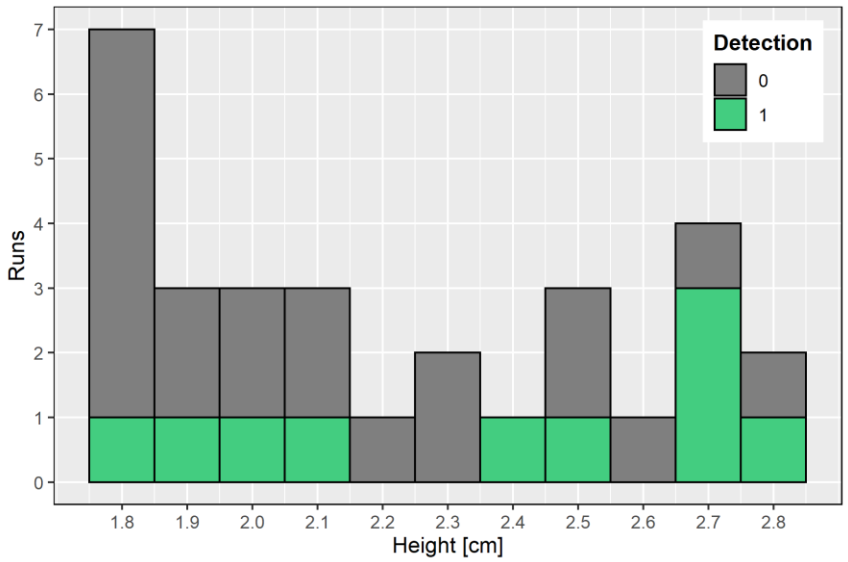

Figure 25. Impact plate detection threshold analysis. Impacts were exerted upon the plate centre by dropping a gravel particle (Particle-A) from measured heights.

The results of the detection threshold analysis demonstrate that plate response was fairly erratic across the range of observations.

3.3.3 Cold Temperature Performance Analysis

Impact plate cold temperature performance was evaluated by placing the plate and mount in a freezer for a total duration of 67 hours prior to repeating the detection threshold test. Once the plate was removed from the freezer, a layer of frozen condensation was cleared from the plate

surface. The plate was unable to detect impacts exerted by dropping Particle-A from heights similar to and greater than the previous detection threshold experiment, so a larger particle was used in its place. This larger particle, herein referred to as Particle-B, weighed 0.5 g and possessed a b-axis diameter of 8.51 mm. A total of 20 runs were completed as demonstrated in Figure 26.

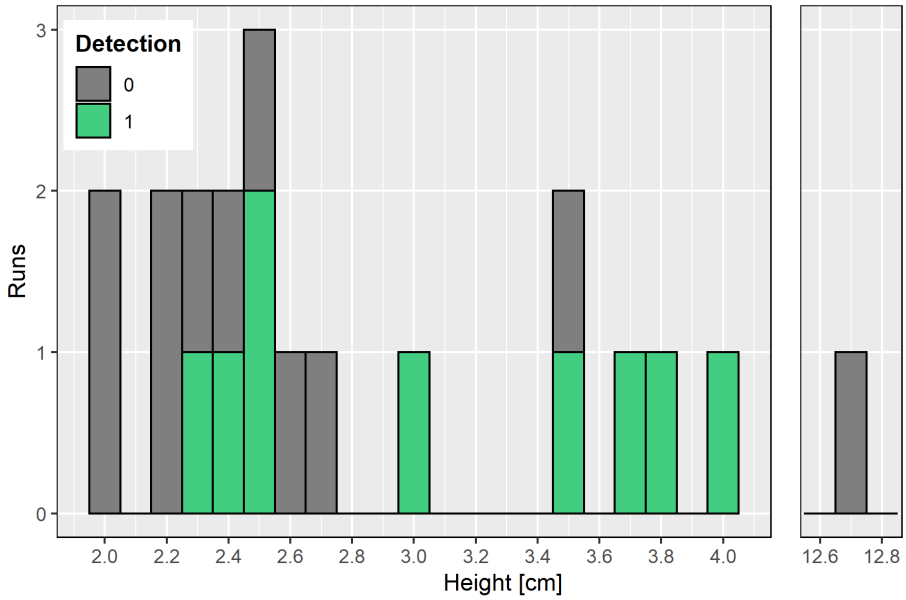

Figure 26. Impact plate detection threshold analysis under cold operating temperatures. Impacts were exerted upon the plate centre by dropping a gravel particle (Particle-B) from measured heights.

The results of the detection threshold analysis revealed that the impact plate centre was typically triggered by dropping Particle-B from a height of 2.5 cm. In order to evaluate general robustness against cold temperature field conditions, the impact plate and mount were submerged in a container of water and then placed in a chest freezer for a duration of 21 hours to completely encase the plate in ice. Once the container was removed from the chest freezer, a heat gun was used to melt away the ice covering the plate surface and it was verified that the plate was still functional.

3.3.4 Recommendations

The experiments completed with the modified Type-A impact plate were unable to make any strong conclusions about plate performance. One major remaining question concerns how securing the plate to a concrete mount influences plate response. A series of flume experiments were planned for this thesis to better understand impact plate performance and the corresponding output signal in an applied setting; however, these experiments were not completed due to campus closures and restrictions enacted by the University of Waterloo in response to the COVID-19 global pandemic. Flume experimentation is highly recommended as a future step to clarify the uncertainties surrounding the impact plate monitoring device.

4 Baseline Flow and Sediment Characterization of a Semi-Alluvial Creek

The following chapter describes a study site at Carruthers Creek in Southern Ontario and the implementation of the remote, integrated, automatic and continuous bedload monitoring station to perform baseline flow and sediment characterization. An overview of watershed characteristics and study site selection is provided in Chapter 4.1. A detailed summary of the methods applied to perform baseline data collection and analysis is described in Chapter 4.2. The findings of the baseline characterization study are presented in Chapter 4.3.

4.1 Study Site

Carruthers Creek is located within the City of Pickering and Town of Ajax, Ontario, Canada as illustrated in Figure 27. Carruthers Creek is approximately 30 km in length with an associated watershed drainage area of nearly 40 km^2. At its headwaters in the City of Pickering, Carruthers Creek is primarily surrounded by rural agricultural lands outfitted with tile drains. Further downstream, Carruthers Creek makes its way through the Town of Ajax before discharging into Lake Ontario. The Quaternary geology of the watershed consists of Halton till situated to the north, an undifferentiated till unit to the south, and an intermediary divide of geolacustrine deposits splitting these two till units (Ontario Ministry of Energy Northern Development and Mines, 2017). The landscape of the watershed basin has been subjected to significant modifications and morphologic change over the past century as a result of agricultural development and urbanization (Conservation Authorities Moraine Coalition, n.d.). A study reach within the headwaters was selected to investigate baseline geomorphic conditions of the system in a location absent of urban hydromodification impacts. Information gathered from desktop analyses and site reconnaissance were used to select a study reach that was accessible for field instrumentation and demonstrated signs of active channel adjustment with minimal anthropogenic impacts.

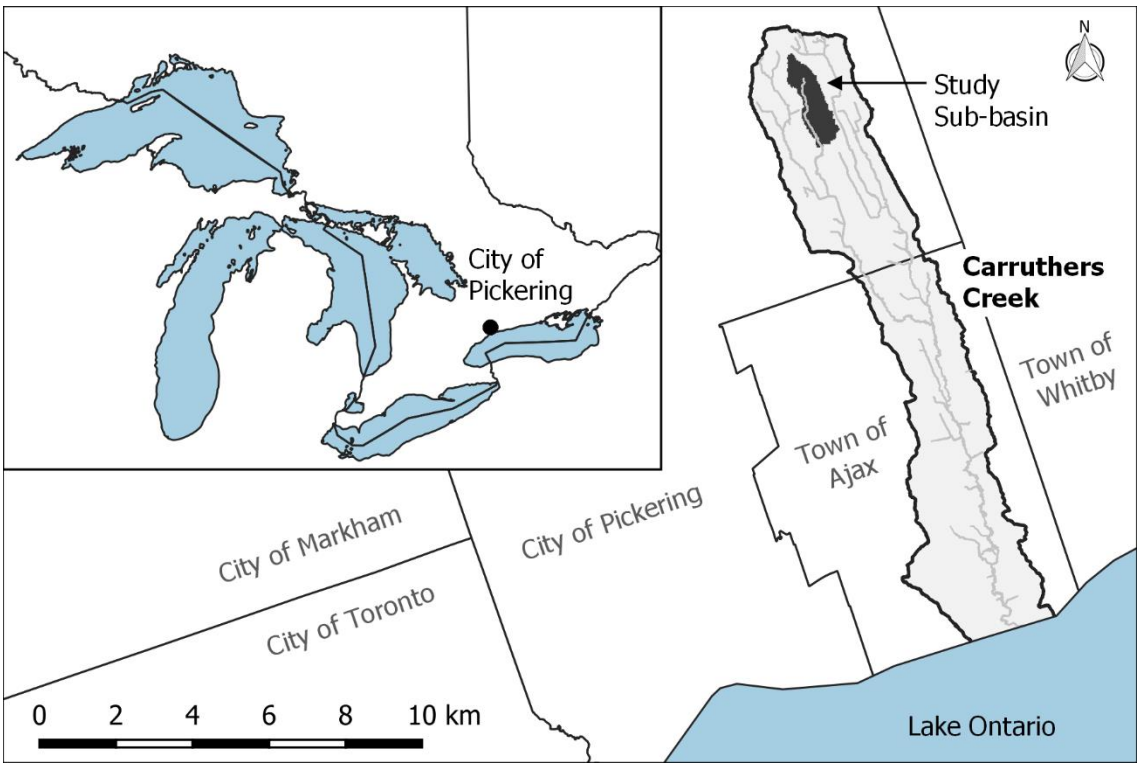

Figure 27. Carruthers Creek watershed basin and study sub-basin area.

4.1.1 Stream Power Analysis

A stream power analysis was completed for the Carruthers Creek watershed using an ArcGIS spatial analysis tool developed by Ghunowa (2017). Stream power is a flow metric that describes the power supplied by streamflow per unit channel length that is available to perform geomorphic work (Bagnold, 1966). Specific stream power (ω) is an alternative derivation that describes power per unit channel area [W/m^2] calculated as follows:

$$\omega = \frac{\rho_w g Q S}{B} \quad (1)$$

where ρ_w is the density of water [kg/m^3]; g is the gravitational acceleration constant [m/s^2]; Q is streamflow discharge [m^3/s]; S is the channel slope [-]; and B is the channel bed width [m]. The spatial analysis tool requires a hydrology-enforced digital elevation model (DEM) of the watershed to discretize the stream network and estimate specific stream power (Ghunowa, 2017). The

enforced DEM was obtained from the Ontario Integrated Hydrology (OIH) Data catalog created by the Ontario Ministry of Natural Resources and Forestry (MNRF) and distributed through Land Information Ontario (LIO). The enforced DEM has a spatial resolution of 30 m but is hydrologically conditioned by an Enhanced Watercourse network that incorporates watercourse features into the DEM (Ontario Ministry of Natural Resources and Forestry, 2020). The resulting stream power analysis of Carruthers Creek is presented in Figure 28.

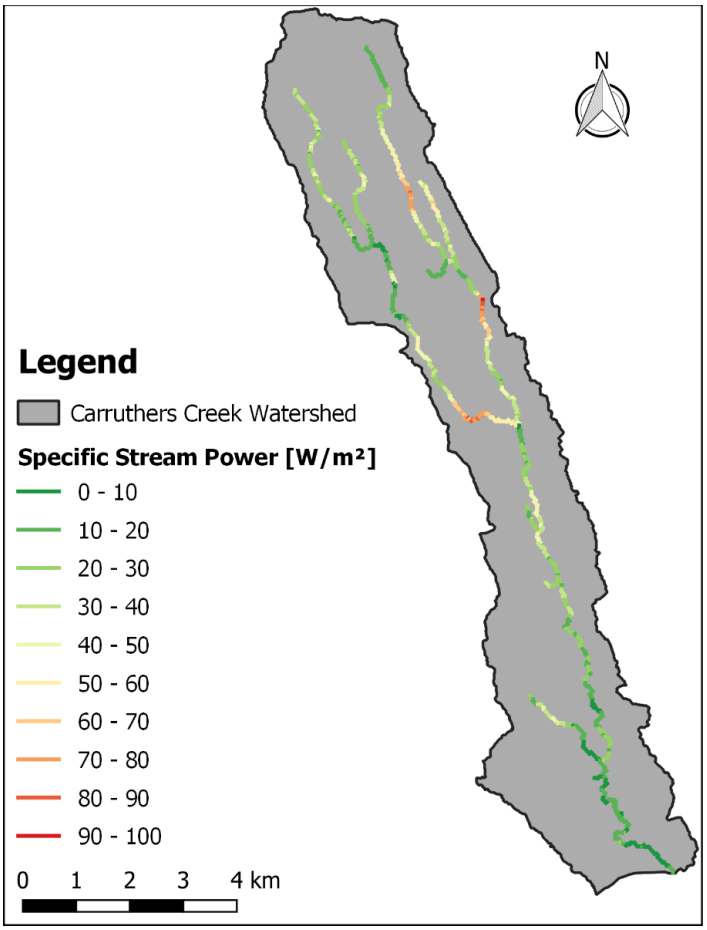

Figure 28. Carruthers Creek specific stream power analysis.

The assessment served as a preliminary desktop-level investigation of channel form along the watershed where specific stream power was interpreted as a geomorphic indicator. Greater specific stream power means greater capacity to perform geomorphic work. Stream segments that contain

abrupt changes in specific stream power represent areas that are most likely susceptible to, or actively undergoing, accelerated channel adjustment relative to the system (Phillips & Desloges, 2014). Abrupt changes of specific stream power within the northern headwaters of the watershed were investigated during site reconnaissance where land access was permitted.

4.1.2 Site Reconnaissance

The headwaters of Carruthers Creek consist of two main branches that merge at a confluence located near the middle of the watershed. These two branches, herein referred to as the West and East Branch, were investigated during site reconnaissance occurring on May 23, 2019. Land use in the headwaters of Carruthers Creek is predominantly rural cropland that is extensively tile drained. Based on observations made during site reconnaissance, the East and West Branches exhibit contrasting differences in channel and valley characteristics despite being surrounded by virtually identical land use and hydrologic conditions. The West Branch is characterized by unconfining valley walls, a wide floodplain, tall grass and shrub riparian vegetation, a low width to depth ratio, meandering planform geometry and riffle-run-pool morphology. The East Branch is characterized by confining valley walls, a densely wooded riparian vegetation buffer, a high width to depth ratio, straight planform geometry, and a relatively high proportion of cobbles and boulders. Available aerial photography dating as far back as 1955 can neither confirm nor deny if historical channel straightening occurred along the East Branch to expand adjacent agricultural table lands. It is also unclear if the uncharacteristically large cobbles and boulders present in the East Branch were fluvially deposited or cleared off adjacent agricultural fields into the channel. The study reach was ultimately established along the West Branch to eliminate the added uncertainty of potential historic anthropogenic channel impacts suspected along the East Branch.

The study reach consists of an approximate 190 m long segment of the West Branch situated within the sub-basin outlined in Figure 27. The study reach extents were delineated to include an observed headcut erosional feature while remaining far enough upstream of a beaver dam structure to avoid backwater effects. The headcut is a prominent geomorphic feature that represents active channel adjustment. The channel bed immediately upstream of the headcut is composed of consolidated till material with embedded gravel particles. Similar till material is exposed sporadically throughout the study reach along the channel toe-of-bank. Coarse sediment appears to be supplied to the system through release from exposed till material as it progressively and episodically erodes. The study reach is classified as semi-alluvial as the channel is composed of a shallow mobile layer containing eroded till material that overlays the largely immobile consolidated till layer.

Beavers were observed throughout the West Branch during site reconnaissance where a series of several dam structures exist. The beaver dam situated furthest upstream along the West Branch is located approximately 150 m downstream of the study reach. A review of aerial photography and satellite imagery was completed to investigate historic changes in the creek and identify any modifications possibly made by humans or beavers along the study reach. No beaver activity or direct human modifications were noted along the study reach based on the review of imagery dating as early as 1955.

4.2 Methods

The following chapter describes methods that were adopted to perform baseline data collection and analysis at the Carruthers Creek study site. Procedures were undertaken to characterize channel morphology and monitor water levels and bedload transport.

4.2.1 Hydrology

Water levels were recorded using a Seametrics PT2X pressure and temperature sensor. Temperature and barometrically compensated water depth measurements were recorded at 5-minute intervals. The sensor was housed within a perforated well situated immediately upstream of the riffle that contains bedload monitoring instruments. This configuration was arranged so that water level measurements and bedload transport observations were gathered at a single location.

The water level record was verified against data collected by GeoProcess Research Associates Inc. (GRA) at Carruthers Creek. GRA maintains a streamflow gauge located approximately 450 m upstream of the bedload monitoring station and has established a stage-discharge rating curve. A watershed drainage area scaling relationship was applied to the GRA streamflow record to obtain a discharge hydrograph at the monitoring station outlet:

$$Q_1 = Q_2 \left(\frac{A_{d1}}{A_{d2}}\right)^{\beta} \quad (2)$$

where Q_1 is the instantaneous discharge of drainage area one [m^3/s]; Q_2 is the instantaneous discharge of drainage area two [m^3/s]; A_{d1} is the area of drainage area one [m^2]; A_{d2} is the area of drainage area two [m^2]; and β is an empirical exponent set to a value of 0.863 as estimated by statistical regression for the Toronto and Region area (Phillips & Desloges, 2014).

4.2.2 Substrate Characterization

Channel bed substrate was studied by conducting modified Wolman (1954) pebble counts, and collecting diagnostic volumetric bedload samples (Bunte & Abt, 2001; M.G. Wolman, 1954). A Pebble count is a two-dimensional sampling method which characterizes the population of surficial streambed particles, thus providing insight into bed roughness. Pebble counts were completed along representative channel lengths predominantly consisting of riffle bedforms. One pebble

count was conducted downstream of the headcut and a second was completed upstream of the headcut to examine differences with respect to this erosional feature. For each pebble count, the a-, b-, and c-axis dimensions were recorded for a minimum of 200 randomly sampled bed particles following the Bevenger and King (1995) zig-zag sampling pattern.

Diagnostic volumetric bedload sampling is a three-dimensional method which encompasses vertical stratification of the active armour layer and describes a different population of streambed particles than a pebble count (Bunte & Abt, 2001). Diagnostic volumetric bedload samples were collected along active gravel bars using an open-bottomed bucket sampler with a diameter of 30 cm. Individual samples were gathered by driving a bucket sampler into a gravel bar and excavating the enclosed substrate to a depth of twice the b-axis dimension of the D_{90} surface particle (Bunte & Abt, 2001; Simons & Şentürk, 1992). A sieve analysis was completed to determine the grain size distribution of each sample using successive half-phi class sieves.

4.2.3 Geomorphic Survey

A geomorphic survey was completed along the study reach to characterize channel cross-sectional geometry, gradient, and bed morphology. Topographic survey points were collected using a Sokkia GRX2 real time kinematic (RTK) global positioning system (GPS) receiver (± 4 cm error). Cross-sections were surveyed along the study reach capturing representative valley geometry and morphological geometry of riffle, run and pool features. Survey points were collected along the channel centerline profile approximately every 1 - 2 channel widths in addition to inflection points and geomorphic features. Geomorphic features encompassed in the channel profile survey included riffle heads, tails and crests, and the bottom of prominent pools.

4.2.4 Photographic Inventory

A photographic inventory was compiled to visually document field conditions and geomorphic features of interest during successive site visits. Photographs of vegetation growth, water level, bedload transport activity, bank erosion, and headcut advancement were collected. The record provided visual verification that was compared against bedload transport data collected by the monitoring station.

4.2.5 Bedload Transport Monitoring

Bedload transport dynamics were monitored at Carruthers Creek using a remote, integrated, automatic and continuous bedload monitoring station setup as described in Chapter 3. The station integrates three unique bedload monitoring methods including automatic RFID tracer stone particle tracking, passive acoustic monitoring with a series of two modified Benson Type-A impact plates, and direct physical sampling with a Bunte sediment trap.

4.2.5.1 Tracer Particle Tracking

Particle movement was tracked using custom synthetic tracer stones equipped with embedded RFID passive integrated transponder (PIT) tags. A total of 400 synthetic RFID tracer stones divided into 4 half-phi size classes were seeded at the study site as summarized in Table 3.

Table 3. Summary of Bedload Monitoring Method Characteristics

Phi Class	Surface Particle Size Percentile	Avg. Tracer Diameter [mm]	Quantity	Tracer Type
-4.5	D_{60}	28.5	125	Standard
-5.0	D_{75}	41.5	125	Standard
-5.5	D_{80}	56.2	75	Wobblestone
-6.0	D_{90}	89.2	75	Wobblestone

The four synthetic tracer stone half-phi size classes were selected to represent the coarse fraction of the surface particle grain size distribution. The a-, b-, and c-axis dimensions of the pebble count

particles were analyzed to identify the typical particle shape of each size class following the approach outlined by Zingg (1935) as presented in Figure 29. Synthetic tracer molds were made from actual stones selected from Carruthers creek with shape factors that generally matched the typical particle shape of the respective size class.

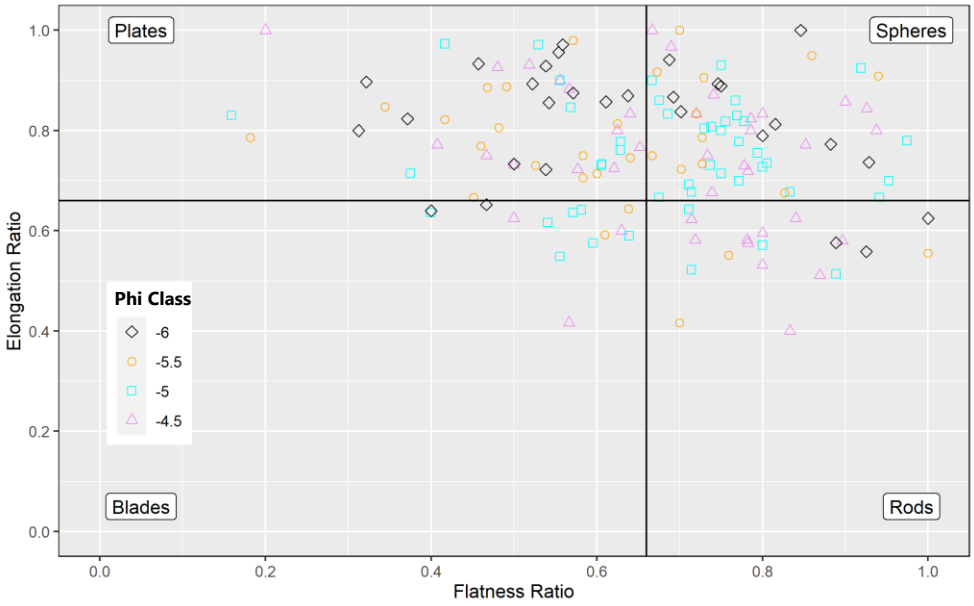

Figure 29. Pebble count particle shape categorized by half-phi class.

Ideally it would be desirable if all tracer stones were manufactured as Wobblestones due to their advantages over standard tracers; however, the minimum size of a Wobblestone synthetic tracer is limited by the size of the tag insert (16 mm) and the resulting clast density due to the void space created by the tag insert. As a result, the smallest two tracer size classes were manufactured with a directly embedded RFID transponder tag to maintain a clast density comparable to that of a natural stone. The minimum size of a standard synthetic tracer stone is physically limited by the c-axis dimension which must accommodate the length of the 12 mm RFID tag. Thus, the smallest tracer size class signifies the smallest manufacturable particle that can house a RFID tag and retain a representative shape factor. The likelihood of losing a small standard RFID tracer stone due to

burial or electromagnetic masking is greater than a Wobblestone because the orientation of the RFID tag will be variable, thus a greater quantity of standard tracer stones were manufactured to compensate for anticipated tracer loss (Ferguson & Hoey, 2002; Papangelakis, 2019).

Wobblestone inserts and synthetic tracer stone clasts were manufactured according to the process outlined by Papangelakis et. al (2019). Stages of the Wobblestone insert assembly process are illustrated in Figure 30. Insert parts were cast from high-density polyethylene (HDPE) pellets using an injection mold machine and a custom aluminum mold. Individual inserts were assembled according to the following process: the bottom half of the inner ball was weighted with a mixture of coarse aluminum oxide (Al_2O_3) blasting abrasive and ©Smooth-On Smooth-Cast® 380 polyurethane resin at a ratio of 2:1, respectively. A RFID tag was placed into the bottom half holder with the copper coil oriented upwards. The inner ball was then assembled by securing the two halves together with a waterproof epoxy sealant. The bottom half of the outer ball was filled with a glycol lubricant consisting of 70% glycerin and 30% water. The assembled inner ball was then placed into the outer ball bottom half. Finally, the outer top and bottom halves were secured together with an exterior coating of waterproof epoxy sealant.

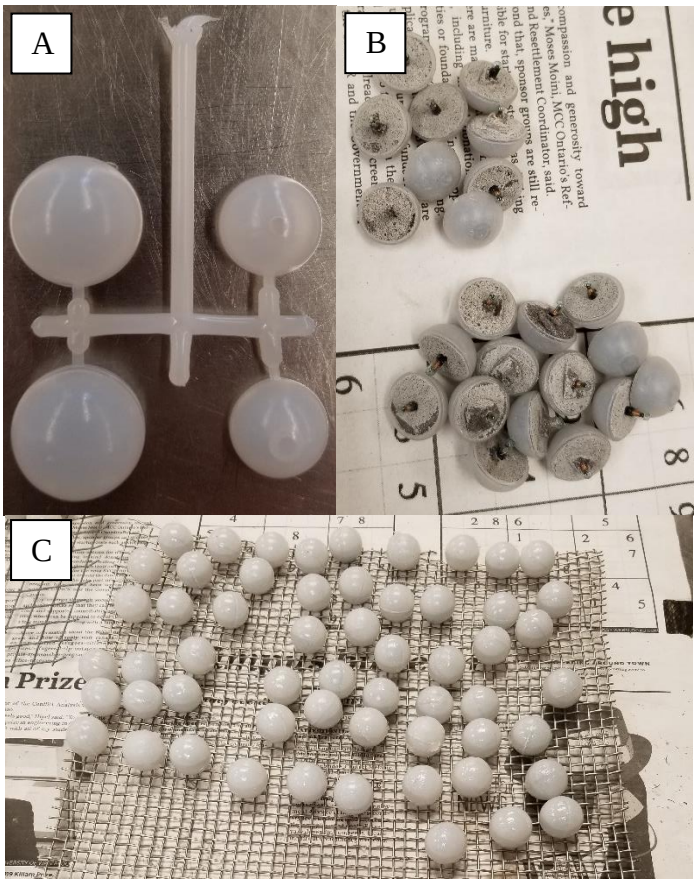

Figure 30. Wobblestone insert parts and assembly stages. (A) Raw part cast from HDPE injection mold. (B) Weighted inner ball bottom halves containing RFID tags. (C) Assembled Wobblestone inserts.

Reusable silicone molds of the 4 selected natural stones were created out of ©Smooth-On Mold Star™ 15 Slow silicone. Synthetic tracer stones were subsequently cast from the molds using a mixture of coarse aluminum oxide (Al_2O_3) blasting abrasive and ©Smooth-On Smooth-Cast® 380 polyurethane resin at a ratio of 2:1, respectively. To cast a synthetic tracer stone, the two halves of a given silicone mold were filled with the aluminum oxide and resin mixture. Then, either a Wobblestone insert or RFID tag oriented parallel to the c-axis was partially inserted into the centre of one mold half. Finally, the two halves of the mold were aligned together and placed under weight for approximately 1 hour to cast. As stone manufacturing progressed, Quikrete® all-purpose gravel was gradually added to the synthetic tracer stone mix as a filler to help offset the

high cost of resin and aluminum oxide materials. The stone molds, original stones, and synthetic tracer stones are displayed in Figure 31.

Figure 31. Particle tracking synthetic tracer stones, stone molds, and original stones.

A set of 20 additional standard synthetic tracer stones were manufactured to test tracer durability. The tracer stones were combined with a gravel mixture and placed inside a 0.55 m wide cement drum mixer for a total duration of 80 minutes at a speed of approximately 20 rpm. Based on visual observation, tracers were assumed to travel approximately 1.4 m per rotation for an estimated total travel length of approximately 2200 m. The percent difference of each tracer's pre- and post-experimental mass was calculated to quantify degradation. The average percent difference in tracer mass was 0.3% which represents a negligible difference that is unlikely to affect particle entrainment and mobility dynamics (Cain, 2019).

The 400 synthetic tracer stones were seeded upstream of the monitoring station by following a *pick-and-replace* methodology where a particle similar in size to a respective synthetic tracer stone was located on the creek bed and replaced by the tracer. When coarse gravel particles were not present on the creek bed (i.e. run and pool morphology) tracer stones were lightly pressed into the fine substrate of the bed. These procedures were adopted to emulate natural particle interlocking and imbrication, and minimize false preliminary tracking observations as a result of the

experimental design (Chapuis et al., 2015; Papangelakis, MacVicar, et al., 2019). To evenly distribute the tracer stones, the study reach was divided into 9 m segments where a subset of 16 synthetic tracer stones (3 each of the Wobblestone size classes and 5 each of the standard tracer size classes) were seeded. The first 4 segments upstream of the bedload monitoring station were seeded with twice this density (32 tracer stones per 9 m segment) to increase the opportunity for preliminary automatic tracking observations.

To facilitate automatic RFID tracer stone tracking, an appropriately sized rectangular loop antenna was configured to align with the dimensions of Carruthers Creek. The configured loop antenna complies with the OregonRFID ATC inductance range of 25 - 102 µH (Oregon RFID, 2019). A summary of the Carruthers Creek in-stream antenna characteristics is provided in Table 4.

Table 4. Carruthers Creek In-stream Antenna Characteristics

Property	Value	Units
Length	1.6	m
Width	1.0	m
Loop Turns	3	-
Antenna Inductance	43.5	µH

The antenna was buried slightly below the mean streambed elevation along a relatively straight riffle section located downstream of the seeded tracer stones. The antenna housing was keyed into the channel banks with the upstream edge aligned with the riffle crest. An antenna tuner box was mounted above ground on a wood post located within the floodplain floor adjacent to the in-stream antenna to compensate for natural electromagnetic interference (Oregon RFID, 2019). The SAR is configured to scan for tracer stones at a rate of 5 Hz consisting of a 50 ms charge time and a 150 ms listening period during competent flow events when the water level rises to 0.2 m above the PT2X sensor. Manual tracking was periodically conducted using a mobile loop antenna (OregonRFID pole antenna and LF HDX Backpack Reader) and stick antenna (OregonRFID

AEA580 antenna with a Data Tracer II FDX/HDX Reader). The loop and stick antenna possess a detection range of approximately 0.5 m and 0.2 m, respectively (Chapuis et al., 2014).

4.2.5.2 Passive Acoustic Monitoring

Bedload acoustic monitoring was conducted using a series of two modified Benson Type-A impact plates. The plates were instrumented along the same riffle as the in-stream antenna to make direct comparisons and minimize environmental variability between the two monitoring methods. The Type-A impact plates were modified by the manufacturer for increased plate sensitivity to typically detect particles with a b-axis diameter of 10 - 12 mm. The impact plates were mounted on top of individual concrete blocks buried into the streambed. The surface of the impact plates rested flush with the local mean streambed surface.

The impact plate data record was analyzed using a bedload transport rate estimation model developed by Soar & Downs (2017) called "Bedload from Impact Plates" (BLIP). The BLIP model produces a supply-limited, location specific, high resolution times series of bedload transport rates using the impact plate counts, a corresponding water level record, and information about channel geometry, substrate size, and particle shape (Soar & Downs, 2017). The model includes a user-specified parameter range for Shields' dimensionless critical shear stress corresponding to the median particle size (D_{50}). The dimensionless critical shear stress range was set to 0.04 – 0.05 which is typical of gravel bed rivers according to visually-based incipient motion research studies (Buffington & Montgomery, 1997).

The BLIP model accepts a time series of impact count aggregates for each plate and outputs a corresponding time series of bedload sediment yield ($\bar{Y}_{(N)t}$). Total bedload yield at each timestep ($\bar{Y}_{(total)t}$) is calculated by applying a linear interpolation equation that interprets each plate as a

shear stress panel along the channel cross-section and assumes zero transport at the section margins as shown in Figure 32.

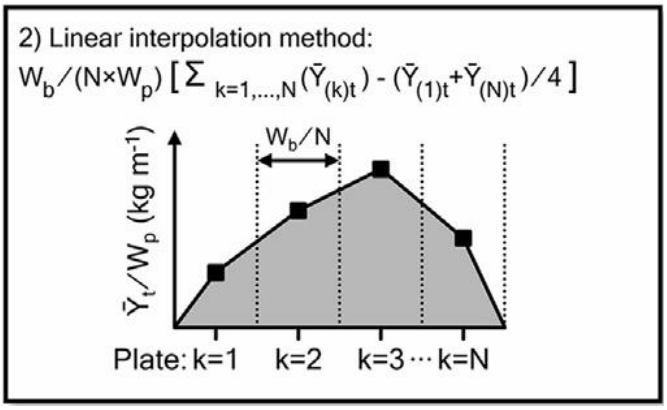

Figure 32. Linear interpolation method applied to obtain total bedload sediment yield from BLIP model outputs. From (Soar & Downs, 2017).

4.2.5.3 Direct Physical Sampling

A Bunte trap physical sampler was installed along the riffle located immediately downstream of the impact plates (Bunte et al., 2007). The trap was aligned with the channel thalweg and was secured to an aluminum ground plate that rested flush with the local mean streambed surface. The trap consisted of a mesh netting that allowed passage of particles with a b-axis diameter less than 3 mm. Samples were periodically retrieved from the trap following significant flow events for lab analysis.

4.2.6 Field Installation

The bedload monitoring station was installed at the Carruthers Creek study site over a period of four days from August 13, 2019 to August 16, 2019. A tabletop frame was constructed to elevate the electronics enclosure above the floodplain floor and to function as a solar panel mount. All wires and cabling were routed underground from the instruments to the electronics enclosure. The bedload monitoring station field setup is displayed in Figure 33 and the contents of the electronics enclosure are shown in Figure 34.

Figure 33. Carruthers Creek bedload monitoring station. (A) Tabletop frame, solar panels, and electronic equipment enclosure located within river-left overbank zone. (B) View facing upstream showing water level sensor (top-right), in-stream antenna (centre) and impact plates (bottom). (C) View facing downstream showing sediment trap. (D) Seeded tracer stone (photo credit: Bruce MacVicar).

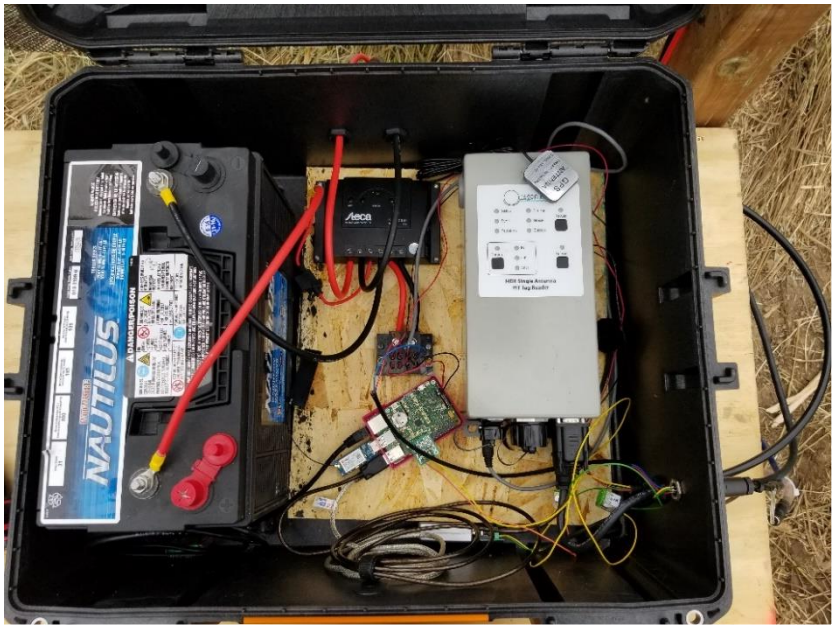

Figure 34. Electronics enclosure contents including MotoMaster deep cycle battery, Steca solar charge controller, OregonRFID SAR, and Raspberry Pi. Wire and cables enter enclosure via water-tight feedthrough seals.

4.3 Results

4.3.1 Geomorphic Characterization

The geomorphic survey included the collection of 2 volumetric bedload samples, 2 pebble counts, and 9 surveyed cross-sections (4 riffle-run sections and 5 pool sections) across the surveyed longitudinal profile. Figure 35 illustrates points of interest along the surveyed longitudinal profile including the locations of substrate samples, and study reach extents as delineated by the monitoring station and tracer stone upstream seeding limit. The monitoring station riffle crest cross-sectional and corresponding bankfull stage is illustrated in Figure 36. The grain size distributions of the sediment samples are presented in Figure 37.

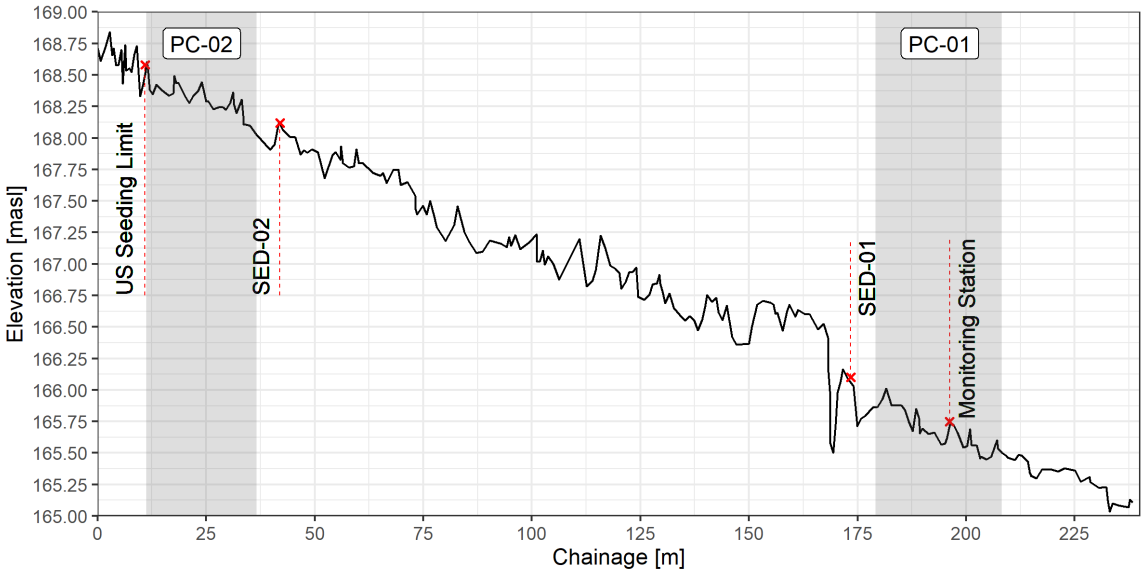

Figure 35. Study reach longitudinal profile displaying locations of the volumetric bedload samples (SED), pebble counts (PC), monitoring station and upstream tracer stone seeding limit.

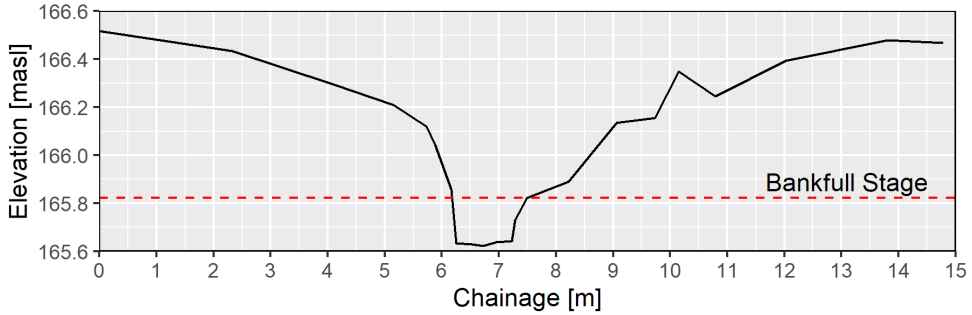

Figure 36. Carruthers Creek monitoring station riffle crest cross-section and bankfull stage.

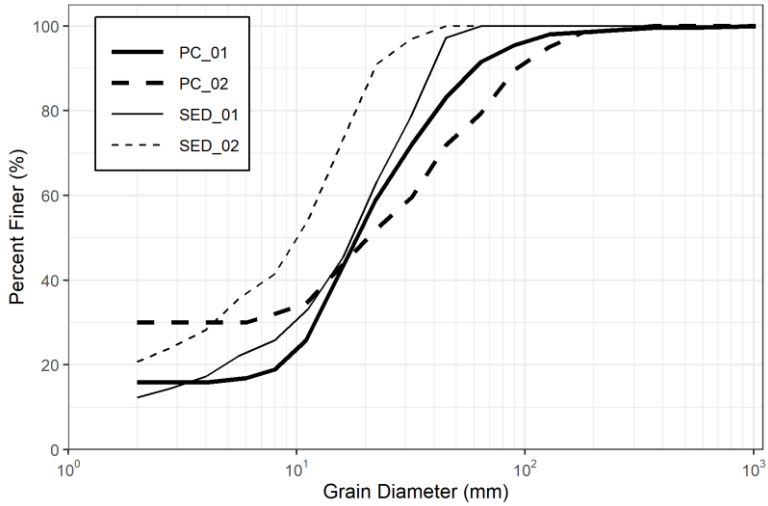

Figure 37. Grain size distributions of pebble count and volumetric bedload samples.

The pebble count data was used to estimate a bed surface roughness coefficient (n) according to the following equation:

$$n = 0.039\, k_s^{1/6} \tag{3}$$

where k_s is the equivalent bed roughness (D. A. Chin, 2013). Equivalent bed roughness was calculated according to the relationship proposed by López and Barragan (2008):

$$k_s = 2.8\, D_{84} \tag{4}$$

where D_{84} is the 84th percentile surface particle diameter of the combined pebble counts set to a value of 0.06 m. The study reach geomorphic characteristics are summarized in Table 5.

Table 5. Carruthers Creek Study Reach General Characteristics

Parameter	Value	Units
Sub-Basin Drainage Area	1.5	km^2
Study Reach Length	190	m
Slope	1.47	%
Surface Roughness Coefficient (n)	0.029	-
Mean Bottom Width	0.80	m
Mean Bankfull Width	1.15	m
Mean Bankfull Depth	0.22	m

The riffle cross-section presented in Figure 36 is characterized as moderately entrenched with an entrenchment ratio of 2.1 based on the quantitative expression defined by Rosgen (1994). This moderate ratio indicates that the creek may have undergone downcutting. The headcut located at chainage station 165 m in Figure 35 is a significant geomorphic feature that represents active channel adjustment. Differences in geomorphic parameters are evident when comparing the segments situated upstream and downstream of the headcut. Channel widening is apparent downstream of the headcut as evidenced by surveyed cross-sections for both riffle-run and pool cross-sections. Pebble counts and volumetric bedload samples indicate that channel bed substrate

also differs slightly along the study reach depending on location relative to the headcut. The downstream grain size distribution is generally coarser than upstream in exception to the surficial substrate data (pebble counts) in which case the fraction of particles with a diameter greater than approximately 15 mm is coarser upstream. The headcut appears to be a prominent sediment supply source to the creek through gradual and episodic erosion, which may account for general downstream coarsening and excess supply of fine to moderately sized sand and gravel particles along the bed surface. Headcut advancement was periodically surveyed over the duration of the study as illustrated in Figure 38.

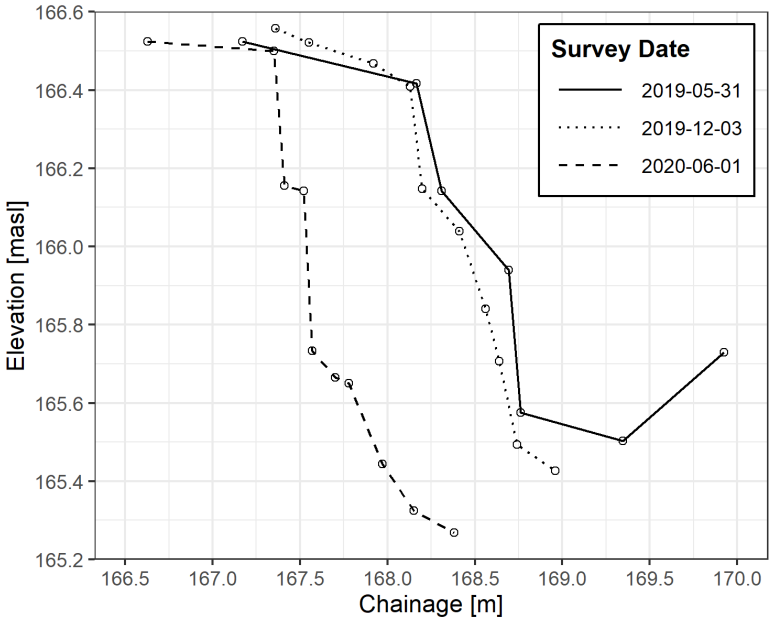

Figure 38. Profile view of headcut advancement over study period.

The profile surveyed on June 1, 2020 demonstrates the result of a significant episodic erosion event that occurred sometime between March 3 - 17, 2020. The headcut advanced approximately 0.8 m upstream during this event. It is believed that freeze-thaw cycles likely contributed towards the abrupt and clear-cut release of till. Figure 39 compares the headcut before and after the event and shows the size of gravel particles embedded within the till layer.

Figure 39. Visual comparison of headcut over study duration. (A) Headcut location on May 23, 2019. (B) Significant advancement first observed on March 17, 2020. (C) View of gravel particles embedded within till on June 1, 2020 (Photo credit: Bruce MacVicar).

4.3.2 Critical Threshold Assessment

Papangelakis et al. (2020) developed a predictive model of bedload particle transport using extensive RFID bedload tracer data collected from three study streams in Southern Ontario, each characterized by unique catchment hydrology (rural, urbanized with SWM, and urbanized without SWM). For every tracer recovery survey completed, Papangelakis et al. (2020) calculated bedload transport parameters for each tracer stone size class "*i*" including the fraction of tracer stones that moved (f_{mi}), the geometric mean travel distance of the tracer stones that moved (L_i), and the weighted median travel length ($\tilde{L}_i$) calculated as the product of f_{mi} and the median travel length. Papangelakis et al. (2020) performed single- and multi- parameter linear regression analyses to relate the resulting parameters with a variety of peak and cumulative flow metrics to determine which metrics best predict bedload transport. Peak flow metrics describe flow magnitude and are determined as the maximum parameter value observed during an event, while cumulative flow metrics describe both flow magnitude and duration as illustrated in Figure 40.

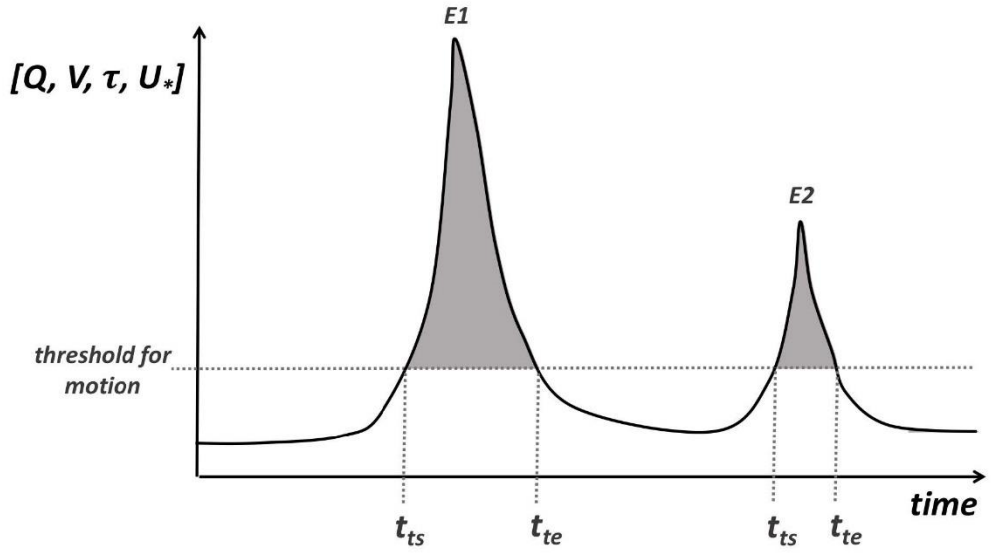

Figure 40. Conceptual diagram of cumulative flow metrics. From (Papangelakis, 2019)**.**

A cumulative flow metric, such as discharge (Q), velocity (V), shear stress (τ), or shear velocity (U_*), is calculated as the area under the hydrograph curve that exceeds the particle entrainment threshold, as indicated by the grey shaded area in Figure 40. The result of the linear regression analysis was the development of an equation that performed exceptionally well at modelling weighted median travel lengths across the observed rural and urban study sites ($R^2 = 0.91$):

$$\frac{\tilde{L}_i}{B} = 1.4\text{x}10^{-5}(CEQ) \tag{5}$$

where CEQ [m^3] is the cumulative excess discharge calculated as the instantaneous discharge (Q_t) less the critical discharge ($Q_{c(i)}$) (Papangelakis et al., 2020). Equation (5) was applied to the Carruthers Creek study site for the purpose of making predictions of bedload transport. Critical discharge was estimated for each tracer size class by first determining the respective dimensionless criticial shear stress ($\tau^*_{c(i)}$). In order to account for interactions between particle size classes (entrapment and interlocking), a hiding function was applied (Parker & Klingeman, 1982; Wilcock, 1988):

$$\frac{\tau^*_{c(i)}}{\tau^*_{c(D50)}} = \left[\frac{D_i}{D_{50}}\right]^b \tag{6}$$

Where $\tau^*_{c(D50)}$ is the dimensionless critical shear stress of the median particle size [-]; D_i is the diameter of the respective tracer size class [mm]; D_{50} is the median particle diameter [mm]; and b is the exponential coefficient set to a value of -0.75 [-] to match Papangelakis' field calibrated value of the rural Ganatsekiagon Creek study site. Three values of the parameter $\tau^*_{c(D50)}$ were assessed to consider the range in typical values for gravel bed rivers (Buffington & Montgomery, 1997): a) 0.047 [-] typical of visually-based incipient motion studies; b) 0.07 [-] typical of reference-based incipient motion studies; and c) 0.082 [-] which is Papangelakis' field calibrated

value for Ganatsekiagon Creek. Critical shear stress ($\tau_{c(i)}$) was then calculated following the relationship developed by Shields (1936):

$$\tau_{c(i)} = \tau^*_{c(i)}(\rho_s - \rho_w)gD_i \quad (7)$$

where ρ_s is the tracer density [kg/m^3]. Critical shear stress was then expressed in terms of channel geometry by calculating hydraulic radius:

$$R_{h(i)} = \frac{\tau_{c(i)}}{\rho_w g S} \quad (8)$$

Critical discharge was calculated with respect to the geometry of the gauged cross-section (Figure 36) using an at-a-station hydraulic model that follows Manning's equation:

$$Q_{c(i)} = \frac{A(R_{h(i)})^{\frac{2}{3}} S^{\frac{1}{2}}}{n} \quad (9)$$

Where *A* is the wetted cross-sectional area [m^2]. The resulting critical threshold estimates for each tracer size class with respect to the varying $\tau^*_{c(D50)}$ parameter is summarized in Table 6 to Table 8.

Table 6. Summary of Tracer Stone Critical Thresholds ($\tau^*_{c(D50)}$ = 0.047 [-])

Phi Class	Mean Tracer Diameter [mm]	Dimensionless Critical Shear Stress [-]	Critical Shear Stress [Pa]	Critical Discharge [m^3/s]	Critical Stage [masl]
-4.5	28.5	0.035	16.4	0.16	165.78
-5.0	41.3	0.027	18.0	0.20	165.80
-5.5	56.0	0.021	19.4	0.24	165.81
-6.0	89.4	0.015	21.8	0.52	165.91

Table 7. Summary of Tracer Stone Critical Thresholds ($\tau^*_{c(D50)}$ = 0.07 [-])

Phi Class	Mean Tracer Diameter [mm]	Dimensionless Critical Shear Stress [-]	Critical Shear Stress [Pa]	Critical Discharge [m^3/s]	Critical Stage [masl]
-4.5	28.5	0.053	24.4	0.65	165.94
-5.0	41.3	0.040	26.8	0.78	165.97
-5.5	56.0	0.032	28.9	0.91	166.00
-6.0	89.4	0.022	32.5	1.15	166.05

Table 8. Summary of Tracer Stone Critical Thresholds ($\tau^*_{c(D50)}$ = 0.082 [-])

Phi Class	Mean Tracer Diameter [mm]	Dimensionless Critical Shear Stress [-]	Critical Shear Stress [Pa]	Critical Discharge [m^3/s]	Critical Stage [masl]
-4.5	28.5	0.062	28.6	0.89	166.00
-5.0	41.3	0.047	31.3	1.07	166.03
-5.5	56.0	0.037	33.8	1.26	166.07
-6.0	89.4	0.026	38.0	1.69	166.13

The cumulative excess discharge pertaining to each tracer size class and $\tau^*_{c(D50)}$ value was calculated for the period between seeding and the final tracking survey. Resulting weighted median travel length estimates are summarized in Table 9 and compared to surveyed travel lengths in Chapter 4.3.3.

Table 9. Weighted Median Travel Length Estimates for Study Tracking Period

Phi Class	$\tilde{L}_i$ [m] ($\tau^*_{c(D50)}$ = 0.047 [-])	$\tilde{L}_i$ [m] ($\tau^*_{c(D50)}$ = 0.07 [-])	$\tilde{L}_i$ [m] ($\tau^*_{c(D50)}$ = 0.082 [-])
-4.5	2.8	1.5	1.1
-5.0	2.6	1.3	0.9
-5.5	2.5	1.1	0.7
-6.0	1.8	0.8	0.3

4.3.3 Tracer Particle Tracking

The bedload monitoring station documented movement of a single RFID tracer stone during a significant flow event that occurred between January 11 - 13, 2020 as demonstrated in Figure 41.

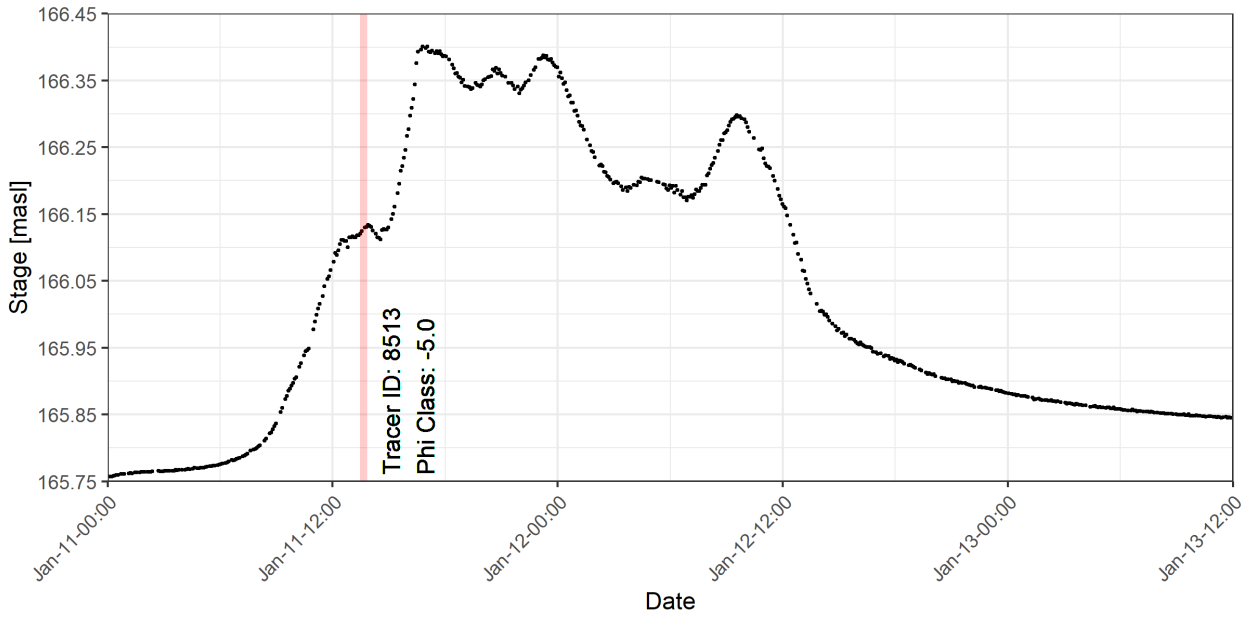

Figure 41. In-flood RFID tracer stone movement during January 2020 flow event**.** Red shading signifies the duration for which tracer stone 8513 remained within the antenna detection zone.

Tracer stone 8513 mobilized over the antenna on January 11 at 08:27:53 EST and remained within the antenna detection zone for a duration of approximately 25 minutes before exiting at 08:51:28 EST. The timing of the movement corresponds with the rising limb of a local peak in the hydrograph. Disruptions to station power supply and storage components (including insufficient capacity and equipment theft) unfortunately precluded further observation of in-flood tracer stone movement during the study period; however, upgrades were added to improve station power capacity and deter theft. As a result, particle tracking observations were largely supplemented in this study through the collection of manual inter-flood tracking data.

Tracer stone movement was tracked manually on two occasions during December 2019 and June 2020 where recovery rates of 91.5% and 86.8% were achieved, respectively. These recovery rates are comparable to other inter-flood particle tracking studies that also use synthetic tracer stones with embedded 12mm RFID tags such as Cain (2019) who achieved recovery rates as high as 88%. A comparison of tracer movement with respect to size class was completed by calculating

fractional mobility, mean travel length, weighted median travel length, and mean annual velocity over the complete study period duration. The fraction of tracers that moved for each size class (f_{mi}) was calculated according to the following equation:

$$f_{mi} = \frac{m_{(i)}}{n_{(i)}} \tag{10}$$

where $m_{(i)}$ is the number of tracers that moved; and $n_{(i)}$ is the total number of tracers recovered. A tracer was considered mobile if it travelled a distance greater than the detection range of the respective antenna device. Tracers located by the stick antenna or loop antenna were deemed mobile if they travelled more than 0.5 m or 1 m, respectively, following recommendations by Papangelakis (2019). A binomial proportion confidence interval of fractional mobility was calculated according to the following equation:

$$CI_{95} = \pm z_{(1-\frac{\alpha}{2})}\sqrt{\frac{F_{mi}(1-F_{mi})}{n_{(i)}}} \tag{11}$$

where α is the significance level set to 0.05; $z_{(1-\frac{\alpha}{2})}$ is the tabulated "z"-factor of a standard normal distribution. The resulting tracer stone fractional mobility is presented in Figure 42.

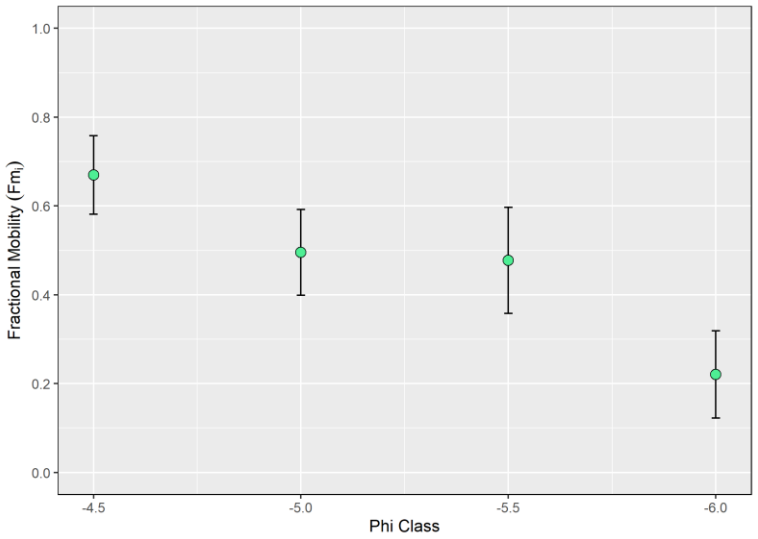

Figure 42. Tracer stone fractional mobility**.**

Figure 42 demonstrates that the study reach exhibits size-selective transport whereby smaller particles have a greater tendency to become entrained compared to larger particles.

The travel length of each recovered tracer was calculated as the distance along the channel centerline between the initial and final tracer position. The average travel length of each size class was then calculated as the geometric mean to accommodate the high level of skewness present within the distribution of travel lengths and better represent the central tendency (MacVicar et al., 2015; Papangelakis, 2019). A confidence interval was calculated for the mean travel length of each size class according to the following equation:

$$CI_{95} = \pm 10^{\left[z_{(1-\frac{\propto}{2})} \cdot \frac{\sigma_{(i)}}{\sqrt{n_{(i)}}} \right]} \quad (12)$$

where $\sigma_{(i)}$ is the standard deviation of the $\log_{10}$ transformed travel lengths. Mean travel lengths are universally characterized in literature through a variety of empirical relationships such as Church and Hassan (1992):

$$\frac{L_i}{L_{D50}} = (1 - log\frac{D_i}{D_{50}})^{1.35} \quad (13)$$

where L_i is the geometric mean travel length of the given tracer size class; L_{D50} is the mean travel length of the tracer size class that represents the median surface substrate particle diameter; D_i is the diameter of the given tracer size class; and D_{50} is the median surface substrate particle diameter (Church & Hassan, 1992). Vazquez-Tarrio et al. (2019) developed an alternative scaled travel length relationship through the analysis of tracer data from 33 scientific papers:

$$log\left(\frac{L_i}{L_{D50}}\right) = -0.26\left(\frac{D_i}{D_{50}}\right) + 0.26 \quad (14)$$

To compare scaled travel lengths of the tracer data to literature relationships, the L_{D50} scaling parameter had to be assumed as the tracer size classes are not representative of the median particle size. As a result, the geometric mean travel length and diameter of the smallest tracer size class (D_{60}) were used for scaling. The resulting scaled travel lengths of the tracer size classes are presented in Figure 43.

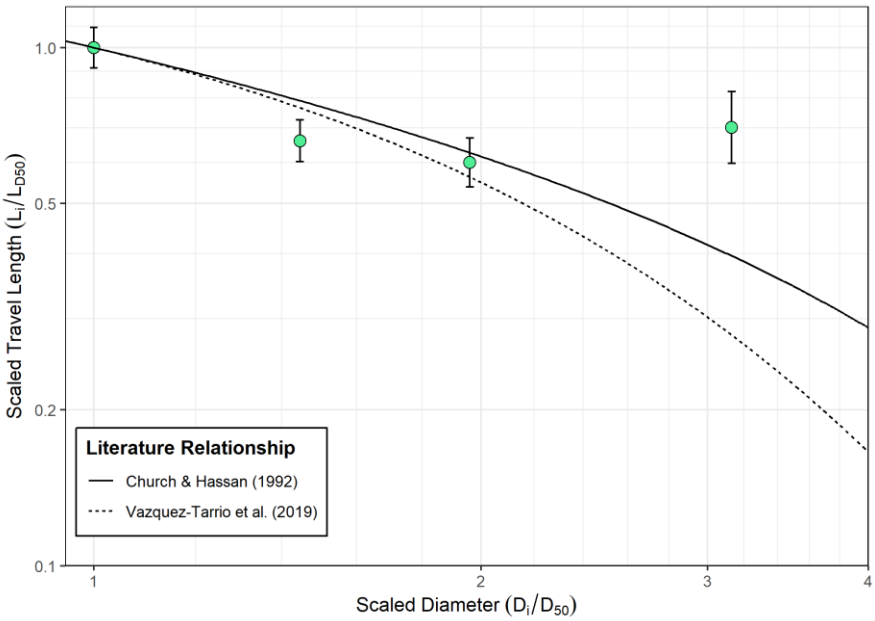

Figure 43. Tracer stone scaled travel lengths compared to literature relationships**.**

The Carruthers Creek scaled travel lengths generally align with the literature relationships in exception to the -6.0 half-phi class. This observation is likely a temporal effect as travel lengths are commonly exaggerated immediately following seeding (MacVicar & Roy, 2011). The scaled travel length of the -6.0 half-phi class will likely align better with the literature relationships over time as tracers become sufficiently water-worked or buried.

The weighted median travel length of each tracer size class ($\tilde{L}_i$) was calculated by multiplying the surveyed median travel lengths by the respective value of f_{mi}. Resulting $\tilde{L}_i$ values are compared to estimates derived from the cumulative excess discharge analysis (Table 9) as demonstrated in Figure 44.

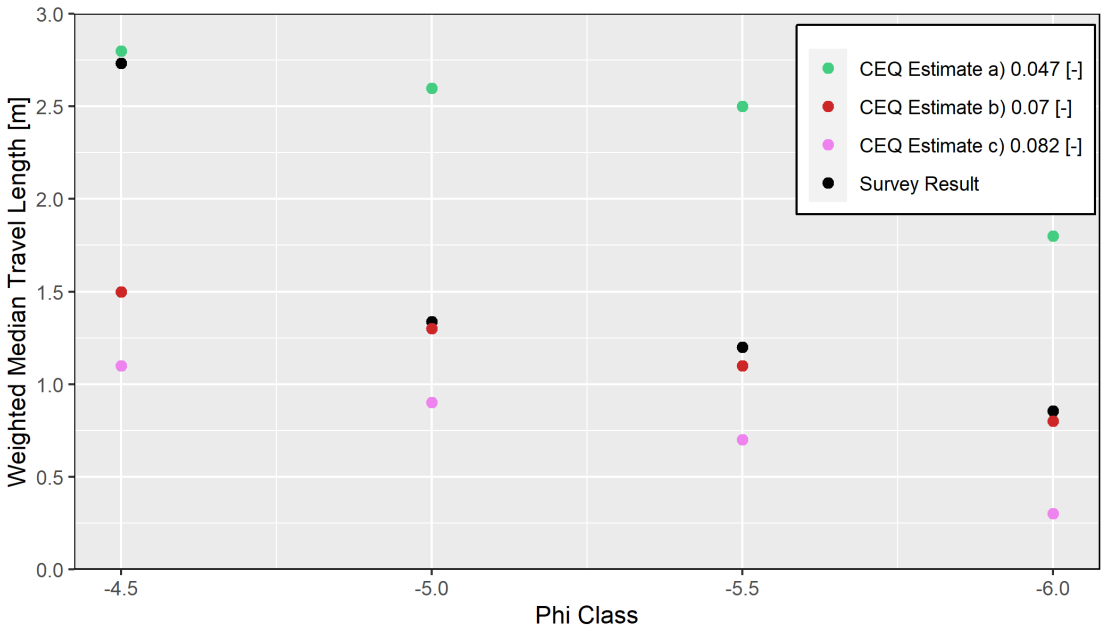

Figure 44. Comparison of surveyed weighted median travel lengths against estimates derived from cumulative excess discharge analysis. Estimates correspond to varying dimensionless critical shear stress values assumed for the median grain size.

Figure 44 reveals that Papangelakis' linear regression model (Equation (5)) is capable of estimating $\tilde{L}_i$ values that are representative of measured field results. Critical thresholds corresponding to an assumed $\tau^*_{c(D50)}$ value of 0.07 [-] result in $\tilde{L}_i$ estimates that nearly match

measured values for the -5.0 to -6.0 phi classes, but underestimate the -4.5 phi class. In contrast, critical thresholds corresponding to an assumed $\tau^*_{c(D50)}$ value of 0.047 [-] result in $\tilde{L}_i$ estimates that closely match the -4.5 phi class, but overestimate the -5.0 to -6.0 phi classes. This observed discrepancy is likely attributed to the effects of channel geometry; assuming a $\tau^*_{c(D50)}$ value of 0.07 [-] results in a critical stage for the -4.5 phi class that is above bankfull stage (Table 7), while assuming a $\tau^*_{c(D50)}$ value of 0.047 [-] results in a critical stage below bankfull (Table 6). Figure 44 indicates that the -4.5 phi class is entrained below bankfull stage and thus is better represented by a relatively lower $\tau^*_{c(D50)}$ value. Accordingly, a relatively higher $\tau^*_{c(D50)}$ value is more appropriate for the larger size classes that appear to become entrained above bankfull stage where energy is dissipated in the floodplain. Overall, the accuracy of the linear regression model is expected to improve over time through continued field calibration of critical thresholds.

The mean annual velocity of each tracer size class was calculated as the geometric mean travel length of all tracers (mobile and immobile) divided by the study duration (approximately 0.8 years). Although the study duration is shorter than the 2-year timeframe recommended by Houbrechts et al. (2015), mean annual velocity was calculated to gain a general sense of how the tracer results compare against other study sites. Figure 45 compares the mean annual velocities of Carruthers Creek to Papangelakis (2019) who conducted RFID tracer studies at comparable sites in the Greater Toronto Area (GTA) including Wilket Creek, Morningside Creek, and Ganatsekiagon Creek.

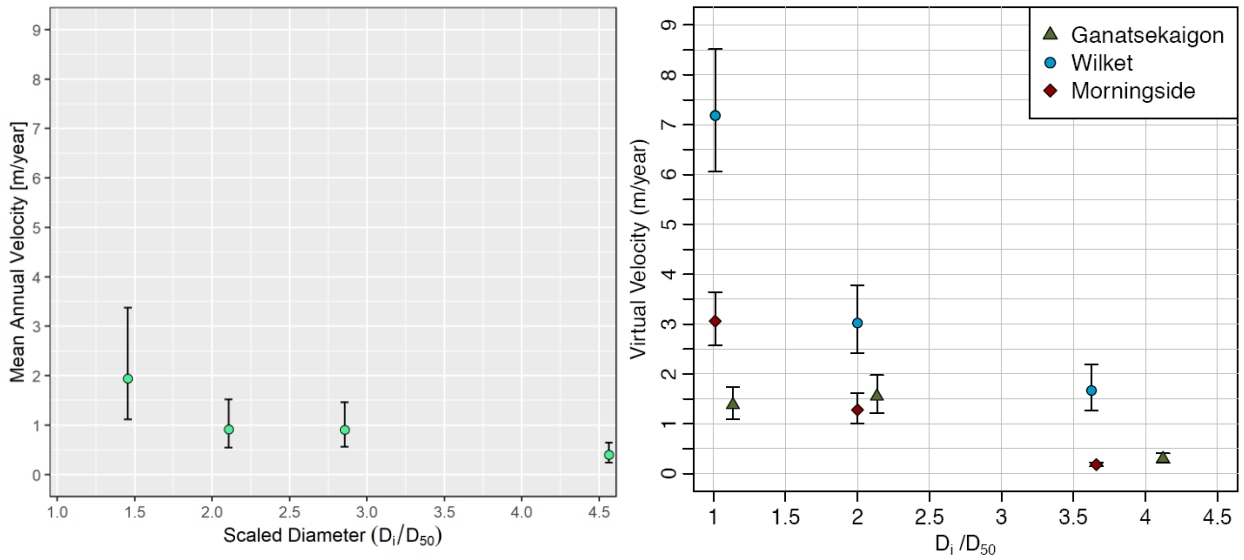

Figure 45. Tracer stone mean annual velocity. Comparing Carruthers Creek results (left) to Papangelakis (2019) (right) including results from Ganatsekaigon Creek, Wilket Creek, and Morningside Creek. From (Papangelakis, 2019).

Mean annual velocity of the Carruthers Creek tracers plots similarly to Papangelakis' (2019) results at Ganatsekaigon Creek (a rural watershed) and Morningside Creek (an urban watershed with SWM). Papangelakis (2019) found that similarities exist between these two watershed types as SWM practices help decrease tracer dispersion in urban settings, particularly for larger particles (Papangelakis, 2019).

The tracer stones are expected to predominantly congregate along riffle bedforms over time. A k-means cluster analysis was completed to evaluate the degree of tracer congregation observed over the study period. Figure 46 illustrates a plan-view layout of the tracer stones locations surveyed at the start and end of the study.

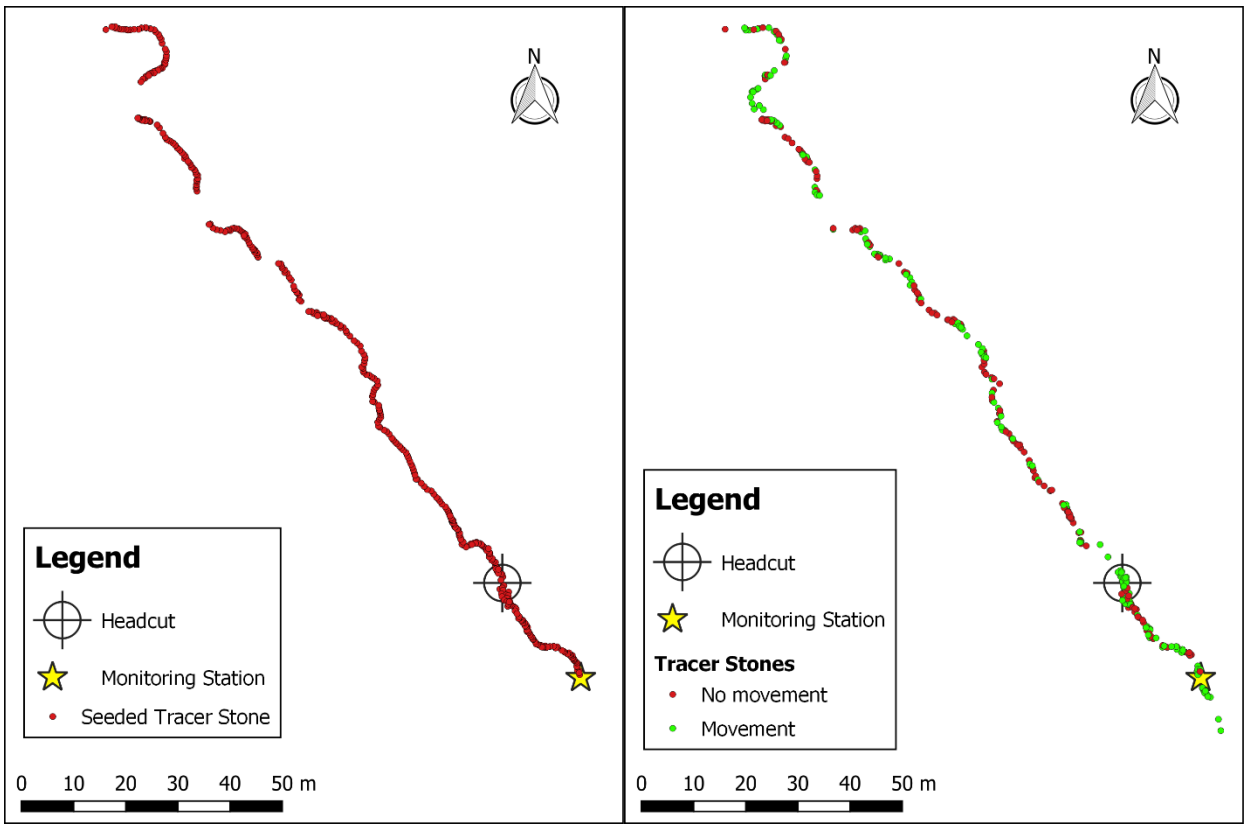

Figure 46. Study reach tracer stone layout. Plan-view of seeded locations on August 15, 2019 (left) and locations documented during the final tracking survey on June 12, 2020 (right).

The k-means cluster analysis was completed following the Hartigan and Wong (1979) algorithm, which functions by grouping the tracer stones into a user-specified number of clusters such that distances between cluster centroids and tracer stone coordinates are minimized. The seeding layout and final tracking survey were each analyzed by applying the k-means cluster algorithm with a varying number of cluster groups. The number of clusters were incrementally increased up to 30 groups, which roughly corresponds to the number of riffle bedforms present along the study reach assuming a typical pool spacing of 5 - 7 bankfull widths (Leopold et al., 1964). For every incremental cluster number, the algorithm was repeated 20 times to obtain a distribution of total within-cluster sum-of-squares error (SSE). Table 10 summarizes the resulting within-cluster SSE ranges corresponding to a 95% confidence interval for each cluster group number.

Table 10. Summary of K-Means Analysis Total Within-Cluster SSE Results

Number of Clusters	Seeding Layout SSE (95% CI Range)	Final Survey SSE (95% CI Range)	Mean SSE Percent Change
5	30352*	28079*	7.5 %
10	7773*	6786*	12.7 %
15	3118*	2909 – 2913	6.6 %
20	1860*	1705 – 1727	7.7 %
25	1197 - 1206	1078 – 1099	9.4 %
30	835 - 847	759 - 778	8.6 %

* Algorithm did not result in variable total within-cluster SSE.

A reduction in total within-cluster SSE is generally observed with increasing cluster group numbers for both the seeding layout and final tracking survey. The final tracking survey total within-cluster SSE is consistently lower than the seeding layout indicating that the tracer stones are forming tighter clusters. The number of tracers present immediately downstream of the headcut has increased over time, which indicates that a large proportion of tracers are accumulating at this erosional zone. The results of the k-means cluster analysis align with the expectation that tracers are forming tighter clusters, which over time may coincide with the typical spacing of riffle bedforms.

4.3.4 Bedload Impact Detections

A preliminary record of bedload impact counts was documented across several competent flow events observed between the period of Fall 2019 to Spring 2020. Rolling particles are expected to have a considerable influence on impact counts at the Carruthers Creek site because a large proportion of channel substrate is characterized as spherical based on pebble count shape factor results, shown in Figure 29, and thus have a greater tendency to roll (Turowski & Rickenmann, 2009). As a result, the raw data record was processed with an imposed sampling frequency filter to counteract multiple counts registered by rolling particles. The sampling frequency filter was set to 5 Hz, similar to Downs et al. (2016), and effectively suppresses impact counts recorded less

than 0.2 s apart. The filtered impact count data record was then aggregated over 5-minute intervals to visualize bedload transport intensity with respect to the streamflow hydrograph as demonstrated in Figure 47.

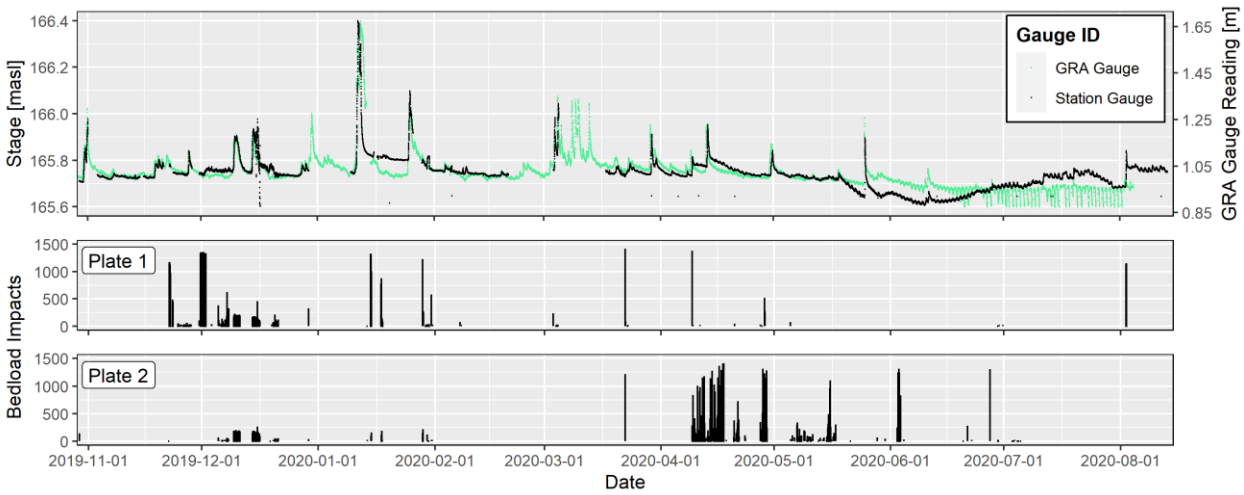

Figure 47. Aggregate bedload impacts summed over 5-minute time intervals. GRA gauge record superimposed onto station water level timeseries.

The preliminary record contains a number of data gaps caused by insufficient system power supply and storage. System power storage was upgraded on December 3, 2019 through the addition of a second battery. The station solar panel was stolen in late-February 2020, which precluded data collection until mid-March 2020 (in exception to a brief period in early-March when the system batteries were charged with a generator). The single stolen solar panel was eventually replaced by two new panels on March 17, 2020 to improve system power supply. The GRA water level record demonstrates that several significant flow events were missed by the station in late-December 2019 and early- to mid-March 2020.

The aggregate bedload impact record demonstrates a high degree of variability in impact count occurrence and magnitude between the two plates, and with respect to the water level record. In principle these observations are consistent with Downs et al. (2016) who noted lateral variability

in impact counts across a section of three plates, and inter-event variability in bedload transport intensity for flow events characterized by similar magnitude and duration. However, overall confidence in the collected data record is diminished by the unanswered uncertainties associated with the impact plate device as previously identified in Chapter 3.3. Furthermore, it was noted during a site visit on January 24, 2020 that partial freezing of the water column in winter months creates altered hydraulic conditions that emulate pressurized flow. It is expected that these altered conditions would likely produce conflicting impact count observations when compared against open channel flow events. Figure 48 demonstrates the shallow depth of the under-ice water profile over an uncovered impact plate.

Figure 48. Study reach under-ice water profile over an uncovered impact plate on January 24, 2020 (viewing upstream)**.** Ice previously covering the impact plate was removed to visualize flow conditions.

Data reliability is further complicated by instances of a third *phantom* plate signal noted within the raw data record in addition to the two instrumented impact plates. This observation suggests that the station contains poor electrical contacts between the plates and raspberry pi, which is potentially manifesting as noise and spikes within the data record. A custom hardware piece for the raspberry pi was designed to improve the electrical contacts and is pending installation.

Due to the many nuances present within the data record over the study duration, a single flow event was isolated for detailed examination. The flow event occurring between December 9 – 11, 2019 was selected as the occurrence of bedload impacts between the two plates appear strongly correlated and coincide with the water level record as illustrated in Figure 49.

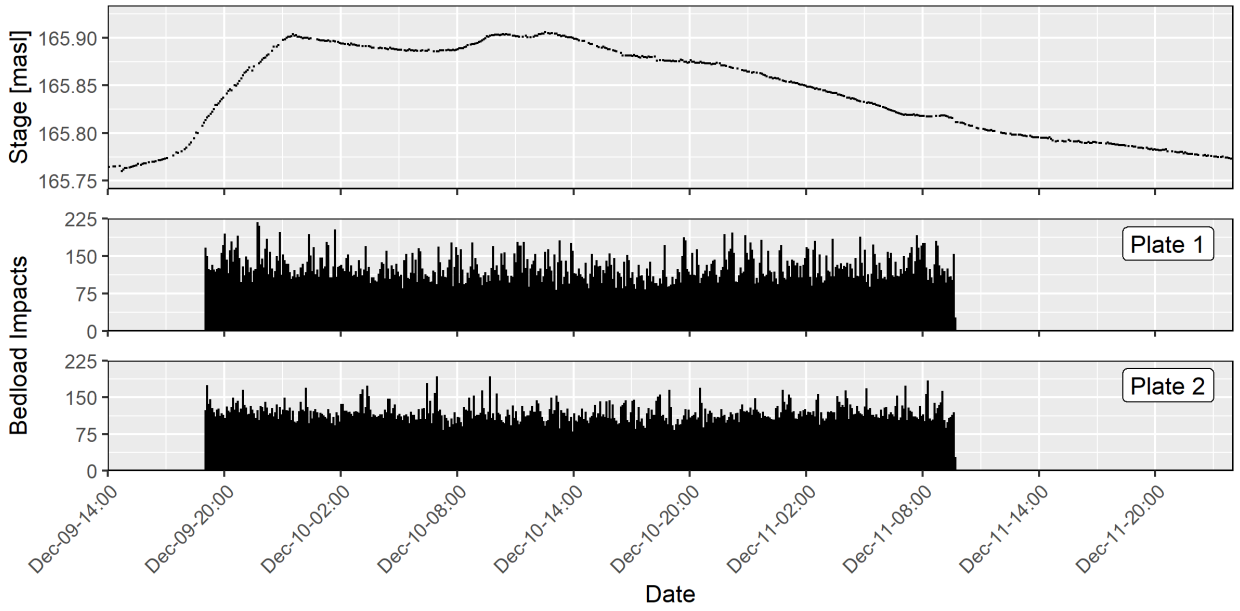

Figure 49. December 2019 flow event. Aggregate bedload impacts summed over 5-minute time intervals.

Bedload impacts recorded during the flow event appear extremely idealized with detections essentially resembling a step function. Bedload impacts are only detected while the stage remains above 165.8 masl, which approximately coincides with bankfull discharge. Bedload impact intensity remains fairly consistent throughout the flow event, which is attributed to floodplain energy dissipation as the right channel bank overtops.

Data quality was evaluated by analyzing time between successive raw data points, impact aggregate magnitude frequency, and a normal probability plot of aggregate values as presented in Figure 50. These metrics were examined to identify patterns that contradict or align with the anticipated stochastic nature of bedload transport.

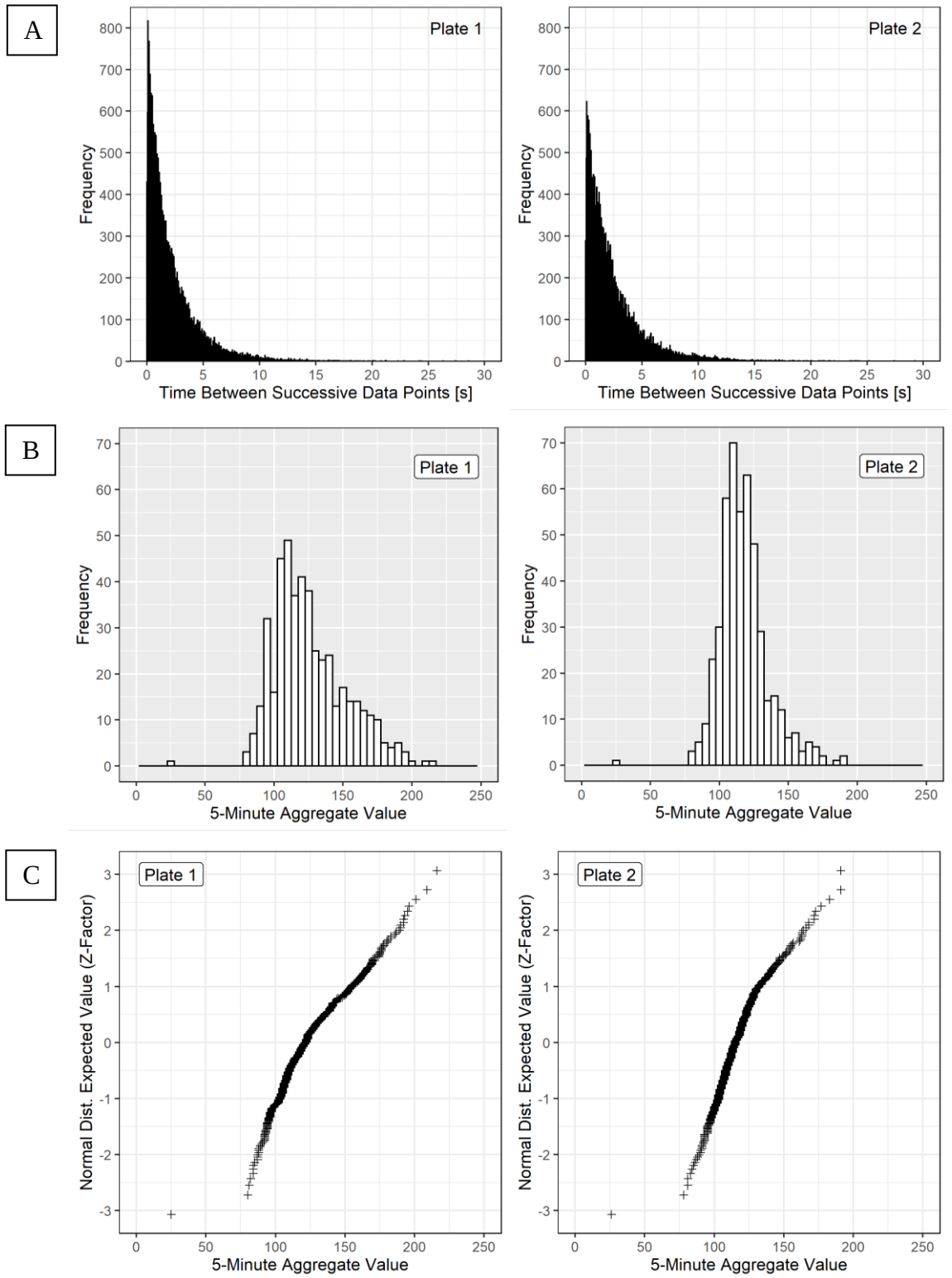

Figure 50. December 2019 flow event data quality analysis. (A) Frequency of time between successive raw data point observations. (B) Magnitude frequency of aggregated bedload impacts. (C) Normal probability plot of aggregated bedload impacts.

The time between successive data points for both plate 1 and 2 follows a pattern of exponential decay. Magnitude frequency of the 5-minute aggregate values appears to follow a slightly positive-skewed distribution where both plates share a similar mode with plate 1 demonstrating a wider variance. The normal probability plots reveal that in the case of both plates, aggregate values less than the mode deviate from a normal distribution. This observation might be attributed to an inability of representing the lower tail of the curve due to the detection threshold of the impact plate device. The aggregate values might be better described in general as a slightly positive-skewed Laplace distribution. Regardless, these patterns do appear to align with the anticipated stochastic processes associated with bedload transport.

Bedload transport rate estimates were derived for the December 2019 flow event according to the processes developed by Soar & Downs (2017). While it is acknowledged that the data record contains many uncertainties, estimates are presented as a point of comparison to Soar & Downs (2017) and to demonstrate the theoretical capability of the impact plate as a bedload monitoring device. The bedload transport rate predictions resulting from the Soar & Downs (2017) BLIP model are shown in Figure 51.

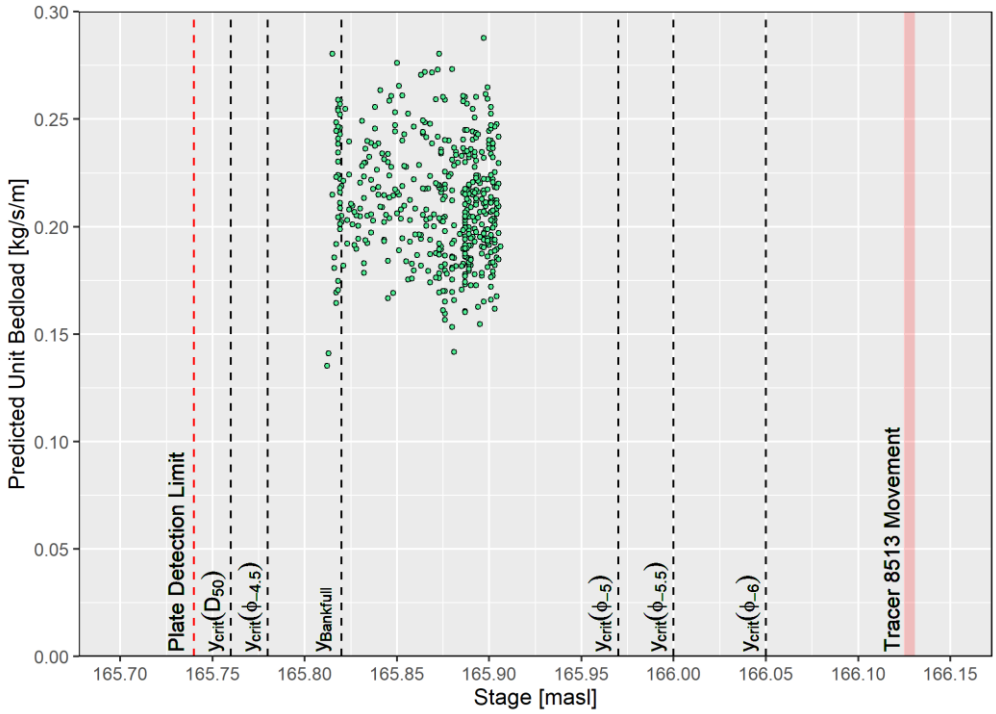

Figure 51. December 2019 flow event instantaneous stage versus predicted unit bedload rates (plate 1 and 2 average) derived from Soar & Downs (2017) BLIP model. Stage is specified for points of interest including bankfull discharge, critical threshold estimates, and the automatically tracked movement of tracer stone 8513.

Predicted unit bedload rates are compared against the stage corresponding to the estimated plate detection limit, estimated critical threshold of the median surface particle, estimated critical threshold of the tracer stone half-phi classes, bankfull discharge, and the movement of tracer stone 8513 (-5 half-phi class). As per the findings drawn from Figure 44, critical thresholds below bankfull stage were estimated assuming a $\tau^*_{c(D50)}$ value of 0.047 [-], while critical thresholds above bankfull stage were estimated assuming a $\tau^*_{c(D50)}$ value of 0.07 [-]. Bedload impacts were absent for a considerable range of discharge expected to trigger plate detections below bankfull. Bedload impacts were detected for flows estimated to entrain particles belonging to the -4.5 half-phi class. Discharge did not reach the estimated critical thresholds for the -5 to -6 half-phi classes over this period of observation.

Soar & Downs (2017) observed consistent intra-event hysteresis of bedload impacts where bedload spikes occurred during the rising and falling limbs of hydrographs. Soar & Downs (2017) attributed this observation to temporal variations in bedload supply related to armour layer break-up during the rising limb and "bank failures and flood-routing of non-local sediment sources" during the falling limb. Soar & Downs (2017) also noted that bedload peaks typically occurred just below bankfull discharge along the hydrograph falling limb. The bedload impacts and predicted transport rates of the December 2019 event do not follow the patterns observed by Soar & Downs (2017), which indicates that temporal variations in bedload supply related to armour layer break-up, bank-failure, or flood-routing may not have occurred. The absence of bedload impacts for flows below bankfull might indicate that particles with a diameter greater than 10 - 12 mm up to the -4.5 half-phi class were supply limited and not readily available on the bed for transport.

An alternative interpretation of the December 2019 event might be explicated by the movement of tracer stone 8513. Tracer 8513 was seeded closest to the bedload monitoring station approximately 0.55 m upstream of the in-stream antenna. An early-November 2019 flow event that exhibits a greater peak than the December 2019 event should have entrained tracer 8513 based on estimated critical thresholds; however, the tracer was found immobile on December 3, 2019 during the first manual tracking survey. The January 2020 flow event mobilized tracer 8513 over the in-stream antenna with a stage of approximately 166.12 masl, which might imply that the estimated critical thresholds are lower than actual site conditions. Higher critical thresholds could explain the sudden observation of impacts near bankfull discharge, which might coincide with the detection limit of the impact plates.

4.3.5 Direct Physical Sampling

The contents of the Bunte sediment trap were retrieved a total of three times during the study period. The three samples largely consisted of cohesive till clumps with some embedded fine sand material. At the individual grain scale, the entrapped material was finer than the sediment trap mesh and should have passed through the trap; however, the cohesive strength of the large till clumps overcame erosive forces and thus remained in the trap as a block. Consequentially, a sieve analysis could not be completed upon the sediment trap samples and direct physical sampling data was not available to calibrate indirect bedload monitoring data.

The Bunte sediment trap failed to collect samples indicative of mobile bedload due to several noted complicating factors. The physical dimensions of the Bunte trap appear too large relative to the size of the channel. As a result, the trap obstructs flow and appears to have directly influenced undercutting of the adjacent channel bank and diversion of the preferential flow path. Furthermore, the trap opening was observed to be jammed on several occasions by thick and woody vegetation, and in one instance completely sealed off by ice during the winter of 2020 as displayed in Figure 52.

Figure 52. Bunte sediment trap sealed by ice and vegetation on January 24, 2020. (A) Ice and vegetation removed from trap opening. (B) Sand and gravel substrate found resting on top of sediment trap netting.

4.4 Alternative Land Use Modelling

The baseline flow and sediment data presented in Chapter 4.3 can be applied to make predictions about bedload transport under alternative land use scenarios. The hydrology of alternative land use scenarios within the Carruthers Creek study sub-basin was simulated using a semi-distributed Raven model (Craig et al., 2020). The hydrologic model was not specifically developed in support of the scope of this thesis, but rather was built as part of a final project for the University of Waterloo Principles of Hydrologic Modelling course (CIVE 781). The CIVE 781 final project report is provided for reference in Appendix A and outlines details regarding model discretization, calibration, and performance. The model was strictly used to obtain outflow hydrographs for demonstration purposes only. Chapter 4.4.1 summarizes the details of each modelled land use

scenario. Predictions of bedload transport for each scenario were derived by performing an analysis of cumulative excess discharge upon the modelled outflow hydrographs as presented in Chapter 4.4.2.

4.4.1 Hydrologic Model Scenarios

The CIVE 781 Carruthers Creek Raven model was updated to include an observation point at the location of the bedload monitoring station so that direct comparisons could be made between the baseline field data record and modelled outflow hydrographs. To enable this update, the study sub-basin was spatially delineated into discrete hydraulic response units (HRUs). Each HRU corresponds to the area within a given sub-basin characterized by unique hydrologic properties. In the case of the Carruthers Creek Raven model, HRUs are delineated based on land use designation alone. The HRUs within the study sub-basin were then manipulated to simulate two alternative land use scenarios: 1) an urbanized study sub-basin with no stormwater management controls; and 2) an urbanized study sub-basin with LID SWM. Scenario 1 was configured by converting the cropland HRU within the study sub-basin into a residential HRU. Scenario 2 was configured by adjusting two hydrologic properties of the newly converted residential HRU from Scenario 1 to emulate LID SWM. The first adjustment consisted of reducing the runoff coefficient from a value of 0.75 to 0.6, which corresponds to the lower limit for residential areas as specified by the Town of Ajax stormwater management design guidelines (Town of Ajax, 2016). The second adjustment consisted of increasing the maximum percolation rate of the primary soil horizon to a value of 5 mm/hr.

A synthetic design storm event was created in accordance with the Town of Ajax stormwater management design guidelines to be used as the precipitation input for the model. The storm event incorporates the Town of Ajax's intensity-duration-frequency (IDF) parameters for the 5-year

return period and follows a 3-hour Chicago distribution. Each alternative land use model scenario was executed using the design storm precipitation input to obtain a corresponding outflow hydrograph at the study sub-basin outlet as illustrated in Figure 53.

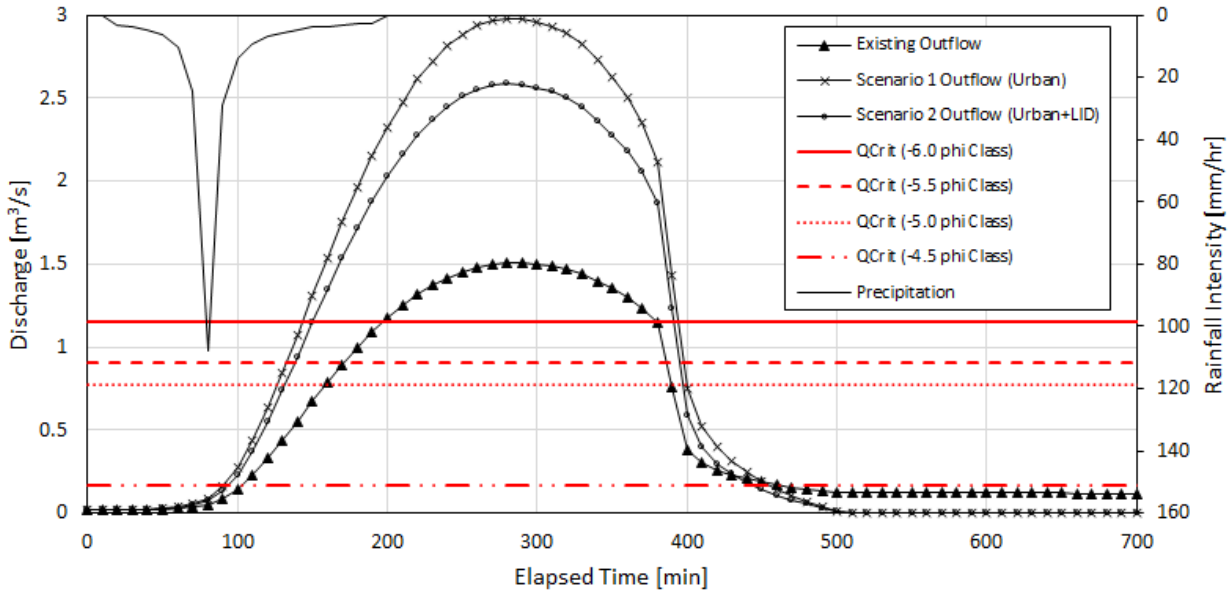

Figure 53. Raven model outflow hydrograph for 5-year return period 3-hour Chicago distribution design storm.

4.4.2 Cumulative Excess Discharge Analysis

A cumulative excess discharge analysis was performed upon each modelled outflow hydrograph to estimate weighted median travel lengths according to Equation (5). The resulting cumulative excess discharge values and travel lengths are presented in Table 11.

Table 11. Cumulative Excess Discharge Results for Modelled Outflow Hydrographs

Phi Class	Land Use Scenario	Cumulative Excess Discharge [m^3]	Estimated Weighted Median Travel Length ($\tilde{L}_i$) [m]
-4.5	1 (Urban)	3.7×10^4	0.41
	2 (Urban+LID)	3.2×10^4	0.35
	Existing	1.7×10^4	0.19
-5.0	1 (Urban)	2.6×10^4	0.29
	2 (Urban+LID)	2.1×10^4	0.23
	Existing	7.3×10^3	0.08
-5.5	1 (Urban)	2.4×10^4	0.26
	2 (Urban+LID)	1.9×10^4	0.21
	Existing	5.6×10^3	0.06
-6.0	1 (Urban)	2.0×10^4	0.22
	2 (Urban+LID)	1.5×10^4	0.17
	Existing	2.6×10^3	0.03

The cumulative excess discharge analysis demonstrates that the addition of LID SWM to an urban land use scenario results in reduced cumulative excess discharge and subsequently lower $\tilde{L}_i$ estimates for all tracer size classes. This effect is expected based on an elementary understanding of urban hydrology. The key takeaway here is the model demonstrates a method with which predictions of bedload transport can be made, used to quantify the impact of land use change on fluvial systems, and ultimately help inform land development decision making based on relative comparisons. For example, if the baseline sediment regime of a study reach is at a relatively stable state of quasi-equilibrium, alternative land development layouts could be modelled with the goal of minimizing differences in pre- and post-development $\tilde{L}_i$ estimates. The idea behind this goal would be to avoid increasing predicted travel lengths, which could result in higher sediment transport rates, more export of sediment from the system, and a greater rate of channel incision if geomorphic thresholds are exceeded.

4.5 Conclusions

Baseline field data reveals that Carruthers Creek is a sediment supply limited semi-alluvial system that is undergoing active channel adjustment. Coarse substrate embedded within the underlying Halton till unit is supplied to the fluvial system via till erosion. These characteristics are prominently exemplified by the headcut geomorphic feature situated along the study reach, which was observed to advance considerably during the study period. Manual tracer particle tracking results demonstrated good alignment with previous studies conducted by Papangelakis (2019) and Cain (2019) within the neighbouring Ganatsekiagon Creek rural watershed. Manual inter-flood particle tracking proved to be a reliable technique compared to the automated bedload transport methods that were implemented. In general, maintaining the bedload transport monitoring station proved to be challenging despite what appeared to be a robust design. The modified Benson Type-A impact plates and RFID in-stream antenna were both less informative than manual tracking results. Furthermore, Papangelakis' cumulative excess discharge linear regression model was able to accurately describe manual tracer particle tracking results. Predictions of bedload transport under alternative watershed land-use scenarios were made by applying Papangelakis' model to hydrographs obtained from a hydrologic model.

5 Conclusions and Recommendations

The goal of this thesis was to develop a robust field method capable of collecting comprehensive baseline data that can be used to inform stream restoration targets and land use decision making. While some aspects of this goal were accomplished, this thesis elicits new questions and presents opportunities for further study.

A novel bedload monitoring station was designed, which integrates existing methods into an automated system that alleviates challenges commonly faced when obtaining bedload transport data. This novel methodology was implemented in the field to characterize baseline conditions of a study reach along Carruthers Creek, Pickering, ON. The baseline field data was used to make relative predictions of bedload transport under alternative watershed land-use scenarios. It is beyond the scope of this study to explicitly answer if an urban development undertaking can improve upon an agriculturally impacted stream system; however, this body of work contributes to the long-term exploration of this concept by putting methods in place to predict and monitor changes to stream stability resulting from land-use change. The following conclusions and recommendations pertain to the Carruthers Creek study site:

- Tracer particle transport dynamics measured over the study period were accurately described by Papangelakis' cumulative excess discharge linear regression model. This thesis demonstrates how the model can be easily applied as a predictive tool to make relative comparisons of bedload transport dynamics pertaining to alternative watershed hydrology. This process can be adopted by high-level decision makers to predict relative changes to stream stability corresponding to alternative land-use scenarios.
- Manual tracer particle tracking results fit with the regional expectation of how stream systems in agricultural watersheds behave as compared to previous studies conducted by

Papangelakis (2019) and Cain (2019) within the neighbouring Ganatsekiagon Creek watershed.

- The narrow channel geometry of the study reach necessitated a tracer stone seeding layout that was uniformly distributed along the channel longitudinal profile. This experimental setup allowed for observations to be drawn regarding how coarse particles tend to distribute along the longitudinal profile over time. Mobilized tracer stones tended to form cluster groups as opposed to being uniformly transported downstream. This observed tendency aligns with the expectation that the coarse substrate will predominantly congregate along riffle bedforms over time.
- This study examines the baseline characteristics of a study reach along Carruthers Creek where anthropogenic modifications within the riparian corridor are minimal and agricultural land use in the watershed is the primary factor affecting channel health and stability. Carruthers Creek is generally characterized as a sediment supply limited semi-alluvial system that is undergoing active channel adjustment. The headcut present along the study reach is a prominent erosional feature that exhibits local effects of high upstream sediment transport and downstream deposition. The headcut advanced approximately 0.8 m upstream during the study period and is believed to be a prominent sediment supply source to the creek through gradual and episodic erosion.

The following conclusions and recommendations pertain to the novel bedload monitoring station design:

- While promising, the modified Benson Type-A impact plates were unable to yield meaningful bedload transport insight for this application over the short study period duration. The data record contains high variability that is partially believed to be the result

of poor electrical connections between the plates and bedload monitoring station system controller. In general, the monitoring station design introduces an added level of complexity to the impact plate device when compared to other studies that use an un-modified version of the Benson plate, which incorporates an internal data logger. The integration of hard-wired connections appears to introduce an additional source of error, which likely explains why this application of the device was largely unsuccessful. A custom hardware piece for the raspberry pi system controller was designed to improve the electrical contacts; installation of this hardware piece is recommended.

- The performance of the impact plate device was highly uncertain in both field and lab applications. It is recommended that the impact plates are evaluated through flume experimentation to gain a better understanding of device performance and limitations under controlled laboratory settings.
- The impact plate data record requires field calibration; however, the Bunte sediment trap was unable to obtain direct physical samples for this purpose. The Bunte sediment trap was not an appropriate physical sampling device for this small headwater system because of its large size relative to the channel. The device posed as a flow obstruction that appeared to divert the preferential flow path, and the device opening was regularly blocked by thick woody vegetation and ice during the winter. An alternative physical sampling device that does not obstruct flow, such as a pit trap, is recommended for this study site.
- Automatic tracer particle tracking observations were very limited due to operational disruptions. At the beginning of the study period, the station power system did not meet the demands of the monitoring equipment, which caused several gaps in the data record. Power demands have since been satisfied after upgrades were made to the station power

system; however, automatic tracer particle tracking is largely a proof-of-concept in this study. The station is expected to yield more consistent automatic tracking results in the future as tracer stones progress downstream.

References

Allan, J. C., Hart, R., & Tranquili, J. V. (2006). The use of Passive Integrated Transponder (PIT) tags to trace cobble transport in a mixed sand-and-gravel beach on the high-energy Oregon coast, USA. Marine Geology, 232(1–2), 63–86. https://doi.org/10.1016/j.margeo.2006.07.005

Arnaud, F., Piégay, H., Vaudor, L., Bultingaire, L., & Fantino, G. (2015). Technical specifications of low-frequency radio identification bedload tracking from field experiments: Differences in antennas, tags and operators. Geomorphology, 238, 37–46. https://doi.org/10.1016/j.geomorph.2015.02.029

Ashworth, P. J., & Ferguson, R. I. (1986). Interrelationships of channel processes, changes and sediments in a proglacial braided river. Geografiska Annaler, Series A, 68 A(4), 361–371.

Askarizadeh, A., Rippy, M. A., Fletcher, T. D., Feldman, D. L., Peng, J., Bowler, P., et al. (2015). From Rain Tanks to Catchments: Use of Low-Impact Development To Address Hydrologic Symptoms of the Urban Stream Syndrome. Environmental Science and Technology, 49(19), 11264–11280. https://doi.org/10.1021/acs.est.5b01635

Bagnold, R. A. (1966). An approach to the sediment transport problem from general physics. Professional Paper. https://doi.org/10.3133/pp422I

Bevenger, G. S., & King, R. M. (1995). A pebble count procedure for assessing watershed cumulative effects. Research Paper - US Department of Agriculture, Forest Service, (RM-RP-319).

Beylich, A. A., & Laute, K. (2014). Combining impact sensor field and laboratory flume measurements with other techniques for studying fluvial bedload transport in steep mountain streams. Geomorphology, 218, 72–87. https://doi.org/10.1016/j.geomorph.2013.09.004

Blann, K. L., Anderson, J. L., Sands, G. R., & Vondracek, B. (2009). Effects of agricultural drainage on aquatic ecosystems: A review. Critical Reviews in Environmental Science and Technology, 39(11), 909–1001. https://doi.org/10.1080/10643380801977966

Bledsoe, B. P., & Watson, C. C. (2001). Effects of urbanization on channel instability. Journal of the American Water Resources Association, 37(2), 255–270. https://doi.org/10.1111/j.1752-1688.2001.tb00966.x

Buffington, J. M., & Montgomery, D. R. (1997). A systematic analysis of eight decades of incipient motion studies, with special reference to gravel-bedded rivers. Water Resources Research, 33(8), 1993–2029. https://doi.org/10.1029/96WR03190

Bunte, K., & Abt, S. R. (2001). Sampling Surface and Subsurface Particle-Size Distributions in Wadable Gravel- and Cobble-bed Streams for Analyses in Sediment Transport, Hydraulics, and Streambed Monitoring. USD A-Rocky Mountain Research Station, General Technical Report RMRS-GTR-74 (Vol. 74).

Bunte, K., Swingle, K. W., & Abt, S. R. (2007). Guidelines for using bedload traps in coarse-bedded mountain streams: Construction, installation, operation, and sample processing. USDA Forest Service - General Technical Report RMRS-GTR, (191 RMRS-G), 1–97.

Burkhead, N. M., & Jelks, H. L. (2001). Effects of suspended sediment on the reproductive success of the tricolor shiner, a crevice-spawning minnow. Transactions of the American Fisheries Society, 130(5), 959–968. https://doi.org/10.1577/1548-8659(2001)130<0959:EOSSOT>2.0.CO;2

Cain, A. (2019). *High-precision Sediment Tracking for Characterization of Sediment Transport of a Rural Stream in Southern Ontario Conditioned by Glacial Legacy Deposits* (Master's thesis, pp. 78). University of Waterloo, Waterloo, Canada. 78 pp. Retrieved from UWSpace.

Cain, A., & MacVicar, B. (2020). Field tests of an improved sediment tracer including non-intrusive measurement of burial depth. Earth Surface Processes and Landforms. https://doi.org/10.1002/esp.4980

Cassel, M., Piégay, H., & Lavé, J. (2017). Effects of transport and insertion of radio frequency identification (RFID) transponders on resistance and shape of natural and synthetic pebbles: applications for riverine and coastal bedload tracking. Earth Surface Processes and Landforms, 42(3), 399–413. https://doi.org/10.1002/esp.3989

Chapuis, M., Bright, C. J., Hufnagel, J., & Macvicar, B. (2014). Detection ranges and uncertainty of passive Radio Frequency Identification (RFID) transponders for sediment tracking in gravel rivers and coastal environments. Earth Surface Processes and Landforms, 39(15), 2109–2120. https://doi.org/10.1002/esp.3620

Chapuis, M., Dufour, S., Provansal, M., Couvert, B., & de Linares, M. (2015). Coupling channel evolution monitoring and RFID tracking in a large, wandering, gravel-bed river: Insights into sediment routing on geomorphic continuity through a riffle-pool sequence. Geomorphology, 231, 258–269. https://doi.org/10.1016/j.geomorph.2014.12.013

Chatanantavet, P., Whipple, K. X., Adams, M. A., & Lamb, M. P. (2013). Experimental study on coarse grain saltation dynamics in bedrock channels. Journal of Geophysical Research: Earth Surface, 118(2), 1161–1176. https://doi.org/10.1002/jgrf.20053

Chin, A. (2006). Urban transformation of river landscapes in a global context. Geomorphology, 79(3–4), 460–487. https://doi.org/10.1016/j.geomorph.2006.06.033

Chin, D. A. (2013). Water-Resources Engineering (Third). New Jersey: Pearson.

Church, M., & Hassan, M. A. (1992). Size and distance of travel of unconstrained clasts on a streambed. Water Resources Research, 28(1), 299–303. https://doi.org/10.1029/91WR02523

Classens, M. (2017). The transformation of the Holland Marsh and the dynamics of wetland loss: a historical political ecological approach. Journal of Environmental Studies and Sciences, 7(4), 507–518. https://doi.org/10.1007/s13412-016-0407-4

Craig, J. R., Brown, G., Chlumsky, R., Jenkinson, R. W., Jost, G., Lee, K., et al. (2020). Flexible watershed simulation with the Raven hydrological modelling framework. Environmental Modelling and Software, 129. https://doi.org/10.1016/j.envsoft.2020.104728

Dawson, B. (2003). The roots of agriculture: A historiographical review of first nations agriculture and government Indian Policy. Prairie Forum, 28(1), 99–116.

Dey, S. (2014). Bed-load transport. GeoPlanet: Earth and Planetary Sciences (Vol. 4). https://doi.org/10.1007/978-3-642-19062-9_5

Downs, P. W., Singer, M. S., Orr, B. K., Diggory, Z. E., & Church, T. C. (2011). Restoring ecological integrity in highly regulated rivers: The role of baseline data and analytical references. Environmental Management, 48(4), 847–864. https://doi.org/10.1007/s00267-011-9736-y

Downs, P. W., Soar, P. J., & Taylor, A. (2016). The anatomy of effective discharge: The dynamics of coarse sediment transport revealed using continuous bedload monitoring in a gravel-bed river during a very wet year. Earth Surface Processes and Landforms, 41(2), 147–161. https://doi.org/10.1002/esp.3785

Eaton, J. G., & Scheller, R. M. (1996). Effects of climate warming on fish thermal habitat in streams of the United States. Limnology and Oceanography, 41(5), 1109–1115. https://doi.org/10.4319/lo.1996.41.5.1109

Eidman, V. (1997). Minnesota farmland drainage: Profitability and concerns. Agricultural Economist, No. 688.

Elliott, K. A. (1998). The forests of southern Ontario. The Forestry Chronicle, 74(6), 850–854.

Emmett, W. W., & Wolman, M. G. (2001). Effective discharge and gravel-bed rivers. Earth Surface Processes and Landforms, 26(13), 1369–1380. https://doi.org/10.1002/esp.303

Ferguson, R. I., & Hoey, T. B. (2002). Long-term slowdown of river tracer pebbles: Generic models and implications for interpreting short-term tracer studies. Water Resources Research, 38(8), 17-1-17–11. https://doi.org/10.1029/2001wr000637

Fulton, R. J. (1986). Quaternary stratigraphy of Canada. Quaternary Science Reviews, 5(C), 207–209. https://doi.org/10.1016/0277-3791(86)90187-3

Ghunowa, K. (2017). *Spatial Decision Support System for Urban Streams* (Master's thesis, pp. 140). University of Waterloo, Waterloo, Canada. Retrieved from UWSpace.

Graf, W. L. (1979). DEVELOPMENT OF MONTANE ARROYOS AND GULLIES. Earth Surf Processes, 4(1), 1–14. https://doi.org/10.1002/esp.3290040102

Gray, J. R., Laronne, J. B., Osterkamp, W. R., & Vericat, D. (2010). Bed Load Research International Cooperative - BRIC. U.S. Geological Survey Scientific Investigations Report 2010-5091, 1–8.

Gray, J. R., Laronne, J. B., & Marr, J. D. G. (2010). Bedload-Surrogate Monitoring Technologies. U.S. Geological Survey Scientific Investigations Report 2010-5091.

Gregory, S. v, Swanson, F. J., McKee, W. A., & Cummins, K. W. (1991). An Ecosystem Perspective of Riparian Zones: Focus on links between land and water. BioScience, 41(8), 540–551. https://doi.org/10.2307/1311607

Habersack, H., Seitz, H., & Liedermann, M. (2010). Integrated Automatic Bedload Transport Monitoring. U.S. Geological Scientific Investigations Report 2010-5091, 218–235.

Habersack, H., Kreisler, A., Rindler, R., Aigner, J., Seitz, H., Liedermann, M., & Laronne, J. B. (2017). Integrated automatic and continuous bedload monitoring in gravel bed rivers. Geomorphology, 291, 80–93. https://doi.org/10.1016/j.geomorph.2016.10.020

Hartigan, J. A., & Wong, M. A. (1979). HYBRID CLUSTERING. Proceedings - American Petroleum Institute, Refining Department, 137–143.

Houbrechts, G., Levecq, Y., Peeters, A., Hallot, E., van Campenhout, J., Denis, A.-C., & Petit, F. (2015). Evaluation of long-term bedload virtual velocity in gravel-bed rivers (Ardenne, Belgium). Geomorphology, 251, 6–19. https://doi.org/10.1016/j.geomorph.2015.05.012

Integrated Power Systems. (n.d.). Sun hours per day. Retrieved from: http://ipwr.net/sun-hours-per-day/.

Johnston, C. E., & Shute, J. R. (1997). Observational notes on the spawning behavior of the blue shiner (Cyprinella caerulea) and the holiday darter (Etheostoma brevirostrum), two rare fishes of the Conasauga River, Georgia and Tennessee. In Southeastern Fishes Council Proceedings: No. 35.

Jordan, T. E., Correll, D. L., & Weller, D. E. (1993). Nutrient interception by a riparian forest receiving inputs from adjacent cropland. Journal of Environmental Quality, 22(3), 467–473. https://doi.org/10.2134/jeq1993.00472425002200030010x

Killey, M. M. (2007). Illinois' Ice Age Legacy. Illinois State Geological Survey.

Lacroix, P. (2019). Promises to keep: French Canadians as revolutionaries and refugees, 1775-1800. Journal of Early American History, 9(1), 59–82. https://doi.org/10.1163/18770703-00901004

Lamarre, H., MacVicar, B., & Roy, A. G. (2005). Using Passive Integrated Transponder (PIT) tags to investigate sediment transport in gravel-bed rivers. Journal of Sedimentary Research, 75(4), 736–741. https://doi.org/10.2110/jsr.2005.059

Lambert, R. S., & Pross, P. (1967). Renewing Nature's Wealth: A Centennial History of the Public Management of Lands, Forests & Wildlife in Ontario, 1763-1967. Toronto: Ontario Dept. of Lands and Forests.

Lane, E. W. (1955). The importance of fluvial morphology in hydraulic engineering. Proceedings of the American Society of Civil Engineers, 81, 1–17.

Lane, S. N., & Richards, K. S. (1997). Linking river channel form and process: Time, space and causality revisited. Earth Surface Processes and Landforms, 22(3), 249–260. https://doi.org/10.1002/(SICI)1096-9837(199703)22:3<249::AID-ESP752>3.0.CO;2-7

Leopold, L. B., Wolman, M. G., & Miller, J. P. (1964). Fluvial processes in geomorphology. San Francisco, CA: WH Freeman and Co.

Leyton, L., Reynolds, E. R. C., & Thompson, F. B. (1967). Rainfall Interception in Forest and Moorland. International Symposium on Forest Hydrology; 1965 August 29-September 10; Pennsylvania State University, University Park, PA, 163–178.

López, R., & Barragan, J. (2008). Equivalent Roughness of Gravel-Bed Rivers. Journal of Hydraulic Engineering, 134, 847–851. https://doi.org/10.1061/(ASCE)0733-9429(2008)134:6(847)

Mackin, H. J. (1948). Concept of the graded river. Bulletin of the Geological Society of America, 59(5), 463–512. https://doi.org/10.1130/0016-7606(1948)59[463:COTGR]2.0.CO;2

MacVicar, B., & Roy, A. G. (2011). Sediment mobility in a forced riffle-pool. Geomorphology, 125(3), 445–456. https://doi.org/10.1016/j.geomorph.2010.10.031

MacVicar, B., Chapuis, M., Buckrell, E., & Roy, A. (2015). Assessing the performance of in-stream restoration projects using Radio Frequency Identification (RFID) transponders. Water (Switzerland), 7(10), 5566–5591. https://doi.org/10.3390/w7105566

Madramootoo, C. A., Johnston, W. R., Ayars, J. E., Evans, R. O., & Fausey, N. R. (2007). Agricultural drainage management, quality and disposal issues in North America. Irrigation and Drainage, 56(SUPPL. 1). https://doi.org/10.1002/ird.343

Meyer, J. L., Paul, M. J., & Taulbee, W. K. (2005). Stream ecosystem function in urbanizing landscapes. Journal of the North American Benthological Society, 24(3), 602–612. https://doi.org/10.1899/04-021.1

Mion, J. B., Stein, R. A., & Marschall, E. A. (1998). River discharge drives survival of larval walleye. Ecological Applications, 8(1), 88–103. https://doi.org/10.1890/1051-0761(1998)008[0088:RDDSOL]2.0.CO;2

Muirhead, C. (2018). *Advances in River Bedload Tracking Technology: Self-righting Radio Frequency Identification Tracers and an In-stream Automated Station* (Master's thesis, pp. 109). University of Waterloo, Waterloo, Canada. Retrieved from UWSpace.

Naiman, R. J., & Décamps, H. (1997). The ecology of interfaces: Riparian zones. Annual Review of Ecology and Systematics, 28, 621–658. https://doi.org/10.1146/annurev.ecolsys.28.1.621

Newcombe, C. P., & Jensen, J. O. T. (1996). Channel suspended sediment and fisheries: A synthesis for quantitative assessment of risk and impact. North American Journal of Fisheries Management, 16(4), 693–727. https://doi.org/10.1577/1548-8675(1996)016<0693:CSSAFA>2.3.CO;2

Nichols, M. H. (2004). A radio frequency identification system for monitoring coarse sediment particle displacement. Applied Engineering in Agriculture, 20(6), 783–787.

Nir, D. (1983). Man, A Geomorphological Agent: An Introduction to Anthropic Geomorphology. (D. Ashboren, Ed.). Israel: Keter Publishing House.

Ontario Ministry of Energy Northern Development and Mines. (2017). Ontario's Quaternary Geology. Queen's Printer for Ontario, 2020.

Ontario Ministry of Natural Resources and Forestry. (2020). User Guide for Ontario Integrated Hydrology. Queen's Printer for Ontario.

Ontario Ministry of the Environment & Climate Change. (2017). DRAFT Low Impact Development (LID) Stormwater Management Guidance Manual.

Ontario Royal Commission on Forestry. (1947). Report of the Ontario Royal Commission on Forestry. Baptist Johnston, Printer to the King's Most Excellent Majesty, Toronto.

Oregon RFID. (2019). HDX Single Antenna PIT Tag Reader User Guide.

Osborne, L. L., & Kovacic, D. A. (1993). Riparian vegetated buffer strips in water-quality restoration and stream management. Freshwater Biology, 29(2), 243–258. https://doi.org/10.1111/j.1365-2427.1993.tb00761.x

Owens, P. N., Batalla, R. J., Collins, A. J., Gomez, B., Hicks, D. M., Horowitz, A. J., et al. (2005). Fine-grained sediment in river systems: Environmental significance and management issues. River Research and Applications, 21(7), 693–717. https://doi.org/10.1002/rra.878

Papangelakis, E. (2019). *Bedload sediment transport regimes of urban gravel-bed rivers under different management scenarios* (PhD thesis, pp. 144). University of Waterloo, Waterloo, Canada. Retrieved from UWSpace.

Papangelakis, E., MacVicar, B., & Ashmore, P. (2019). Bedload Sediment Transport Regimes of Semi-alluvial Rivers Conditioned by Urbanization and Stormwater Management. Water Resources Research, 55(12), 10565–10587. https://doi.org/10.1029/2019WR025126

Papangelakis, E., Muirhead, C., Schneider, A., & Macvicar, B. (2019). Synthetic Radio Frequency Identification Tracer Stones with Weighted Inner Ball for Burial Depth Estimation. Journal of Hydraulic Engineering, 145(12). https://doi.org/10.1061/(ASCE)HY.1943-7900.0001650

Papangelakis, E., Montakhab, F., MacVicar, B., & Ashmore, P. (2020). (In preparation) Competent volume of discharge predicts the displacement of bed sediment particles in rivers with different hydrograph shapes. Nature Geoscience.

Parker, G., & Klingeman, P. C. (1982). On why gravel bed streams are paved. Water Resources Research, 18(5), 1409–1423. https://doi.org/10.1029/WR018i005p01409

Peterjohn, W. T., & Correll, D. L. (1984). Nutrient dynamics in an agricultural watershed: observations on the role of riparian forest. Ecology, 65(5), 1466–1475. https://doi.org/10.2307/1939127

Phillips, R. T. J., & Desloges, J. R. (2014). Glacially conditioned specific stream powers in low-relief river catchments of the southern Laurentian Great Lakes. Geomorphology, 206, 271–287. https://doi.org/10.1016/j.geomorph.2013.09.030

Pimentel, D., Harvey, C., Resosudarmo, P., Sinclair, K., Kurz, D., McNair, M., et al. (1995). Environmental and economic costs of soil erosion and conservation benefits. Science, 267(5201), 1117–1123. https://doi.org/10.1126/science.267.5201.1117

Plumb, B. D., Annable, W. K., Thompson, P. J., & Hassan, M. A. (2017). The Impact of Urbanization on Temporal Changes in Sediment Transport in a Gravel Bed Channel in Southern Ontario, Canada. Water Resources Research, 53(10), 8443–8458. https://doi.org/10.1002/2016WR020288

Raso, T. (2017). *The Impacts of Stormwater Management on Hydromodification and Bedload Sediment Transport in a Gravel-bed Stream* (Master's thesis, pp. 108). University of Waterloo, Waterloo, Canada. Retrieved from UWSpace.

Reid, S. C., Lane, S. N., Berney, J. M., & Holden, J. (2007). The timing and magnitude of coarse sediment transport events within an upland, temperate gravel-bed river. Geomorphology, 83(1–2), 152–182. https://doi.org/10.1016/j.geomorph.2006.06.030

Rickenmann, D. (1997). Sediment transport in swiss torrents. Earth Surface Processes and Landforms, 22(10), 937–951. https://doi.org/10.1002/(SICI)1096-9837(199710)22:10<937::AID-ESP786>3.0.CO;2-R

Rickenmann, D. (2017). Bed-load transport measurements with geophones and other passive acoustic methods. Journal of Hydraulic Engineering, 143(6). https://doi.org/10.1061/(ASCE)HY.1943-7900.0001300

Rickenmann, D., & Fritschi, B. (2010). Bedload Transport Measurements Using Piezoelectric Impact Sensors and Geophones. U.S. Geological Survey Scientific Investigations Report 2010-5091, 407–423.

Rickenmann, D., & McArdell, B. W. (2007). Continuous measurement of sediment transport in the Erlenbach stream using piezoelectric bedload impact sensors. Earth Surface Processes and Landforms, 32(9), 1362–1378. https://doi.org/10.1002/esp.1478

Rickenmann, D., Turowski, J. M., Fritschi, B., Klaiber, A., & Ludwig, A. (2012). Bedload transport measurements at the Erlenbach stream with geophones and automated basket samplers. Earth Surface Processes and Landforms, 37(9), 1000–1011. https://doi.org/10.1002/esp.3225

Rickenmann, D., Turowski, J. M., Fritschi, B., Wyss, C., Laronne, J., Barzilai, R., et al. (2014). Bedload transport measurements with impact plate geophones: Comparison of sensor calibration in different gravel-bed streams. Earth Surface Processes and Landforms, 39(7), 928–942. https://doi.org/10.1002/esp.3499

Rickenmann, D., Steeb, N., & Badoux, A. (2018). Improving bedload transport determination by grain-size fraction using the Swiss plate geophone recordings at the Erlenbach stream. In E3S Web of Conferences (Vol. 40). https://doi.org/10.1051/e3sconf/20184002009

Riley, J. L., & Mohr, P. (1994). The Natural Heritage of Southern Ontario's Settled Landscapes: A Review of Conservation and Restoration Ecology for Land-Use and Landscape Planning. Aurora: Ontario Ministry of Natural Resources, Southern Region, Science and Technology Transfer.

Robinson, M., & Rycroft, D. W. (1999). The impact of drainage on streamflow. Agronomy Monograph, Agricultural Drainage, 38, 767–800.

Rollet, A. J., Macvicar, B., Piegay, H., & Roy, A. (2008). A comparative study on the use of passive integrated transponders to estimate sediment transport: First results | L'utilisation de transpondeurs passifs pour l'estimation du transport sédimentaire: Premiers retours d'expérience. Houille Blanche, (4), 110–116. https://doi.org/10.1051/lhb:2008047

Rosgen, D. L. (1994). A classification of natural rivers. Catena, 22(3), 169–199. https://doi.org/10.1016/0341-8162(94)90001-9

Rosgen, D. L. (1996). Applied river morphology. Pagosa Springs, Colo: Wildland Hydrology.

Royal Commission on Aboriginal Peoples. (1996). Report of the Royal Commission on Aboriginal Peoples. Ottawa: Canada Communication Group.

Schumm, S. A. (1984). Incised channels : morphology, dynamics, and control. (M. D. Harvey & C. C. Watson, Eds.). Littleton, Colo: Water Resources Publications.

Schumm, S. A., & Lichty, R. W. (1965). Time, space, and causality in geomorphology. American Journal of Science, 263(2), 110–119. https://doi.org/10.2475/ajs.263.2.110

Shields, A. (1936). Anwendung der Aehnlichkeitsmechanik und der Turbulenzforschung auf die Geschiebebewegung. Berlin, Germany: Mitteilungen de Preussischen Versuchsanstalt für Wasserbau und Schiffbau.

Shields Jr., F. D. (1998). Rehabilitation of aquatic habitats in warmwater streams damaged by channel incision in Mississippi. Hydrobiologia, 382(1–3), 63–86.

Simon, A. (1989). A model of channel response in disturbed alluvial channels. Earth Surface Processes and Landforms, 14(1), 11–26. https://doi.org/10.1002/esp.3290140103

Simons, D. B., & Şentürk, F. (1992). Sediment Transport Technology: Water and Sediment Dynamics. Water Resources Publications. Retrieved from https://books.google.ca/books?id=_eScptWZAeIC

Soar, P. J., & Downs, P. W. (2017). Estimating bedload transport rates in a gravel-bed river using seismic impact plates: Model development and application. Environmental Modelling and Software, 90, 182–200. https://doi.org/10.1016/j.envsoft.2017.01.012

Statzner, B., & Highler, B. (1986). Stream hydraulics as a major determinant of benthic invertebrate zonation patterns. Freshwater Biology, 16(1), 127–139. https://doi.org/10.1111/j.1365-2427.1986.tb00954.x

Stevens, V., Backhouse, F., & Eriksson, A. (1995). Riparian Management in British Columbia: An Important Step Towards Maintaining Biodiversity. Victoria: Province of British Columbia.

Sweeney, B. W., Bott, T. L., Jackson, J. K., Kaplan, L. A., Newbold, J. D., Standley, L. J., et al. (2004). Riparian deforestation, stream narrowing, and loss of stream ecosystem services. Proceedings of the National Academy of Sciences of the United States of America, 101(39), 14132–14137. https://doi.org/10.1073/pnas.0405895101

Sweka, J. A., & Hartman, K. J. (2001). Effects of turbidity on prey consumption and growth in brook trout and implications for bioenergetics modeling. Canadian Journal of Fisheries and Aquatic Sciences, 58(2), 386–393. https://doi.org/10.1139/f00-260

Todd, A. K., & Kaltenecker, M. G. (2012). Warm season chloride concentrations in stream habitats of freshwater mussel species at risk. Environmental Pollution, 171, 199–206. https://doi.org/10.1016/j.envpol.2012.07.040

Town of Ajax. (2016). Town of Ajax Design Criteria Section C: Stormwater Management and Storm Drainage.

Trenhaile, A. (2007). Geomorphology: A Canadian Perspective (Third Edition). Canada: Oxford University Press.

Tsakiris, A. G., Papanicolaou, A. N. T., Moustakidis, I. V. D., & Abban, B. K. (2015). Identification of the burial depth of radio frequency identification transponders in riverine applications. Journal of Hydraulic Engineering, 141(6). https://doi.org/10.1061/(ASCE)HY.1943-7900.0001001

Turowski, J. M., & Rickenmann, D. (2009). Tools and cover effects in bedload transport observations in the Pitzbach, Austria. Earth Surface Processes and Landforms, 34(1), 26–37. https://doi.org/10.1002/esp.1686

Vázquez-Tarrío, D., Recking, A., Liébault, F., Tal, M., & Menéndez-Duarte, R. (2019). Particle transport in gravel-bed rivers: Revisiting passive tracer data. Earth Surface Processes and Landforms, 44(1), 112–128. https://doi.org/10.1002/esp.4484

Vericat, D., Church, M., & Batalla, R. J. (2006). Bed load bias: Comparison of measurements obtained using two (76 and 152 mm) Helley-Smith samplers in a gravel bed river. Water Resources Research, 42(1). https://doi.org/10.1029/2005WR004025

Walsh, C. J., Roy, A. H., Feminella, J. W., Cottingham, P. D., Groffman, P. M., & Morgan II, R. P. (2005). The urban stream syndrome: Current knowledge and the search for a cure. Journal of the North American Benthological Society, 24(3), 706–723. https://doi.org/10.1899/04-028.1

Walsh, C. J., Fletcher, T. D., & Burns, M. J. (2012). Urban Stormwater Runoff: A New Class of Environmental Flow Problem. PLoS ONE, 7(9). https://doi.org/10.1371/journal.pone.0045814

Ward, J. v, & Stanford, J. A. (1982). THERMAL RESPONSES IN THE EVOLUTIONARY ECOLOGY OF AQUATIC INSECTS. Annual Review of Entomology, 27(1), 97–117. https://doi.org/10.1146/annurev.en.27.010182.000525

Weijters, M. J., Janse, J. H., Alkemade, R., & Verhoeven, J. T. A. (2009). Quantifying the effect of catchment land use and water nutrient concentrations on freshwater river and stream biodiversity. Aquatic Conservation: Marine and Freshwater Ecosystems, 19(1), 104–112. https://doi.org/10.1002/aqc.989

Wenger, S. J., Roy, A. H., Jackson, C. R., Bernhardt, E. S., Carter, T. L., Filoso, S., et al. (2009). Twenty-six key research questions in urban stream ecology: An assessment of the state of the science. Journal of the North American Benthological Society, 28(4), 1080–1098. https://doi.org/10.1899/08-186.1

Wichert, G. A., & Rapport, D. J. (1998). Fish community structure as a measure of degradation and rehabilitation of riparian systems in an agricultural drainage basin. Environmental Management, 22(3), 425–443. https://doi.org/10.1007/s002679900117

Wilcock, P. R. (1988). Methods for estimating the critical shear stress of individual fractions in mixed-size sediment. Water Resources Research, 24(7), 1127–1135. https://doi.org/10.1029/WR024i007p01127

Wohl, E., Lane, S. N., & Wilcox, A. C. (2015). The science and practice of river restoration. Water Resources Research, 51(8), 5974–5997. https://doi.org/10.1002/2014WR016874

Wolman, M Gordon. (1967). A Cycle of Sedimentation and Erosion in Urban River Channels. Geografiska Annaler. Series A, Physical Geography, 49(2/4), 385–395. https://doi.org/10.2307/520904

Wolman, M.G. (1954). A method of sampling coarse river-bed material. Eos, Transactions American Geophysical Union, 35(6), 951–956. https://doi.org/10.1029/TR035i006p00951

Zingg, Th. (1935). Beitrage zur Schotteranalyse, Schweizer. Mineralog. u. Petrog. Mitt, (15), 39–140.

Appendix A:

CIVE 781 Principles of Hydrologic Modelling Final Project Report

CIVE 781 – Principles of Hydrologic Modelling

Carruthers Creek Raven Model

Submitted by:

Matthew Iannetta

Submitted to:

Dr. James Craig

August 6, 2019

TABLE OF CONTENTS

List of Tables 121
List of Figures 121
1. Introduction 122
2. Input Data 125
3. Watershed Discretization 128
4. Raven Model Overview 129
5. Model Calibration 131
6. Results 137
References 140

List of Tables

Table 1. Summary of Meteorological Gauges 125
Table 2. Summary of Literature Parameter Values for Model Calibration 133
Table 3. Summary of Model Calibration Parameters 134
Table 4. Summary of Manual Model Calibration Diagnostic Metrics 135
Table 5. Summary of Automated Model Calibration Diagnostic Metrics 136

List of Figures

Figure 1. Carruthers Creek Watershed Overview Map 124
Figure 2. Meteorological Gauge Precipitation Records 126
Figure 3. Carruthers Creek Climate Forcings 127
Figure 4. Carruthers Creek Watershed Delineation 129
Figure 5. Visualization of Subsurface Tile Drainage - Excerpt from (Blann, Anderson, Sands, & Vondracek, 2009) 131
Figure 6: Carruthers Creek Raven Model Pre-Calibration Hydrograph 132
Figure 7: Carruthers Creek Raven Model Manual-Calibration Hydrograph 134
Figure 8: Carruthers Creek Raven Model Automated-Calibration Hydrograph 136

1. Introduction

Carruthers Creek is a headwater drainage system located in Southern Ontario that has been subjected to significant morphologic change over the past century as a result of anthropogenic activities including agriculture and urbanization which have modified the surrounding landscape. At its headwaters in the City of Pickering, Carruthers Creek is primarily surrounded by tile drained agricultural lands which rapidly direct infiltrated water to adjacent tributaries. Agricultural development has historically placed a great deal of stress on the integrity of native aquatic ecosystems due to disruptions in natural water and nutrient cycles (Blann, Anderson, Sands, & Vondracek, 2009). Further downstream, Carruthers Creek makes its way through the urbanized lands of the Town of Ajax before discharging into Lake Ontario. An inherent relationship exists between modification of land coverage and the health of receiving stream networks. Agricultural and urban development influences the quantity, quality, and timing of surface runoff routed to stream networks due to a variety of driving mechanisms including increased impervious land coverage and improved network connectivity through traditional stormwater management (SWM) practices and subsurface draining techniques (Walsh, et al., 2005). Urbanization is generally linked to several consistently observed stream symptoms including reduced water quality, reduced biotic richness, and altered channel stability and morphology (Walsh, et al., 2005). These symptoms are commonly referred to as the urban stream syndrome and appear to be the socially accepted trade-off that comes along with any land development undertaking (Walsh, et al., 2005). However, low impact development (LID) is an alternative SWM practice which aims to manage stormwater where it falls, consequentially reducing overall surface runoff volumes routed to adjacent streams and potentially remedying urban stream symptoms (Askarizadeh, 2015).

There is interest in developing the agricultural and rural lands located within the northern portion of the Carruthers Creek basin using LID as the primary SWM technique in order to simulate pre-agricultural hydrology. It is imperative that the layout of any land development undertaking within the watershed is planned such that Carruthers Creek is not adversely impacted downstream where the urban core of Ajax is currently situated and likely already experiencing symptoms of the urban stream syndrome. The Carruthers Creek Raven model was developed with the intent of investigating potential land development scenarios in the upper basin rural and agricultural lands which do not generate adverse downstream impacts. The specific goal of the model is to calculate the maximum permissible impervious fraction which can be implemented in tandem with LID hydrology across the existing rural and cropland areas of the upstream sub-basins (1 and 2) such that the frequency of erosive flow events observed at the downstream basin outlet does not increase. For the purpose of this investigation, erosive flow events are defined as flow rates which meet or exceed the bankfull channel discharge with respect to the cross-section assigned to the outlet basin (sub-basin 3) in the Raven .rvp input file. The results of this analysis can help inform the community master planning phase of a potential land development undertaking by providing impervious land cover targets for alternative plan layouts.

Carruthers Creek is located within the Newmarket Till geologic unit which is characterized by clay and till plains (Conservation Authorities Moraine Coalition, n.d.). The primary tributary is approximately 30 km in length and has an associated watershed drainage area of 40 km^2. Streamflow data along Carruthers Creek is made available online by the Toronto and Region Conservation Authority (TRCA) but is limited. Three (3) streamflow gauges are instrumented along Carruthers Creek; the two (2) northern most gauges (HY089 and HY090) both consist of a 1-year long data record for the year of 2016 while the southern most gauge (HY013) consists of

approximately 9-years of data between 2007 and 2017. Streamflow gauge HY013 was selected to delineate the study basin for the Raven model due to the adequacy in length of its data record. The resulting study basin covers an area of approximately 28 km^2 as illustrated below in Figure 1.

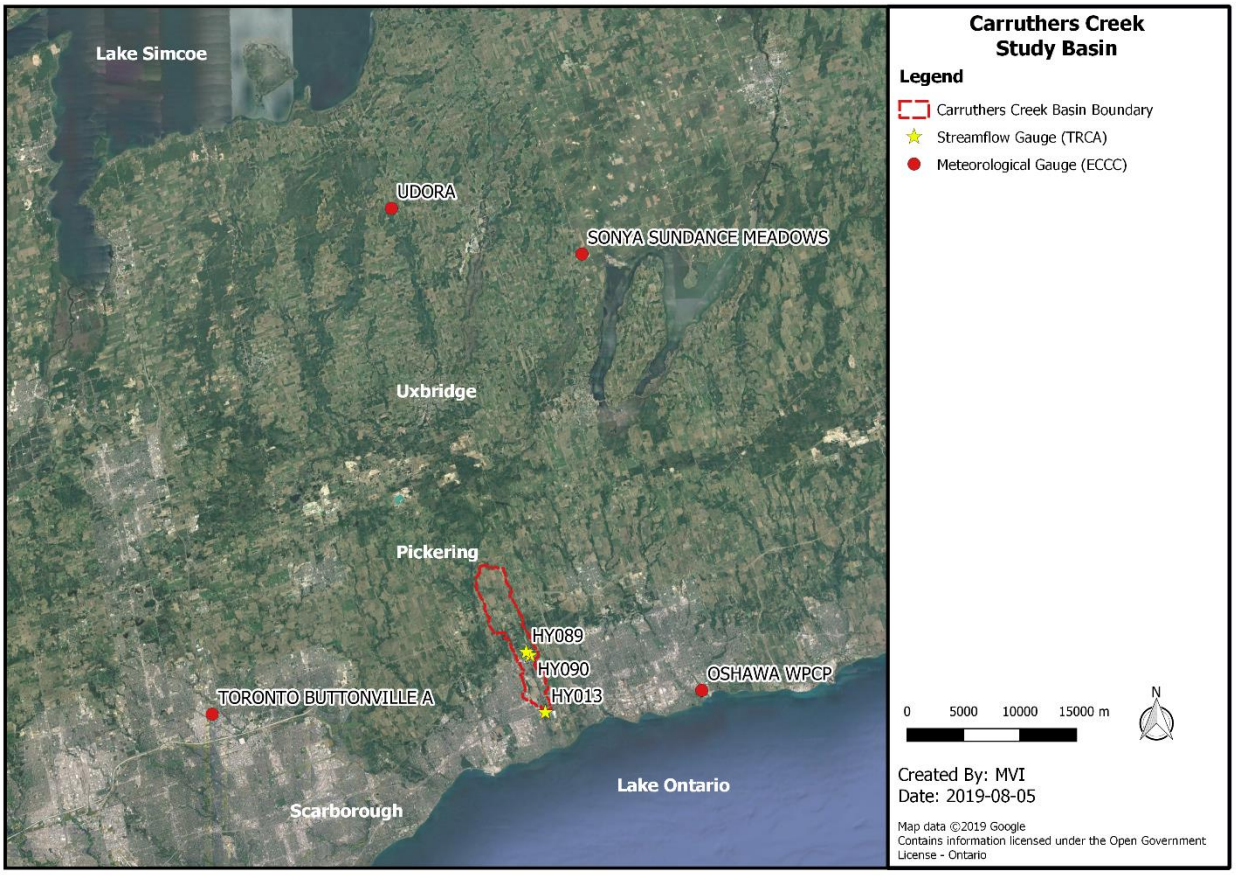

Figure 1. Carruthers Creek Watershed Overview Map

Meteorological data from the Environment and Climate Change Canada online database is limited within the immediate vicinity of Carruthers Creek. The four (4) nearest gauges that contain overlapping records with available streamflow data are all located outside of the study basin boundary with distances ranging from 17.5 – 39 kms from the basin centroid.

2. Input Data

Raven requires a variety of data inputs including observed streamflow records, climate forcing data to drive hydrological processes, and spatial data for model discretization. Daily average streamflow data was obtained from the TRCA online open data portal for the three (3) gauges instrumented along Carruthers Creek. The available streamflow data is relatively sparse as the two (2) upstream gauges HY089 and HY090 only contain a 1-year long data record for the year 2016, and gauge HY013 consists of approximately 9-years of data between 2007 and 2017 which falls short of a desirable 10-year record. Although streamflow data is sparse, the available records are of good quality and complete with no data gaps meaning pre-processing was not necessary for the Raven model.

Daily meteorological data was retrieved from the Environment and Climate Change Canada (ECCC) online database. Four (4) meteorological gauges were selected to provide forcing data for the Raven model based on the criteria of possessing an overlapping data record with the observed streamflow dataset and being of minimal distance away from the Carruthers Creek watershed centroid. The four (4) gauges that meet these criteria are all located outside of the study basin boundary with distances ranging from 17.5 – 39 kms from the basin centroid as summarized below in Table 1.

Table 1. Summary of Meteorological Gauges

Meteorological Gauge ID	Distance from Watershed Centroid [m]
Oshawa WPCP	17,562
Buttonville Airport	27,594
Sonya	33,977
Udora	38,964

The meteorological data records are not of the greatest quality as there are notable discrepancies when comparing precipitation among the gauges as illustrated below in Figure 2.

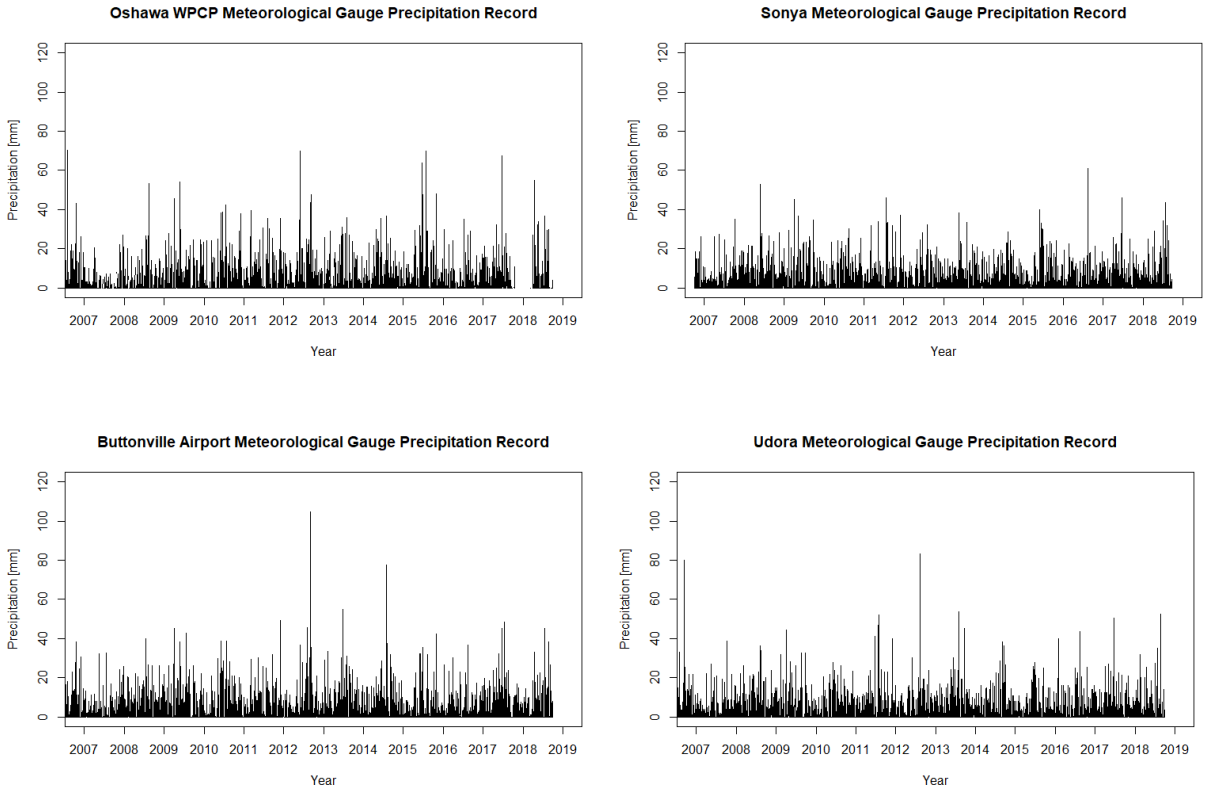

Figure 2. Meteorological Gauge Precipitation Records

The Sonya and Udora gauges appear to consistently report less precipitation overall when compared to the other gauges. Furthermore, the Sonya gauge does not demonstrate comparable peak magnitudes for large rainfall events such as the July 2012 event where all other gauges report maximum precipitation values respectively during the observed timeframe. The Buttonville airport gauge generally appears to report substantially higher precipitation values for some of the largest observed rainfall events when compared to the other gauges as demonstrated by the July 2012 and July 2014 events. The Oshawa WPCP gauge demonstrates suspect data during the second half of 2007 as this segment is seasonally inconsistent with the rest of the observed record, and overall inconsistent with the other gauges. The Oshawa WPCP also reports a relatively significant event around May 2015 which is not reflected by the other gauges to a similar degree of magnitude. In addition to the observed discrepancies, the meteorological data

records for all gauges contain a notable amount of blank data entries. Raven operates with a user specified timestep and is unable to accept input data containing missing or incomplete date entries with respect to the timestep interval. Thus, pre-processing of the meteorological data was a necessary step in order to make the data useful for the Raven model. For a given meteorological gauge, blank data entries were filled in by taking the average value from all other gauges containing data on the specific date of observation. Fortunately, there were no instances where data was unavailable among all gauges for a given time. All forcing data for the Carruthers Creek Raven model is presented below in Figure 3.

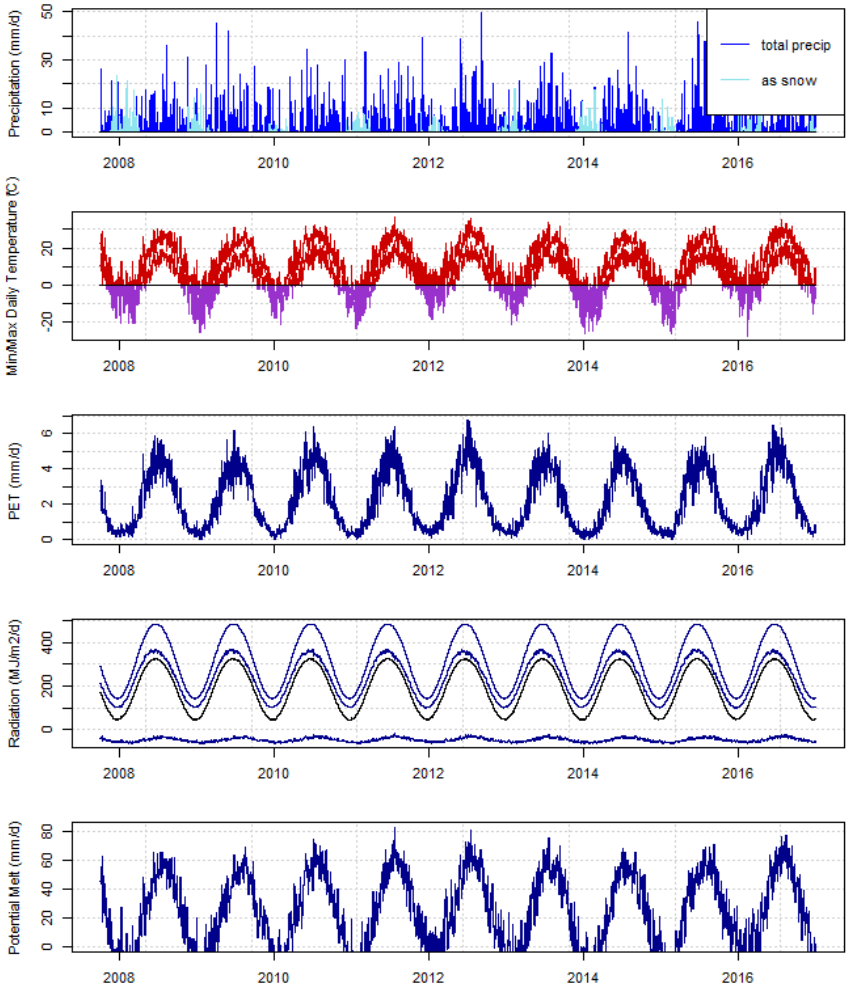

Figure 3. Carruthers Creek Climate Forcings

Spatial land cover data used for model discretization was obtained form the TRCA online open data portal as a polygon shapefile. The shapefile consists of 20 different land use categories within the study basin which is much more detailed than desirable for the purpose of model domain discretization into unique hydraulic response units (HRUs). In order to simplify model discretization, the land cover shapefile was pre-processed such that the default land use categories were consolidated into nine (9) classes characterized by similar runoff properties.

A digital elevation model (DEM) consisting of 30 m x 30 m grid size resolution was obtained from the Land Information Ontario (LIO) online data portal. Using QGIS spatial mapping software, the DEM was clipped to an area that encompasses the Carruthers Creek watershed and was re-projected into the UTM zone 17N EPSG:26917 coordinate system for further pre-processing. The R-SAGA fill sinks algorithm was used to automatically fill in DEM pits in order to facilitate the calculation of realistic drainage basin areas in subsequent watershed discretization steps.

3. Watershed Discretization

The Carruthers Creek study basin was delineated using the GRASS r.watershed spatial analysis tool in QGIS. Streamflow gauge HY013 was selected as the overall study basin pour point as it is situated furthest downstream in the urban core of Ajax and consists of the longest data record compared to the remaining streamflow gauges. The study basin is divided into three (3) sub-basins with outlet pour points corresponding to the locations of the three (3) available streamflow gauges. Although gauges HY089 and HY090 consist of short data records, it is advantageous to delineate sub-basins from these pour points because they divide the study basin into two (2) predominantly agricultural upstream sub-basins, and one (1) predominantly urbanized downstream sub-basin. HRUs were delineated within each sub-basin according to nine (9) land

use classes which are characterized by unique runoff properties as illustrated below in Figure 4.

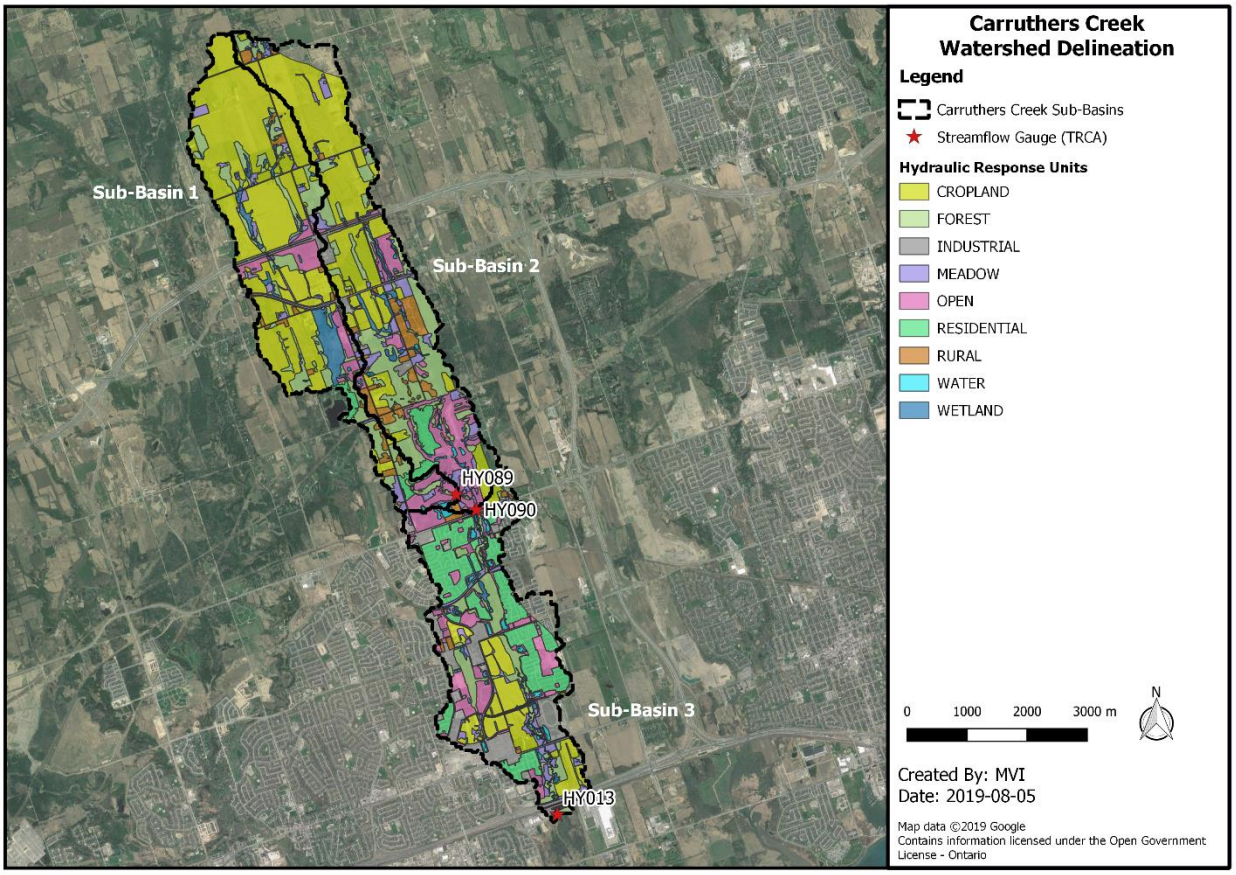

Figure 4. Carruthers Creek Watershed Delineation

This delineation layout aligns well with the intended purpose of the model, which is to make predictions regarding the potential impacts observed downstream as a result of changing upstream agricultural land use. The delineation scheme allows the user to appropriately represent the characteristics of agricultural tile drainage within the basin.

4. Raven Model Overview

The Carruthers Creek Raven model operates according to the following hydrologic processes. Precipitation is partitioned as either abstraction or infiltration using the abstraction percentage algorithm and simple Green-Ampt algorithm respectively. Abstracted water is directed to

depression storage where it can subsequently be evaporated through the open water evaporation process. Infiltrated water is either directed into the preliminary soil horizon if there is sufficient capacity based on soil moisture parameters or is partitioned as surface runoff. The Raven model incorporates two (2) soil horizons to simulate an unsaturated topsoil profile, and a saturated groundwater soil layer. Water that successfully infiltrates into the preliminary soil horizon can subsequently be partitioned as atmospheric water vapour through the linear evaporation-saturation algorithm, interflow through the PRMS interflow algorithm, or can percolate into the next soil horizon through the PRMS percolation algorithm. Water within the final soil horizon is subsequently routed as baseflow using the linear storage analytic baseflow algorithm. Snow melt is modelled using the simple melt algorithm.

The Carruthers Creek Raven model was configured as a simple version of the Eramosa River Raven model as these two regions share similar climatic and physiographic properties within the context of Southern Ontario. The most critical difference is the inclusion of an interflow hydrologic process in the Carruthers Creek model which was used to emulate the effects of tile drained agricultural lands. Tile drains were historically installed with the purpose of draining croplands which would otherwise frequently accumulate ponded water thus generating unfavourable agricultural conditions. Tile drains effectively lower the groundwater table and readily route infiltrated water to adjacent streams or ditches as illustrated below in Figure 5 (Blann, Anderson, Sands, & Vondracek, 2009).

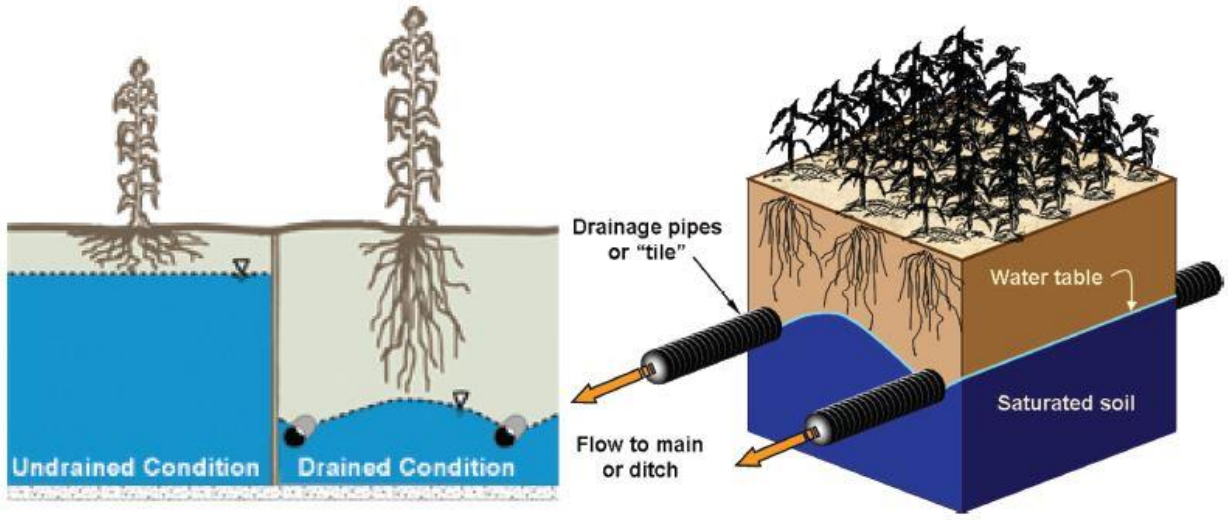

Figure 5. Visualization of Subsurface Tile Drainage - Excerpt from (Blann, Anderson, Sands, & Vondracek, 2009)

The Raven PRMS interflow hydrologic process is similar to a tile drain as it permits the routing of water stored in a shallow soil layer to surface water runoff as outlined in Equation (1):

$$M_{inter} = M_{max}\left(\frac{\varphi_{soil}-\varphi_{tens}}{\varphi_{max}-\varphi_{tens}}\right) \quad (1)$$

where M_{max} is the maximum interflow rate [mm/d]; φ_{max} is the maximum soil moisture content [mm]; φ_{soil} is the soil moisture at the beginning of a given time step [mm]; and φ_{tens} is the maximum soil tension storage [-] (Craig, n.d.).

5. Model Calibration

The Carruthers Creek Raven model was developed using the Eramosa model as a template such that same hydrologic processes were carried over, and the initial .rvp file consisted almost exclusively of Eramosa parameter values by default. A baseline model run was completed which resulted in a NSE value of 0.345 when comparing results to observed flows at the basin outlet (HY013) over the available 9 year data record as demonstrated below in Figure 6.

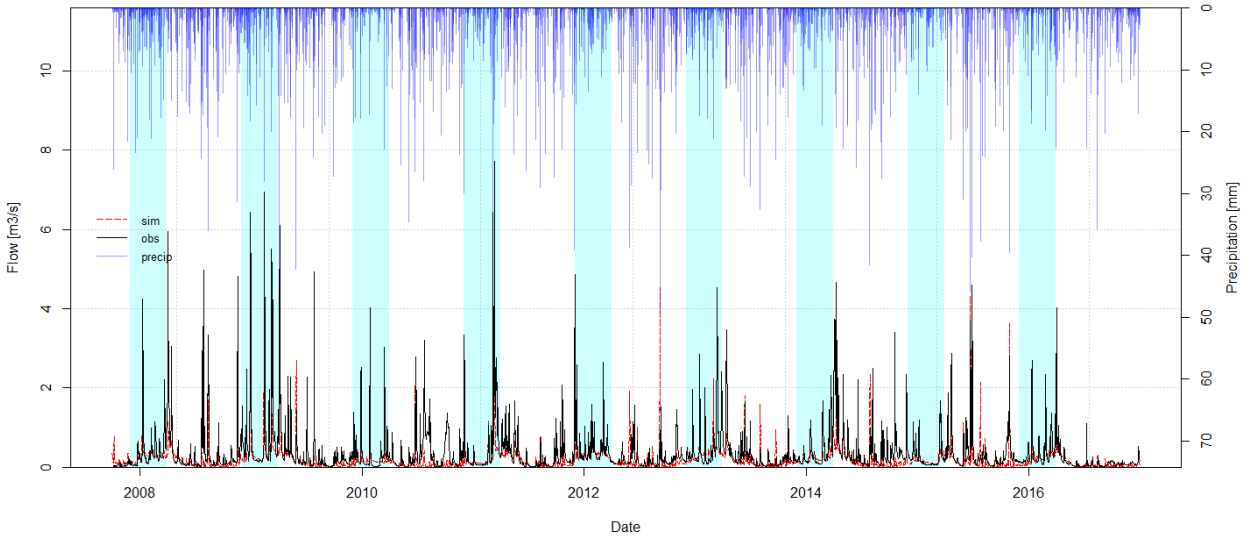

Figure 6: Carruthers Creek Raven Model Pre-Calibration Hydrograph

The pre-calibration hydrograph demonstrates that the model did not effectively capture the peak magnitudes of the larger observed streamflow events, suggesting that the observed system is flashier than modelled. This observation corroborates with the known characteristics of the Carruthers Creek watershed as the system consists of tile drained croplands which readily route shallow infiltrated water to adjacent tributaries of the creek. Furthermore, the watershed is located primarily within the Newmarket Till geologic unit and is characterized by clay and till plains overlain with sandy silt to sandy till surficial material which likely demonstrate different properties than initially specified (Conservation Authorities Moraine Coalition, n.d.). Consequentially, manual calibration was approached by researching appropriate soil properties that sufficiently represent the surficial soils and underlying Newmarket till unit. Appropriate land cover impermeable fractions were obtained from the Town of Ajax stormwater management design criteria manual. A summary of all literature values is provided below in Table 2.

Table 2. Summary of Literature Parameter Values for Model Calibration

Parameter	Literature Value	Units	Literature Source
Tile Drain Installation Depth	0.6 - 1.2	m	(Blann, Anderson, Sands, & Vondracek, 2009)
Newmarket Till Porosity	0.26	-	(Whelan, 2017)
Newmarket Till Hydraulic Conductivity	$10^{-11} – 10^{-10}$	m/s	(Conservation Authorities Moraine Coalition, n.d.)
Newmarket Till Wetting Front Suction Head (Clay)	320 - 1000	mm	(Chin, 2014)
Newmarket Till Field Capacity (Clay)	0.378	-	(Chin, 2014)
Newmarket Till Wilting Point (Clay)	0.265	-	(Chin, 2014)
Surficial Soil Hydraulic Conductivity (Sandy Clay Loam to Silt Loam)	2 - 7	mm/hr	(Chin, 2014)
Surficial Soil Wetting Front Suction Head (Silty Clay to Silt Loam)	170 - 290	mm	(Chin, 2014)
Surficial Soil Porosity (Sandy Clay Loam to Silt Loam)	0.398 – 0.501	-	(Chin, 2014)
Surficial Soil Field Capacity (Sandy Clay Loam to Silt Loam)	0.244 – 0.284	-	(Chin, 2014)
Surficial Soil Wilting Point (Sandy Clay Loam to Silt Loam)	0.135 – 0.136	-	(Chin, 2014)
Residential Impermeable Fraction	0.6 – 0.75	-	(Town of Ajax, 2016)
Industrial Impermeable Fraction	0.9 – 0.95	-	(Town of Ajax, 2016)
Rural Impermeable Fraction	0.05 – 0.35	-	(Town of Ajax, 2016)
Open Impermeable Fraction	0.0 – 0.25	-	(Town of Ajax, 2016)

The above literature values were used to set default model parameters and guide the manual calibration process. A new soil profile was also added to the model and assigned to croplands in order to simulate the characteristics of tile drainage by altering the maximum interflow rate parameter as defined in Equation (1). A summary of eight (8) critical parameters that were adjusted during the manual and automated calibration process is provided below in Table 3.

Table 3. Summary of Model Calibration Parameters

Parameter Value	Parameter Description	Units	Parameter Lower Bound	Parameter Upper Bound	Manual Calibration Value	Automated Calibration Value
par_x1	Porosity (Default)	-	0.398	0.5	0.398	0.5
par_x2	Hydraulic Conductivity (Default)	mm/day	24	168	48	76.33
par_x3	Maximum Interflow Rate (Cropland)	mm/day	0	1000	50	32.16
par_x4	Wetting Front Suction Head (Default)	-mm	170	290	290	191.52
par_x5	Topsoil Depth (Default)	m	0.1	2.0	1.0	0.1162
par_x6	Topsoil Depth (Cropland)	m	0.6	1.2	1.2	1.2
par_x7	Melt Factor	mm/d/K	0.1	5.0	2.7	2.716
par_x8	Rain Snow Temperature	^{o}C	-5.0	3.0	-2.0	-0.809

The simulated hydrograph resulting from manual calibration is presented below in Figure 7.

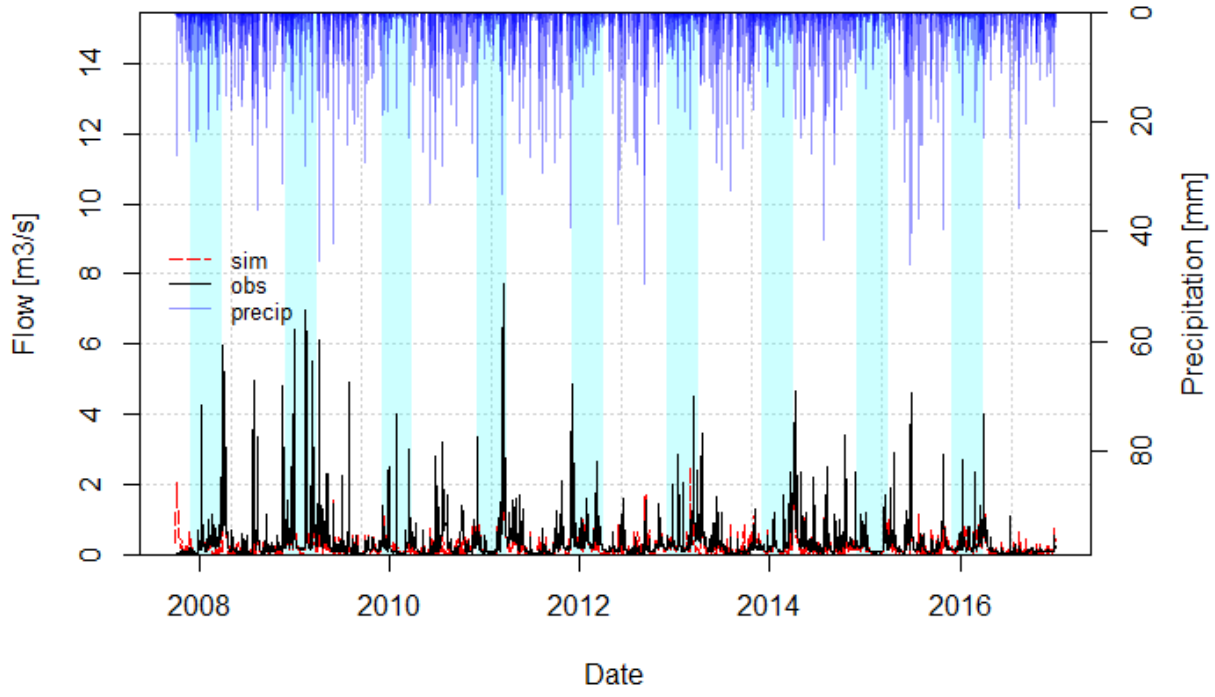

Figure 7: Carruthers Creek Raven Model Manual-Calibration Hydrograph

Model calibration success is quantified through four (4) diagnostic metrics including root mean square error (RMSE), Nash-Sutcliffe efficiency (NSE), number of sign changes (NSC), and peak difference (PDIFF). RMSE is an indicator for the amount of error which is not explained by the model. NSE is a metric that is good at generally describing overall model fit as it quantifies how much better the model is over the average value of the observed streamflow data record. NSC quantifies the number of sign changes that occur between consecutive error values which is an indicator for model tendency to consistently over- or under-predict streamflow (Craig, n.d.). Finally, PDIFF is the difference between the maximum observed and modeled data which is a good indicator of the model's predictive ability during large discharge events (Craig, n.d.). Diagnostic metrics were evaluated for simulated flows at gauge HY013 to assess overall model performance, and for streamflow gauges HY089 and HY090 to isolate the effectiveness of modelling tile drainage as land coverage in these sub-basins is primarily cropland. It is noted that the gauges HY089 and HY090 each contain a 1-year long record which is an insufficiently short period to gauge overall model calibration success in and of itself. The resulting diagnostic metrics from the manual model calibration are presented below in Table 4.

Table 4. Summary of Manual Model Calibration Diagnostic Metrics

Sub-Basin	Outlet Gauge ID	Data Record Period	RMSE	NSE	NSC	PDIFF
1	HY089	2016	0.07	0.595	37	-0.54
2	HY090	2016	0.17	0.624	68	-1.67
3	HY013	2007-2017	0.43	0.499	619	-3.96

Manual calibration resulted in a reasonable model fit with a NSE of 0.499 for the 9-year data period. Agricultural tile drainage appears to be well represented in the model as NSE values for the upstream agricultural sub-basins is approximately 0.6 – 0.62. The Carruthers Creek Raven model was subsequently calibrated using the OSTRICH optimization program to complete a

dynamically dimensioned search (DDS) algorithm with 1000 model evaluations. The resulting optimal parameter estimates are summarized above in Table 3. The simulated hydrograph resulting from automated model calibration is presented below in Figure 8.

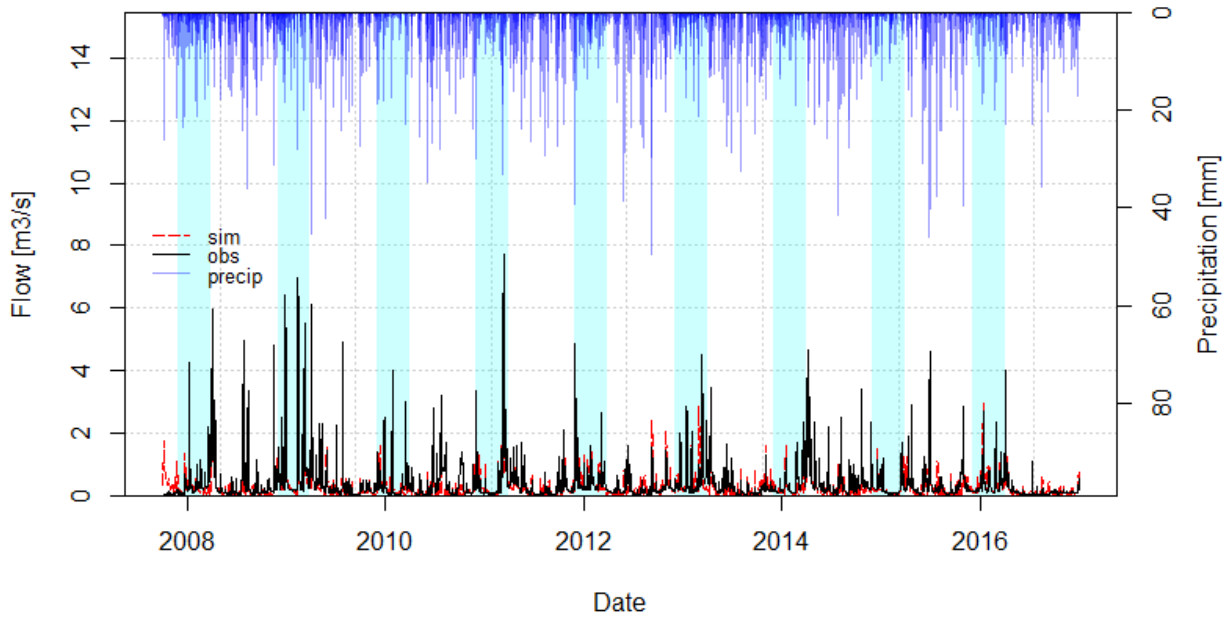

Figure 8: Carruthers Creek Raven Model Automated-Calibration Hydrograph

The resulting diagnostic metrics from automated model calibration are presented in Table 5.

Table 5. Summary of Automated Model Calibration Diagnostic Metrics

Sub-Basin	Outlet Gauge ID	Data Record Period	RMSE	NSE	NSC	PDIFF
1	HY089	2016	0.06	0.702	43	-0.44
2	HY090	2016	0.15	0.735	63	-1.35
3	HY013	2007-2017	0.41	0.560	603	-3.01

Automated calibration improved overall model performance from a NSE fit of 0.499 to 0.560, and resulted in better representation of agricultural tile drainage as indicated by improved NSE values for the upstream agricultural sub-basins which exceed 0.7. Automated calibration also slightly improved PDIFF and RMSE diagnostic metrics while NSC remained relatively the same. Overall model improvement is evident when visually comparing the simulated hydrographs

presented in Figure 7 and Figure 8, however the model still appears to generally underestimate streamflow during large discharge events which is not ideal when completing a bankfull discharge exceedance analysis.

6. Results

The bankfull discharge exceedance analysis was conducted by first estimating bankfull discharge using Manning's equation according to Equation (2):

$$Q = \frac{A^{\frac{5}{3}} S^{\frac{1}{2}}}{n P^{\frac{2}{3}}} \quad (2)$$

where A is the cross-sectional area [m^2]; S is the bed slope [-]; n is the Manning's roughness coefficient [-]; and P is the wetted perimeter [m]. The channel cross-sectional area, wetted perimeter and gradient are based on geomorphic survey data collected from Carruthers Creek on December 5, 2017. The channel roughness was derived from a Wolman's pebble count conducted on May 23, 2019. Bankfull stage is based on cross-sectional geometry and on-site visual indicators resulting in an estimated bankfull discharge of 2.98 m^3/s. The HY013 observed streamflow record validates this estimate as it meets or exceed 2.98 m^3/s approximately 4 times a year on average which is reasonable for a developed catchment such as Carruthers Creek. Comparatively, natural channels in undeveloped catchments usually meet or exceed bankfull discharge twice a year (Leopold, 1973). The calibrated model predicts that under existing conditions, bankfull discharge is equalled or exceeded 13 times during the period of 2007 – 2017. This value is a significant underestimate compared to the observed streamflow record which exceeds bankfull discharge 37 times over the same duration. This discrepancy indicates that the calibrated model is under-predicting streamflow during large flow events which is not ideal for bankfull discharge exceedance analysis.

An LID land development scenario was emulated by assigning a new land use class, vegetation class, and soil profile to the rural and cropland HRUs located within sub-basins 1 and 2. A conservative approach was followed whereby all LID parameters were set to default values used for residential HRUs in exception to the maximum percolation rate which was set to a reasonable value of 5 mm/day. The impervious fraction of the LID land use class was incrementally increased until the number of simulated erosive flow events predicted under the LID development scenario equalled that of existing conditions. The bankfull discharge exceedance analysis reveals that a maximum impervious fraction of 12.1% can be implemented in tandem with LID SWM practices across the existing rural and cropland areas of upstream sub-basins 1 and 2 without increasing the frequency of erosive flow events observed at the downstream basin outlet.

The maximum permissible impervious fraction is associated with a fair amount of uncertainty as the calibrated model under-predicts peak streamflow during larger discharge events. As a result, the model is likely simulating a reduced frequency of bankfull discharge exceedance under the LID development scenario which was the case when comparing the observed streamflow record against the simulated existing conditions record. Other sources of uncertainty originate from the model's use of only one (1) cross-section to represent an entire sub-basin which is a significant assumption when making predictions on a creek reach scale. Geomorphic-survey data would ideally be collected across the entire basin to develop more representative model inputs, and to establish a better bankfull discharge estimate. Furthermore, additional research related to LID drainage characteristics and a more comprehensive delineation of the LID development scenario would assist in refining input parameters estimates and improve the accuracy of the resulting permissible impervious fraction. To improve the overall model, it is recommended that

additional hydrologic processes such as canopy storage are added to provide greater representation of the actual hydrologic mechanisms acting upon the basin. Finally, tt is also recommended that soil parameter estimates derived from actual samples are incorporated into the model to replace literature values.

References

Askarizadeh, A. (2015). From rain tanks to catchments: Use of low impact development to address hydrologic symptoms of the urban stream syndrome. *Environmental Science and Technology*, 49(19), 11264-11280.

Blann, K. L., Anderson, J. L., Sands, G. R., & Vondracek, B. (2009). Effects of Agricultural Drainage on Aquatic Ecosystems: A Review. *Environmental Science and Technology*, 39, 909-1001.

Chin, D. A. (2014). *Water-Resources Engineering Third Edition.* New Jersey: Pearson.

Conservation Authorities Moraine Coalition. (n.d.). *Hydraulic Properties*. Retrieved from Oak Ridges Moraine Groundwater Program: https://oakridgeswater.ca/program-elements/hydrogeologic-analysis/hydraulic

Craig, J. (n.d.). *Raven: User's and Developer's Manual v2.9.1.* Waterloo: University of Waterloo.

Leopold, L. B. (1973). River Channel Change with Time: An Example. *Geological Society of America Bulletin*, 84, 1845-1860.

Town of Ajax. (2016). *Town of Ajax Design Criteria Section C - Stormwater Management and Storm Drainage.* Ajax.

Walsh, C. J., Roy, A. H., Feminella, J. W., Cottingham, P. D., Groffman, P. M., & Morgan, R. P. (2005). The urban stream syndrome: current knowledge and the search for a cure. *Journal of the North American Benthological Society*, 24(3), 706-723.

Whelan, K. (2017). Assessing Aquifer Vulnerability of Private Wells through Geological and Geochemical Analysis near the Clarington Transformer Station. *McMaster University (M.Sc. Thesis)*.